

Development of Molecular Tools for the Investigation of G protein-gated Inwardly Rectifying  
Potassium (GIRK) Channels

By

Susan Joanne Ramos-Hunter

Dissertation

Submitted to the Faculty of the  
Graduate School of Vanderbilt University  
in partial fulfillment of the requirements  
for the degree of

DOCTOR OF PHILOSOPHY

in

Chemistry

May 2017

Nashville, Tennessee

Approved:

Gary A. Sulikowski, Ph.D.

C. David Weaver, Ph.D.

John A. McLean, Ph.D.

Craig W. Lindsley, Ph.D.

Copyright © 2017 by Susan Joanne Ramos-Hunter  
All Rights Reserved

I dedicate this work to my mother, Georgia Ann Ramos Hunter.

You truly taught me how to be a Ramos.

## ACKNOWLEDGEMENTS

I wish I could not be limited by a single page to acknowledge the collective village that helped me to get to this point in my career. First, I would like to thank my advisor, Dr. Gary A. Sulikowski. Mentorship is a key part of this transition from science newbie to professional scientist. I would like to extend a special thank you to my scientific mentors, Dr. C. David Weaver and Dr. Dina Myers Stroud. You both have helped to foster and catalyze a joy of inquisitive learning and exploration. I would also like to extend my thanks to my committee members, Dr. John A. Mclean and Dr. Craig W. Lindsley for their input and support. I owe an unbelievable amount of gratitude to the Fisk-to-Vanderbilt Masters to Ph.D. Bridge Program's faculty, administration and students. Thank you for your mentorship, professional development and friendships. Thank you to the Vanderbilt Department of Chemistry for your support.

Next, I would like to specifically acknowledge the Weaver laboratory: Dr. Yu "Sunny" Du, Kristopher *Keith* Abney, Francis "FJ" Prael III, Brittany (Duerk) Spitznagel and Krystian "Brozek" Andrzej Kozek. Your scientific support and unique conversation topics have been inspiring (and sometimes hilariously questionable). I want to thank the Vanderbilt Institute of Chemical Biology Synthesis Core, specifically: Dr. Kwangho Kim, Dr. Plamen Christov, and Dr. Ian Romaine. I would also like to thank Rocco Gogliotti, James "Jim" Salovich and Dr. Kyuok Jeon. The hours of countless advising, mentoring and helping improve my science has encouraged me to continue my pursuit of research.

Lastly, I would like to thank my family and friends. *Mother*, Aunt Isabell, Aunt Eva and Uncle Ed; you all contributed to my success. You got me here. You kept me going. My friends who have been my support and light-hearted conversations. Thank you. Last but not least, I would like to thank the Flying Spaghetti Monster: All Hail His Noodly Appendages!

## TABLE OF CONTENTS

	Page
DEDICATION .....	iii
ACKNOWLEDGEMENTS .....	iv
LIST OF TABLES .....	vii
LIST OF FIGURES .....	ix
LIST OF SCHEMES.....	xii
Chapter	
1. Introduction .....	1
1.1 GPCRs and GIRK Channels .....	1
Dysregulation of GIRK Channels .....	2
X-ray structure of GIRK2 - $\beta\gamma$ G protein complex .....	4
1.2 Discovery of Small Molecule GIRK Channel Regulators using Metal Sensing Dyes .....	5
Xanthene Based Fluorophores: Fluorescein and Rhodamine .....	6
Photoinduced Electron Transfer .....	7
Development and Use of Thallium Flux Assay .....	11
Thallos™ Dye and Synthesis .....	13
1.3 Prior Small Molecule GIRK Activators (or Inhibitors) .....	14
Development of the Selective and Potent GIRK Activator, ML297 .....	15
1.4 GIRK Selectivity SAR to Development of “Sulfonamides” .....	17
1.5 Statement of Dissertation .....	18
2. Discovery and SAR of a Novel Series of GIRK1/2 and GIRK1/4 Activators “Sulfonamide series” .....	19
2.1 Introduction.....	19
2.2 Identification and Synthesis of Sulfonamide Analogs.....	21
2.3 GIRK Activator CRCs Measuring Tl <sup>+</sup> Flux.....	27

2.4 Conclusion .....	29
2.5 Experimental .....	30
General Experimental .....	30
Synthesis of Urea Library .....	31
Synthesis of Amide Library .....	31
TI <sup>+</sup> Flux Assay Protocol.....	31
Data Analysis .....	32
3. 2-methylcyclopropyl Enantiomers: Selective GIRK1/2 and GIRK1/4 Activators and Inhibitors.....	34
3.1 Introduction.....	34
3.2 Background.....	35
GIRK1/2 Verses GIRK1/4 Selectivity Studies.....	37
3.3 Synthesis of <i>trans</i> 2-Methyl Cyclopropyl Enantiomer Probes .....	42
3.4 Cyclopropyl Enantiomer CRCs Measuring TI <sup>+</sup> Flux .....	43
3.5 Conclusion .....	46
3.6 Experimental.....	47
General Experimental .....	47
Synthesis of ( <i>R,R</i> ) and ( <i>S,S</i> ) <i>trans</i> 2-methyl Cyclopropyl Phenyl Pyrazole Urea Enantiomers .....	48
4. Selective Rhodamine Pro-dye/Enzyme Releasing Pair: Mitochondrion Membrane Potential Sensors.....	62
4.1 Introduction.....	62
4.2 Background.....	63
Metal Ion Sensor Dyes.....	63
“Protected” Dyes Used For Enzymatic Studies .....	64
4.3 Synthesis of PLE-Selective Rhodamine Dyes .....	66
4.4 Enzymatic Reactivity of PLE with Prepared Rhodamines .....	68
4.5 Pro-Dye Selectivity With Transient and Stable PLE cell lines.....	69

Transiently Transfected HEK-293 with PLE .....	69
Stable PLE Expressing HEK-293 Cell Line .....	70
4. 6 Rate of Pro-Dye Deprotection Using Kinetic Plate Reader (Panoptic) .....	71
4. 7 Applying Pro-Dyes in Selectivity Assays .....	74
Rhodamine Pro-Dyes to Study Mitochondria .....	75
Rhodamine Pro-Dyes Cellular Staining.....	76
4.8 Conclusion and Future Directions .....	78
4.9 Experimental .....	80
General Experimental .....	80
Synthesis of Rhodamine Pro-dye PLE substrates .....	81
Cellular Experimental .....	85
Cell Line Formation .....	85
Kinetic Dye Assays .....	85
5. Conclusions and Implications For Further Research .....	91
5.1 Introduction.....	91
5.2 Chapter 2 Conclusions and Future Directions of Discovery and SAR of a Novel Series of GIRK1/2 and GIRK1/4 Activators: “Sulfonamide Series” .....	91
5.3 Chapter 3 Conclusions and Future Directions of Discovery of a Stereo-Specific Modulation of GIRK1/2 and GIRK1/4 Channels: Synthesis and Evaluation of 2-Methylcyclopropyl Enantiomers .....	93
5.4 Chapter 4 Conclusions and Future Directions of Selective Rhodamine Pro-dye/Enzyme Releasing Pair: Mitochondrion Membrane Potential Sensors .....	96
5.5 Concluding Remarks .....	97
Appendix	
A. NMRs For Chapter 3 .....	53
B. NMRs For Chapter 4 .....	87
REFERENCES .....	98

## LIST OF TABLES

Table	Page
1.1 Commonly Used Xanthene Based Dyes Structures and Properties .....	10
2.1 GIRK activity of VU0259369 analogs varied within the Western arylsulfonamide .....	23
2.2 GIRK activity of VU0259369 analogs varied within the Eastern arylsulfonamide .....	25
3.1 Structures and activity of GIRK probe analogs on GIRK1/2 and GIRK1/4.....	38
3.2 Structures and activity of GIRK probe analogs on GIRK1/2 and GIRK1/4.....	40
3.3. EC <sub>50</sub> and IC <sub>50</sub> (μM) of MCP Isomers on GIRK1/2 and GIRK1/4 channels .....	46
4.1. Synthesis of pro-dye rhodamines with VU number, derivative type and yield of reactions ..	67
4.2. Pro-dye rhodamine derivatives rate of deprotection by PLE reported ( $v^{-1}/[S]^{-1}$ ) of PLE expressing cells compared to <i>in situ</i> . .....	73



## LIST OF FIGURES

Figure	Page
1.1. GIRK channels form GIRK2 stable homotetramer or heterotetramers .....	1
1.2. GIRK I/V Chart and Channel Subunits .....	2
1.3. GIRK channels have been implicated in a number of disease states, diagram .....	3
1.4 GIRK channel crystal structure side and overhead view .....	4
1.5. Thallos™ is prepared as bisacetoxo fluorescein with N-(2-methoxyphenyl)iminodiacetate protected acetoxymethyl esters. ....	5
1.6 Jabłoński diagram .....	6
7. In the absence of a metal, PET offers a more efficient relaxation pathway and decreases the optical output of the fluorophore .....	7
1.8. Xanthene fluorophore scaffold in equilibrium between closed-lactone (off) and open quinoid (on) .....	8
1.9. GIRK channels permit the influx of Tl <sup>+</sup> ions when activated by a compound .....	11
1.10. N-(2-methoxyphenyl)iminodiacetate chelation subunit based off of BAPTA Ca <sup>2+</sup> and Zn <sup>2+</sup> sensors .....	13
1.11. Functionalization around initial GIRK channel hit VU0032230 .....	15
1.12. a) Raw trace and slopes plotted for CRCs generated from ML297 on GIRK1/2 containing cells .....	16
1.13. GIRK1 containing GIRK ion channel modulator, VU0456810 (ML297) .....	17
2.1 GIRK1 containing GIRK ion channel modulators, original screening hit VU0032230, SAR study probe, VU0456810 (ML297), “sulfonamide” scaffold modification to amide, VU0259369, and Narigin a known GIRK activator (>100 μM). ....	20
2.2 Optimization plan for synthesis of amide and urea derivatives. ....	21
2.3. A) GIRK activator concentration response curves (CRC) measuring Tl <sup>+</sup> flux .....	28
2.4. B) GIRK activator concentration response curves (CRC) measuring Tl <sup>+</sup> flux .....	29

3.1. Functionalization around ML297 (left). Initially, 3,4-diFluoro was found to be an excellent activator of GIRK1 containing GIRK channels. Recently, selectivity studies have probed the C3 position on the pyrazole to determine GIRK1 containing selectivity and pursued a diversifying SAR (right). .....	36
3.2. Preparation of single enantiomer methylcyclopropanes. ....	42
3.3. Single enantiomer ureas: VU0659392(3.12a), VU0657532(3.12b), VU0657405(3.11a), and VU0657424(3.11b) .....	44
3.4. $\text{Ti}^+$ flux of GIRK1/2 (left) and GIRK1/4 (right) with compounds 3.11a-3.12b, standardized to ML297 fluorescence intensity .....	45
3.5. $^1\text{H-NMR}$ spectrum (400 MHz, $\text{CDCl}_3$ ) of 1 <i>R</i> ,2 <i>R</i> 3.10, $^1\text{H-NMR}$ spectrum (400 MHz, $\text{CDCl}_3$ ) of 1 <i>S</i> ,2 <i>S</i> 3.10b and $^{13}\text{C-NMR}$ spectrum (400 MHz, $\text{CDCl}_3$ ) of 1 <i>R</i> ,2 <i>R</i> 3.10. ....	54
3.6. $^1\text{H-NMR}$ spectrum (400 MHz, $\text{CDCl}_3$ ) of 1 <i>R</i> ,2 <i>R</i> 3.4, $^1\text{H-NMR}$ spectrum (400 MHz, $\text{CDCl}_3$ ) of 1 <i>S</i> ,2 <i>S</i> 3.4b and $^{13}\text{C-NMR}$ spectrum (400 MHz, $\text{CDCl}_3$ ) of 1 <i>R</i> ,2 <i>R</i> 3.4. ....	55
3.7. $^1\text{H-NMR}$ spectrum (400 MHz, $\text{CDCl}_3$ ) of 1 <i>R</i> ,2 <i>R</i> 3.5, $^1\text{H-NMR}$ spectrum (400 MHz, $\text{CDCl}_3$ ) of 1 <i>S</i> ,2 <i>S</i> 3.5b and $^{13}\text{C-NMR}$ spectrum (600 MHz, $\text{CDCl}_3$ ) of 1 <i>R</i> ,2 <i>R</i> 3.5.....	57
3.8. $^1\text{H-NMR}$ spectrum (400 MHz, DMSO) of 1 <i>R</i> ,2 <i>R</i> 3.11a, $^1\text{H-NMR}$ spectrum (400 MHz, DMSO) of 1 <i>S</i> ,2 <i>S</i> 3.11b and $^{13}\text{C-NMR}$ spectrum (600 MHz, DMSO) of 1 <i>R</i> ,2 <i>R</i> 3.11a. ....	59
3.9. $^1\text{H-NMR}$ spectrum (400 MHz, DMSO) of 1 <i>R</i> ,2 <i>R</i> 3.12a, $^1\text{H-NMR}$ spectrum (400 MHz, DMSO) of 1 <i>S</i> ,2 <i>S</i> 3.12b and $^{13}\text{C-NMR}$ spectrum (600 MHz, DMSO) of 1 <i>R</i> ,2 <i>R</i> 3.12a. ....	61
4.1. (Left)1,2-bis(2-aminophenoxy)ethane- <i>N,N,N',N'</i> -tetraacetic acid (BAPTA) developed by Tsien chelates $\text{Ca}^{2+}$ . (Right) 2-triazacryptand[2,2,3]-1-(2-methoxyethoxy)benzene (TAC-RED) are selective for $\text{K}^+$ .....	64
4.2. Trimethyl lock scheme using PLE activated rhodamine protecting group.....	65
4.3. Activated dye from A (Intracellular esterases <sup>35</sup> ) or B (Exogenous hydrolase/amidase) .....	66
4.4. +/-PLE transiently transfected HEK-293 incubated (1h) with pro-dyes [10 $\mu\text{M}$ ]. PLE expressing cells showed fluorescence (0.1ms) when excited at 490nm .....	70
4.5. +PLE stable cell line generated by K. Abney (Weaver). ....	71
4.6. Histogram representing activity ( $\text{v}^{-1}/[\text{S}]^{-1}$ ) of PLE substrate rhodamines in +/-PLE cells .....	74
4.7. (Left) VU0523039 and (right) VU0496934 positive hits for PLE “inhibition” .....	75
4.8. Rhodamine 123 and 110 cellular dyes .....	76

4.9. Cellular staining of HEK-293 cells expressing PLE.....	78
5.1. LOGO5 was found to selectively activate GIRK channels in the presence of 440nm .....	92
5.2. Implementing more sulfonamide probes based off of LOGOs results .....	93
5.3. Examining enantiomer preference with (1 <i>S</i> ,2 <i>S</i> ) 2-methyl cycloproyl probes and <i>R</i> or <i>S</i> phenylethyl pyrazole modification .....	95
5.4. (Left) Proposed Rhodamine 123 based pro-dye off of (Right) Pro-dye 4.1e .....	96

## LIST OF SCHEMES

Scheme	Page
1.1. Synthesis of Fluorescein-based Thallos <sup>TM</sup> with Metal Chelating Unit.....	14
3.1. Synthesis of 2-methylcyclopropyl ( <i>R,R</i> ) or ( <i>S,S</i> ) enantiomers .....	43
4.2. Synthesizing and evaluating PLE-Pro Dye Rhodamines.....	66

# CHAPTER 1

## INTRODUCTION

### 1.1 GPCRs and GIRK Channels

G-Protein Coupled Receptors (GPCRs) are a large family of receptors with numerous functions including regulating electrical excitability in cardiac and neuronal tissue<sup>1</sup> by acting on ion channels. Excitability of nerves and muscles is guided by the membrane potential of cells, or the ability to move ions such as  $\text{Na}^+$ ,  $\text{K}^+$  or  $\text{Cl}^-$  through ion channels. One of these ion channel families is the G Protein-gated Inwardly Rectifying Potassium (GIRK) channels, comprised of the  $\text{K}_{\text{ir}}3.1$ - $3.4$  (GIRK 1/2, 2/2, 2/3, 1/3 and 1/4)<sup>1</sup>.

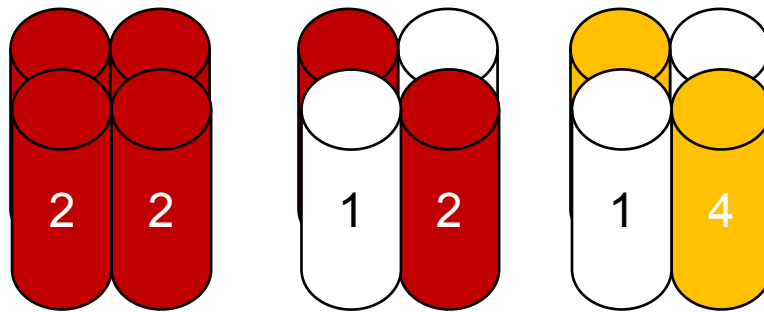


**Figure 1.1.** GIRK channels form GIRK2 stable homotetramer or heterotetramers GIRK1/2, GIRK1/4, GIRK1/3 (not shown) and GIRK2/3 (not shown).

Potassium channels cover a variety of functions such as setting the resting potential, terminate periods of intense activity and generally lower the effectiveness of excitatory inputs<sup>2</sup>. Specifically, GIRKs are expressed as homo and heterotetramers membrane spanning subunits<sup>3</sup> that permit the outward flow of  $\text{K}^+$  ions (efflux) which creates an inhibitory effect, or hyperpolarization<sup>4</sup>. This outward ionic gradient is established by Na/K pumps which regulates the membrane potential. Occlusion of the central pore by intracellular  $\text{Mg}^{2+}$  or polyamines occurs at membrane potentials above the equilibrium potential of  $\text{K}^+$  ( $E_{\text{K}}$ )<sup>1</sup>.

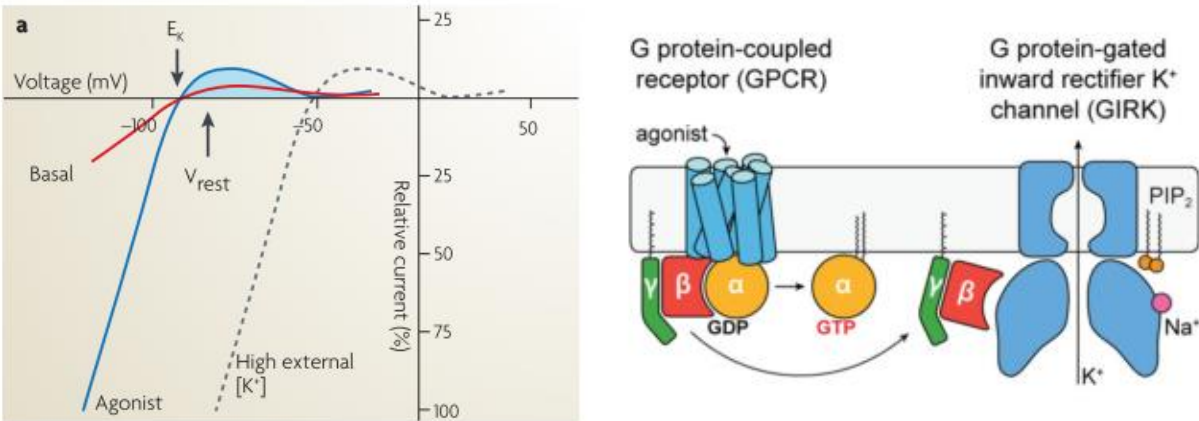


**Figure 1.2.** Used with permission from Luscher<sup>1</sup> and Whorton and McKinnin<sup>3</sup>. (Left) Current plotted as a function of voltage for GIRK channels. Red line (basal) current versus agonist induced current (blue) shows inward rectification (large inward current and small outward current).  $E_K$  indicates equilibrium potential and blue shaded area shows the hyperpolarization of the cell membrane. High external  $K^+$  shifts the  $E_K$ . (Right) GIRK channels are typically activated by an agonist interacting with the GPCR. In the presence of  $PIP_2$ ,  $K^+$  effluxes to the extracellular.

Functionally, when a neurotransmitter (e.g. acetylcholine in cardiac tissue) binds to the G protein-coupled receptor and causes the release of the  $G\beta\gamma$  subunits. These subunits activate the G protein-gated Inward Rectifying potassium channel and causes them to open leading to a release of potassium ( $K^+$ ). Potassium ion release drives the cell membrane towards a resting potential and reduces excitability in the cell signaling<sup>3</sup>. In addition to cardiac tissue (GIRK 1/4), GIRK channels are also dispersed widely in the brain (GIRK 1/2, 2/2, 2/3, 1/3)<sup>5</sup>, and function in a similar way to control neuronal excitability<sup>3</sup>.

### ***Dysregulation of GIRK Channels***

Dysregulation of GIRK channels has been implicated in several disease states such as movement disorders<sup>6</sup>, schizophrenia<sup>7</sup>, drug addiction and withdrawals<sup>8</sup>, epilepsy<sup>9</sup> and pain<sup>10</sup> (Figure 1.3). For example, Harkins and coworkers<sup>8</sup>, studied mice with the *weaver* mutation to better understand ataxia and Parkinson's disease. Not only did these mice suffer from neurological

movement disorders, they also showed signs of degenerating dopaminergic neurons through a mutation that causes neurons to fail to differentiate and migrate. This mutation in GIRK2 channels (G156S) is an altered glycine found in all K<sup>+</sup> channels, causing the loss of K<sup>+</sup> selectivity and permitting Na<sup>+</sup> and Ca<sup>2+</sup> ions to permeate the cell which leads to cell death. As evidenced in the *weaver* mutation study, we have only recently begun to comprehend how important these channels are in normal and pathological central nervous system states. The development of small molecules that can act as selective molecular “switches” that controls activity at specific GIRK channels to first elucidate their role in normal physiology and then evaluate their potential to alleviate can offer us a way of treating or prevent these disorders.

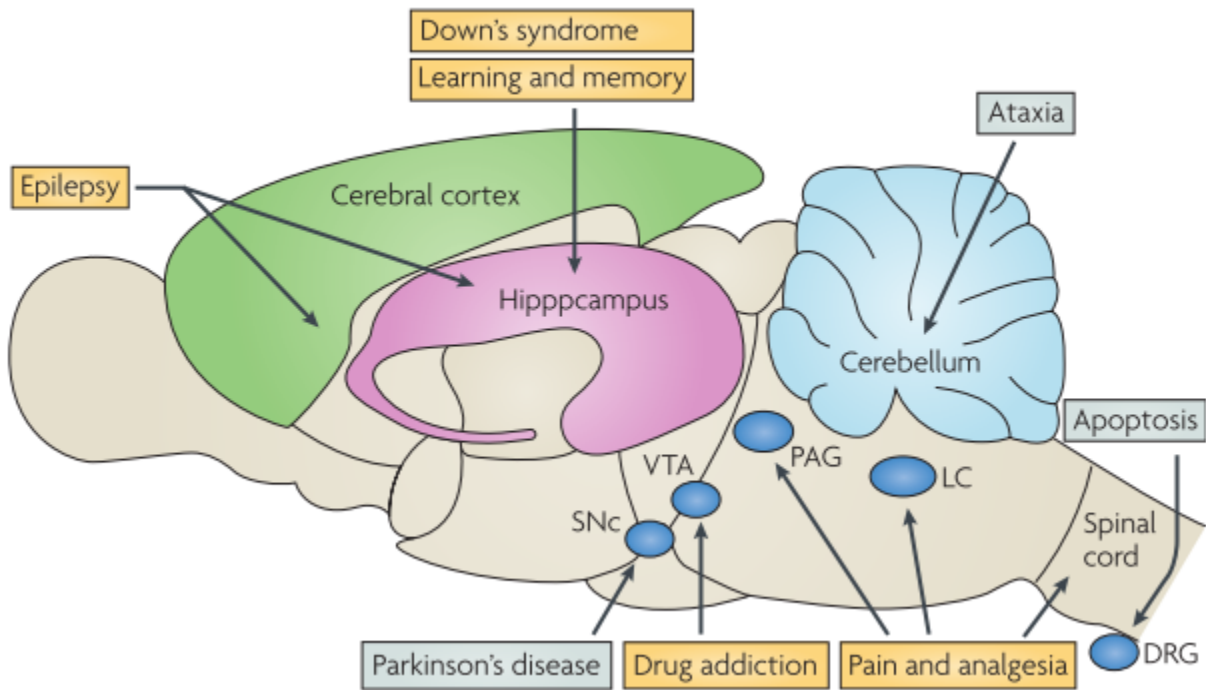


**Figure 1.3.** GIRK channels have been implicated in a number of disease states, diagram used with permission from Lüscher and Slesinger<sup>1</sup>.

### *X-ray structure of GIRK2 - $\beta\gamma$ G protein complex*

Many electrophysiological and biochemical studies have been conducted to determine how GPCR subunit activate GIRK channels. The crystal structure of a GIRK2 channel bound to the  $G\beta\gamma$  subunits also shows the gating regulators of  $Na^+$  and  $PIP_2$  as illustrated in Figure 1.4.

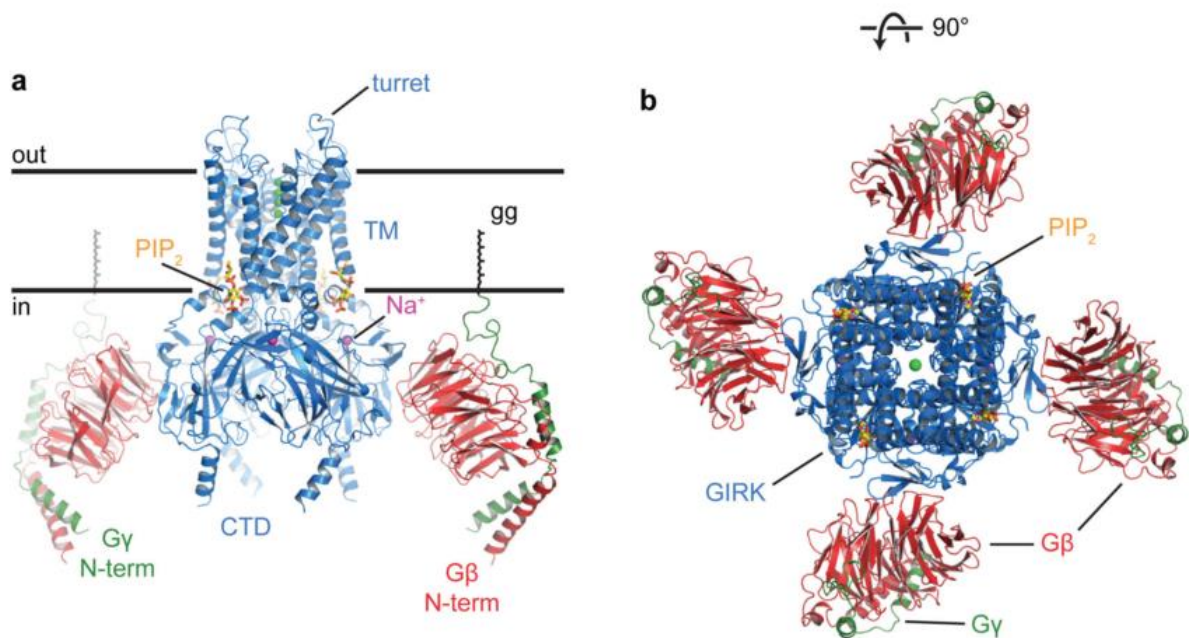


**Figure 1.4.** Used with permission from Whorton and MacKinnon<sup>3</sup>. (a) Side view of crystal structure of GIRK channel with  $G\beta\gamma$  subunits bound to the channel. Front subunits have been removed for clarity. Note transmembrane channel with the turret extruding from the extracellular side. (b) Top view of crystal structure of GIRK channel with  $G\beta\gamma$  subunits bound to the channel. Note  $K^+$  ion passing through the open channel.  $PIP_2$  is also required to be bound for GIRK channel activity.

The authors show the GIRK channels to be modified by the  $G\beta\gamma$  subunits and point out the importance of the G subunits such as how many are required for opening of the channel. They also indicate the importance of the presence of  $PIP_2$  and/or  $Na^+$  which acts as a GIRK channel activator. The stoichiometry of GIRK channels to subunits, as shown, four  $G\beta\gamma$  were found associated with the open conformation due to the stabilizing effect of opening the channel. This study provided an excellent look at how these transmembrane proteins activate but further studies are required to really examine the mechanism of GIRK channel activity.



## 1.2 Discovery of Small Molecule GIRK Channel Regulators using Metal Sensing Dyes

Many currently marketed drugs act target GPCRs for example Atrovent, which targets muscarinic M1 and M2 receptors for chronic obstructive pulmonary disease<sup>11</sup>. Full reviews on this topic are widely available<sup>12</sup>. As GPCRs regulate ion channels monitoring of ion channel activity serves as a common screening paradigm for the discovery of small molecules that regulate GPCR<sup>12</sup> activity as well as ion channel activity directly. One method of monitoring ion channel activity is the use of small molecule probes that change fluorescence upon specific ion binding. Metal detection can occur by either quenching or enhancing fluorescence. In the case of monitoring potassium ion channels, Hille originally determined that  $Tl^+$  was a size surrogate for  $K^+$  channels<sup>2</sup> and Weaver<sup>13</sup> determined upon binding to Thallos<sup>TM</sup> results in enhanced fluorescence presumably by photoinduced electron transfer (PET) (Figure 1.5).

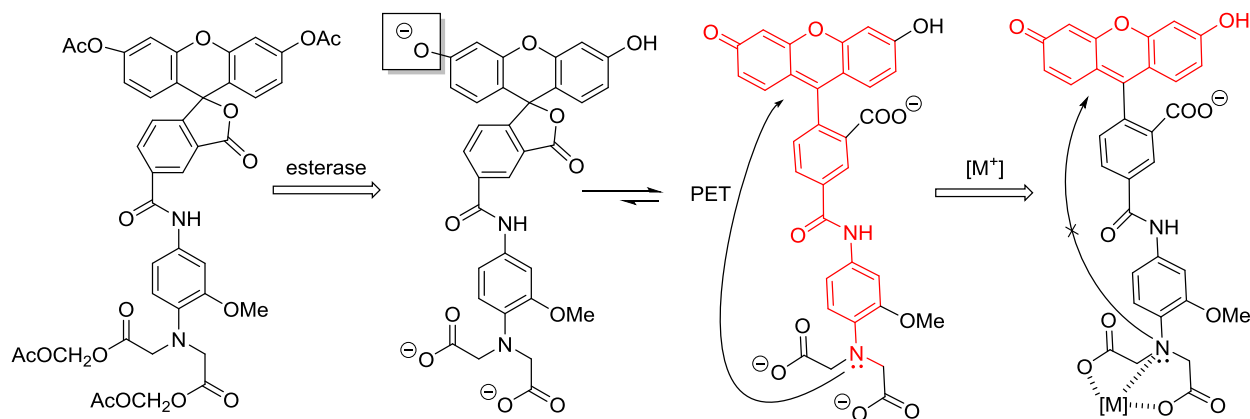


**Figure 1.5.** Thallos<sup>TM</sup> is prepared as bisacetoxymethyl esters with N-(2-methoxyphenyl)iminodiacetate protected acetoxymethyl esters. Cellular esterases deprotect the metal sensor and based on internal pH, the phenol equilibrates to the active dye form. Photoinduced electron transfer (PET) from the amino quenches the fluorescence, as shown as electron density traveling up the “molecular wire” (red). Thallos<sup>TM</sup> in the presence of a metal ion, ( $Tl^+$ ) will quench the fluorescein fluorophore and permit an increase in fluorescence.

## Xanthene Based Fluorophores: Fluorescein and Rhodamine

The process of fluorescence is a molecule absorbing a photon from the ground ( $S^0$ ) to the excited singlet state ( $S^1$ ), as shown in the Jabloński diagram in Figure 1.6. Fluorescence results a release of a photon ( $h\nu$ ) as the fluorophore returns to the ground  $S^0$  from the excited  $S^1$ . Wavelength emission ( $\lambda_{\text{max}}$ ) is typically shifted red compared to the absorbance wavelength ( $\lambda_{\text{abs}}$ ), is known as Stoke's shift, due to interactions

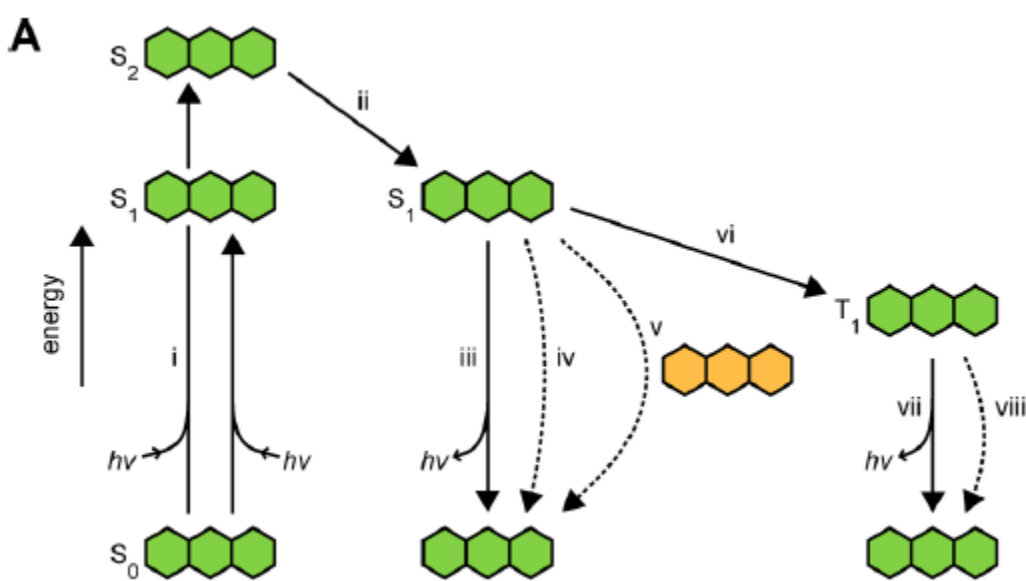


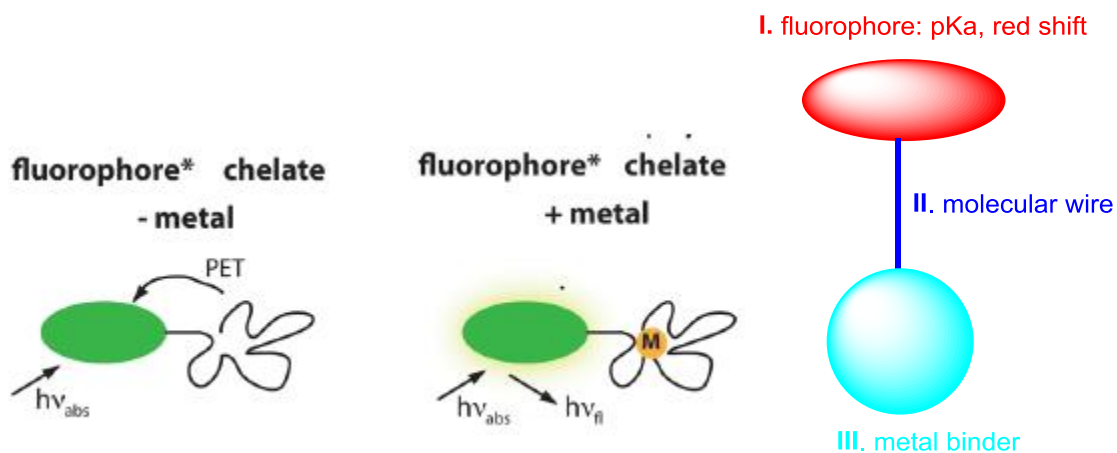
**Figure 1.6.** Taken from Lavis and coworkers<sup>14</sup> i) A photon is being absorbed to give the excited singlet state. ii) Conversion into the singlet state iii) Fluorescence is the relaxation (release of light) of the singlet into the ground state. iv) Describes non-radiative decay (loss as heat) and v) Förster resonance energy transfer vi) Intersystem crossing to triplet state ( $T^1$ ) vii) Phosphorescence and viii) non-radiative decay.

of the excited molecule with surrounding solvent reorganization. Absorption of the molecule is based on the  $\lambda_{\text{abs}}$  and the extinction coefficient ( $\epsilon$ ), which is defined by how strongly a molecule can absorb light. Quantum yield ( $\phi$ ) is a ratio of photons going into the molecule over photons leaving. For example, fluorescein, a xanthene based fluorophore, has an efficient quantum yield ( $\phi = 0.86$ , ideally 1.00), typically absorbs blue light (490 nm) and emits green light (510 nm)<sup>14</sup> with an extinction coefficient of  $9.0 \times 10^4 \text{ M}^{-1} \text{ cm}^{-1}$ . These properties are a part of many

contributing factors that makes xanthene fluorophores one of the most widely utilized fluorophore in research.

### ***Photoinduced Electron Transfer***

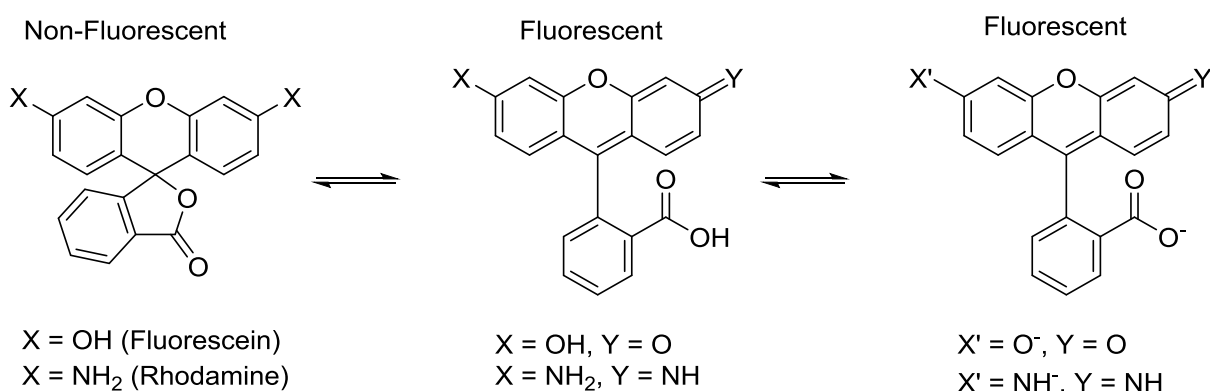
Fluorescence properties of a fluorophore can be modulated by the metal and the fluorophore, known as photoinduced electron transfer (PET)<sup>7</sup>. In the absence of a metal ion, a separation of charge forms on the excited fluorophore and this competes with fluorescence emission. PET then gives rise to a more efficient relaxation pathway ( $S^1$  to  $S^0$ , energy loss through non-radiative decay) than fluorescence and decreases the optical output of the fluorophore. When a metal ion is bound, this disrupts the PET relaxation pathway and increases the quantum yield (Figure 1.7). This tuning of electron density with the choice of fluorophore, linker (molecular wire) and the metal binder can be achieved with electron withdrawing and donating groups that alter the efficiency of the PET



**Figure 1.7.** (Left) In the absence of a metal, PET offers a more efficient relaxation pathway and decreases the optical output of the fluorophore. (Middle) When chelated to a metal ion, the PET effect is disrupted and increases the quantum yield. (Right) Schematic of a metal sensor with a (I) Fluorophore, (II) molecular wire and (III) metal binding unit. Modification of these three parts can tune the PET effect adventitiously.

quenching effect. The depth of small molecule dyes for fluorescence assay is very broad and there are several excellent reviews and resources on the subject<sup>15</sup>. The focus of this dissertation work is

primarily xanthene scaffolds, which hold a unique open-close like switch to the fluorescence. Fluorescein and rhodamine both share a common spirocyclic core scaffold, xanthene, which undergoes an open (fluorescent, quinoid or aza-quinoid) close (non-fluorescent, spiro-lactone) equilibrium. This equilibrium is dependent on  $pK_a$ <sup>16</sup> by introducing an electron withdrawing group adjacent to the aniline or phenol (e.g. F, Cl, etc). This equilibrium can also be controlled by “protecting”, or by alkylating (ether, amino) or acetylating (ester, amide), which forces the xanthene into the closed, non-fluorescent form (Figure 1.8). A large number of fluorescent dyes have been prepared in this protected or masked manner with various trigger groups such as photo-activating releasing groups<sup>17</sup>, enzyme selective cleavage<sup>18</sup> and small-molecule sensors<sup>19</sup>.

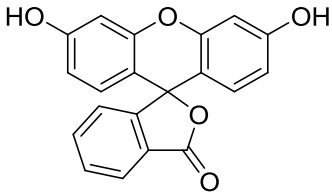
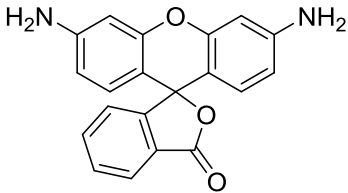
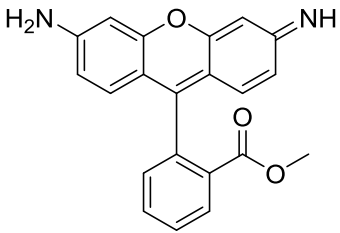
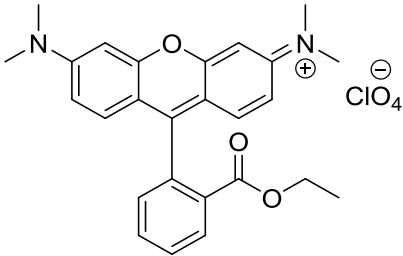


**Figure 1.8.** Xanthene fluorophore scaffold in equilibrium between closed-lactone (off) and open quinoid (on). Dianion species reported as the most fluorogenic<sup>16</sup>.

Dye properties have been exploited based on  $pK_a$  of the functional groups, for example, rhodamine which carries a positive charge (at  $pH < 6.0$ ) when localized in the mitochondrion<sup>20</sup>. In this manner, rhodamine may be used as a dye that is specific for tracking membrane potential in mitochondria. Rhodamine will accumulate in the mitochondria due to its positive charge at cellular  $pH$  and this high concentration will cause a self-quenching (or decrease in fluorescent signal). When the membrane potential is disrupted, rhodamine will then exit the mitochondria and the

increase in fluorescence is detected. Traditionally, the synthesis of xanthene scaffolds consisted of heating of phthalic anhydride with resorcinol under strong acidic conditions (typically condensation with  $\text{CH}_3\text{SO}_3\text{H}$ )<sup>21</sup>. The addition of any functionality to the phenol or anhydride would result in a mixture of isomers that would require careful conditions to separate<sup>22</sup>. Ways around this issue have been proposed synthetically, including Pd cross-coupling chemistry with Buchwald-Hartwig<sup>23</sup> by conversion of an aryl triflate into an aniline. Despite the recent advances in dye chemistry, the coupling of functionality (metal sensor, protein tag) to the fluorescent molecule can prove to be synthetically challenging.

**Table 1.1. Commonly Used Xanthene Based Dyes Structures and Properties<sup>15</sup>**

Structure	Name	$\lambda_{\text{abs}}$ (nm)	$\lambda_{\text{ems}}$ (nm)	$\phi$	$\epsilon(\text{M}^{-1}\text{cm}^{-1})$	Usage
	Fluorescein	490	510	0.92	$9.0 \times 10^4$	Microscopy  Industrial  Applications
	Rhodamine 110	496	520	0.86	$8.3 \times 10^4$	Microscopy  Spectroscopy
	Rhodamine 123	507	529	0.90	$7.5 \times 10^4$	Labeling mitochondria
	Tetramethyl rhodamine ethyl ester perchlorate (TMRE)	549	574	NA	$10.9 \times 10^4$	Mitochondria

### *Development and Use of Thallium Flux Assay*

The work of the late Roger Tsien pioneered cell permeating fluorescent dyes<sup>24</sup> that chelate mono- or divalent cations such as  $\text{Ca}^{2+}$ . Before the development of the Thallium ( $\text{Tl}^+$ ) flux assay, measuring the activity of  $\text{K}^+$  was traditionally done with electrophysiology, rubidium ( $\text{Rb}^+$ ) flux assays or voltage sensitive dyes that measure the change in membrane potential<sup>13</sup>. The utility of fluorescent dyes as indicators for activity was attractive but the only dye at the time that directly bound potassium was benzofuran isophthalate (PBFI)<sup>25</sup>, which was not amenable to the screening of large libraries in a high-throughput manner due to their overlap in excitation (near UV) with many small molecule scaffolds. Similar to  $\text{Rb}^+$ ,  $\text{Tl}^+$  is a monovalent cation that is also permeable to potassium channels<sup>26</sup>. The use of  $\text{Tl}^+$  as a size surrogate for  $\text{K}^+$  channels was promising but the low solubility of  $\text{Tl}^+$  ions in assay buffer ( $\text{TlCl}$  in water, 5mM) required the exclusion of chloride ion to prevent salt precipitation.

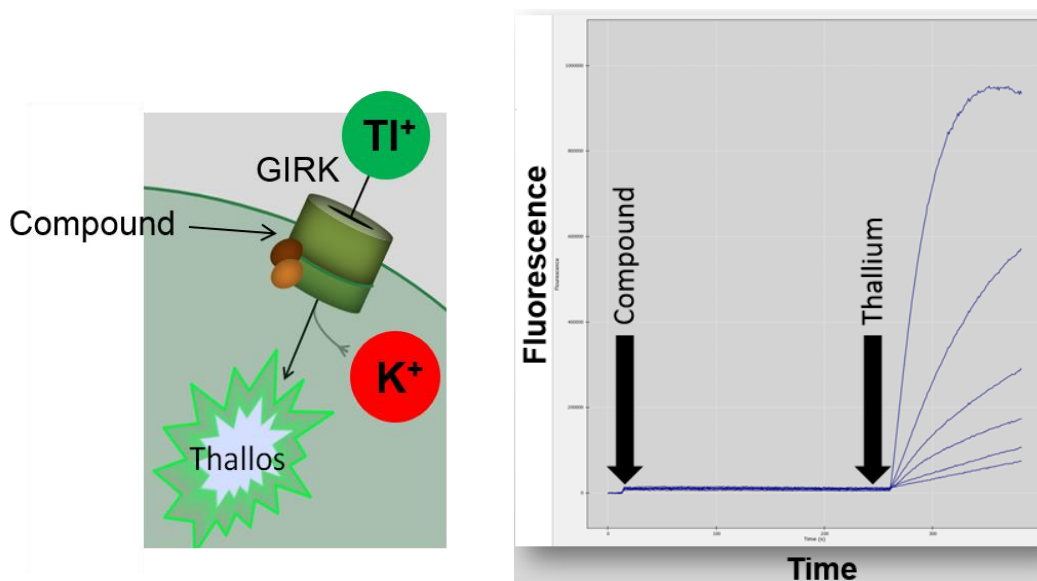


**Figure 1.9.** GIRK channels permit the influx of  $\text{Tl}^+$  ions when activated by a compound. Thallos<sup>TM</sup> dye is incubated in the cells and dequenched (more fluorescent) in the presence of  $\text{Tl}^+$ . Plot shows raw traces of increasing fluorescence over time in concentration response curves (CRC)

A common metal sensing dye utilized the benzothiazolylcoumarin (BTC) scaffold was found to detect  $Tl^+$  ions. The use of FluoZin, originally a  $Zn^{2+}$  dye, presented dequenching metal sensing upon the addition of  $Tl^+$  with the N-(2-methoxyphenyl)iminodiacetate chelation subunit (Figure 1.6). The addition of  $Tl^+$  dequenched the fluorescence and presented a brighter form of the dye. Following this work, many authors reported the dye trapping properties of the cellular uptake and removal of the esterase sensitive acetoxymethyl (AM) ester pendant groups<sup>5</sup>.



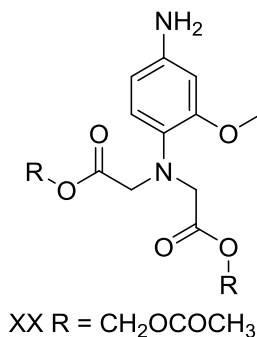


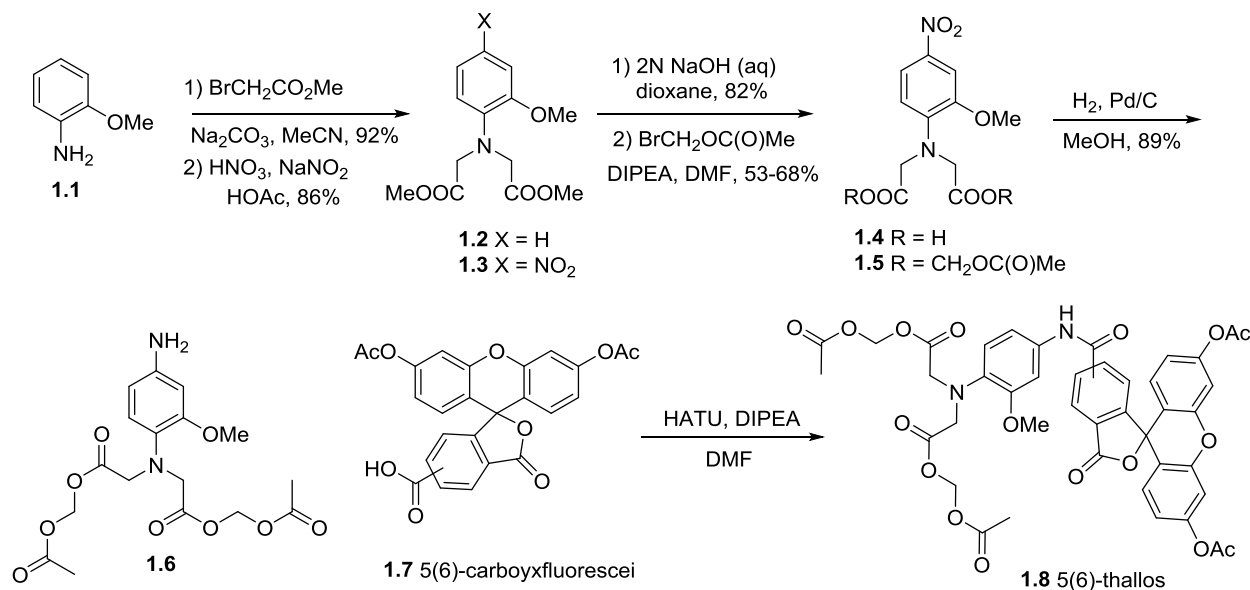
**Figure 1.10.** N-(2-methoxyphenyl)iminodiacetate chelation subunit based off of BAPTA Ca<sup>2+</sup> and Zn<sup>2+</sup> sensors. Cellular esterases remove acetoxymethyl (AM) esters to reveal di-carboxylate, which is considered to contribute to a PET dequenching effect.

The requirement of a metal sensor that was more sensitive to concentrations of Tl<sup>+</sup> drove towards the development of Thallos<sup>TM</sup>, a BAPTA-AM hybrid linked to a xanthene fluorophore. While high-throughput screening of potassium channel activity has certainly benefited from Tl<sup>+</sup> sensitive dyes, there are drawbacks, such as the need higher Tl<sup>+</sup> affinity dyes or a way of detecting localized flux changes.

### *Thallos<sup>TM</sup> Dye and Synthesis*

Based on xanthene scaffolds, a large number of fluorescein based dyes have been functionalized for specific tasks, for example, a Tl<sup>+</sup> sensing chelation moiety. Tl<sup>+</sup> sensing dyes are based on a diacetate fluorescein scaffold with a metal chelation moiety attached through an amide bond. These dyes must diffuse as esters through the cellular membrane of cells expressing GIRK channels, release under the action of endogenous lipases and fluoresce with influx of Tl<sup>+</sup> ions that bind to the metal sensing carboxylate group. The synthesis of Thallos<sup>TM</sup> starts with commercially available *o*-methoxy aniline and under basic conditions, alkylate with methyl bromoacetate build the acetoxymethyl (AM) ester chelation unit. Nitration proceeds smoothly to the para position and

then treatment with strong base gives the bis-acid. Alkylation with bromomethyl acetate prepares the AM esters and a clean reduction with Pd/C reveals the aniline. HATU coupling with bis-acetylated mixture of 5- and 6-carboxyfluorescein gives Thallos™ at comparable yields.



**Scheme 1.1.** Synthesis of Fluorescein-based Thallos™ with Metal Chelating Unit (Special thanks to Dr. Kwangho Kim).

### 1.3 Prior Small Molecule GIRK Activators (or Inhibitors)

As discussed in the introduction GIRK channels have been implicated as therapeutic targets but largely remain unvalidated due to a lack of selective and potent small molecule modulators. Before the work of Lindsley and Weaver, there were few GIRK modulators that had potency below the micromolar range and were selective for GIRK channels. One example, NIP-142, a benzopyrane was found to inhibit atrial GIRK but also inhibited other cardiac potassium channels<sup>27</sup>.

### ***Development of the Selective and Potent GIRK Activator, ML297***

The discovery of small molecules that selectively activate and inhibit GIRK channels is essential for assessing their potential as therapeutic targets. In addition, development of molecules that are selective for neuronal GIRK1/2 channels may limit side effects caused by the activation of GIRK 1/4 in cardiac tissue. Prior to the work of Weaver, Lindsley, and others, there was a current lack of selective and potent small molecule activators except for Narigin, a known GIRK activator (>100  $\mu\text{M}$ ) and ethanol, found to be an activator ( $\text{EC}_{50} > 100 \text{ mM}$ ), but with poor selectivity and low potency<sup>28</sup>. During the course of screening for mGlu<sub>8</sub> small molecule modulators, Weaver, Lindsley and coworkers identified small molecules that modulate GIRK channels directly. Lead optimization resulted in the GIRK1/2 and GIRK1/4 activator urea 1 VU0456810 (ML297)<sup>9</sup>.

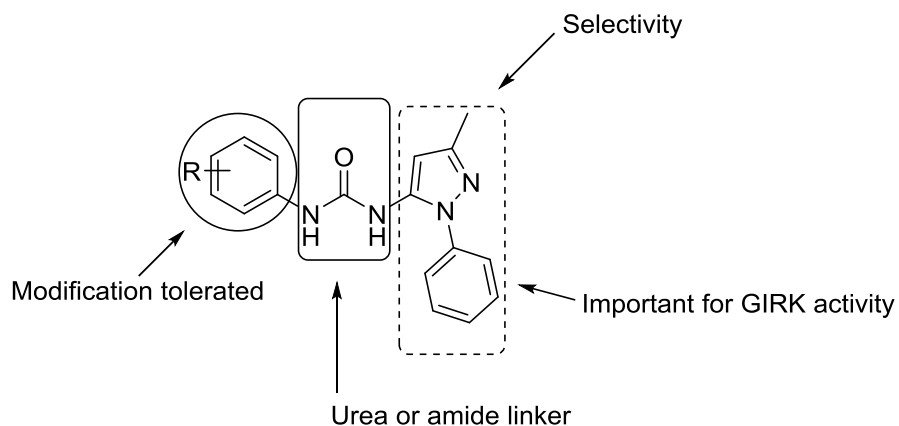


**Figure 1.11.** Functionalization around initial GIRK channel hit VU0032230. ML297 SAR focused primarily around the “western” aryl and the requirement for an amide or urea linker. Later, probes were synthesized to better understand the importance of the eastern phenyl and heterocycle substitution off of the C3 position.

As summarized in Figure 1.11 lead optimization was conducted around a pyrazole urea by variation of the N-aryl group, urea linker and N-arylpyrazole. A number of urea derivatives were produced with a variety of activity on GIRK1/2 found by probing electron withdrawing and releasing groups on the “Western” phenyl. Halogens were well tolerated in the *meta* and *para*

positions where *ortho* substitution were inactive on the GIRK channel. Electron releasing groups such as methoxy and thioether were also tolerated in those positions but with lower potency reported than the electron withdrawing groups. Following up on these reports, the urea nitrogens were methylated to determine if available hydrogen bonds were essential for activity. The methylated urea probe was determined to be inactive, suggesting hydrogen bonding or sterics had a role in binding. Through chemical optimization, ML297 emerged with a very favorable potency ( $EC_{50}$  GIRK1/2 = 160nM) reported for a GIRK1 containing GIRK activator.

Key to this GIRK activator probe was the selectivity for GIRK1 containing GIRK channels, in addition to being inactive on typical voltage gated  $K^+$  ion channels such as  $K_v7.4$ , inward rectifier  $K_{ir}2.1$  and only partially inhibiting hERG with low potency ( $IC_{50} \sim 10\mu M$ ). To fully address ML297's selectivity for GIRK1 containing GIRKs, a radioligand binding assay panel failed to show any significant activity on 68 targets with the exception of three receptors (5-HT<sub>2b</sub>,  $\sigma 1$  and

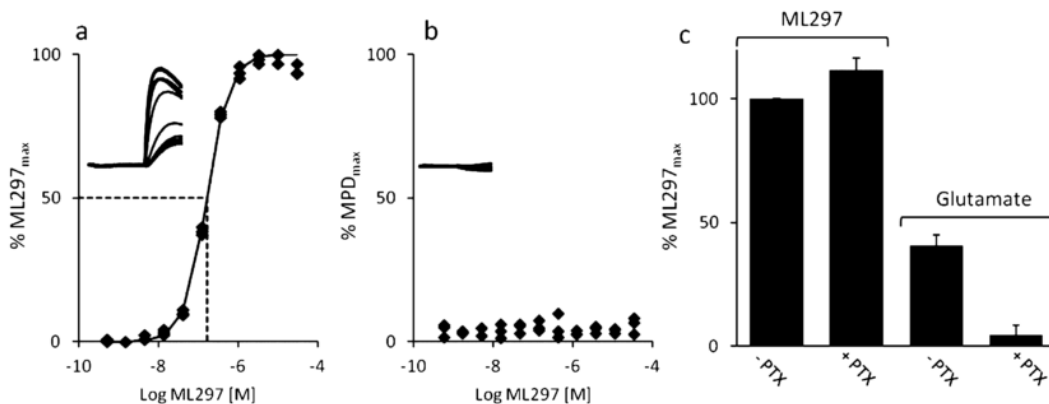


**Figure 1.12.** a) Raw trace and slopes plotted for CRCs generated from ML297 on GIRK1/2 containing cells. b) No activity was reported for GIRK2 containing GIRK channels. c)  $G_{i/o}$  Pertussis (PTX) sensitive G proteins in the presence of PTX were exposed to ML297 and positive control glutamate. ML297 still activated GIRK channels where glutamate did not.

GABA<sub>A</sub>, ~ 10 $\mu$ M). To follow up on selectivity with GABA<sub>A</sub> receptors, whole cell voltage-clamp studies were performed to confirm that ML297 did not demonstrate any activation of GABA-invoked currents. G<sub>i</sub> coupled GPCRs are sensitive to pertussis toxin (PTX) treatment and will inactivate the  $\alpha_i$  subunit by ADP-ribosylation. In the presence of PTX, ML297 still was able to stimulate activity demonstrated by Tl<sup>+</sup> flux assay. These, and the absence of binding from the results of the radioligand assay was used to conclude that ML297 is acting directly on the GIRK channel to activate it.

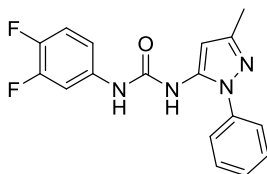


**Figure 1.13.** GIRK1 containing GIRK ion channel modulator, VU0456810 (ML297).

The potential for off-target effects, especially for anti-arrhythmic therapeutics was addressed by the development of the first selective and potent GIRK 1 containing GIRK modulator, **ML297** (Figure 1.13).

#### 1.4 GIRK Selectivity SAR to Development of “Sulfonamides”

Findings with GIRK1 containing GIRK selectivity opened the door to further SAR investigation on GIRK1 selective activation. ML297 had allowed some flexibility around the urea scaffold to probe the alternate substituents on the aryl, heteroaryl alternatives and varying aliphatic groups located at the C3 position of the pyrazole. This was not the case with 2-methylcyclopropyl, as there was a strong preference as a GIRK1/2 activator and inactive on GIRK1/4. The only case of dual GIRK1/2 and GIRK1/4 activation was the ML297 similar, 3,4-difluoro analog, in which

the pyrazole was commercially provided, implied a racemic nature to the 2-methylcyclopropyl. Further investigation into the stereoselective nature of GIRK1/2 and GIRK1/4 selectivity can be found in Chapter 3.

## 1.5 Statement of Dissertation

The work in the following chapters outlines the development and power of molecular tools for use in biological investigation. Prior to 2012, there was only a handful of molecular probes that would selectively activate GIRK channels. The expansion of this library to include various urea and amide derivatives has exponentially increased our understanding of these widely distributed ion channels. We have quickly begun to assess GIRK1 selectivity with amide or urea scaffolds (Chapter 2) and GIRK1/2 versus GIRK1/4 selectivity with enantiomeric preference (Chapter 3). Lately, a dynamic exploration into the world of selectively deprotected dyes for use in GIRK  $TI^+$  flux assay has utilized an exogenous enzyme in an engineered cell line (Chapter 4). By developing and optimizing molecular tools to overcome high background signal, we can probe how GIRK channel activity affects cell function. Through these investigations we can learn about modulation of GIRK channels to ultimately set the stage for better pharmaceutical tools to treat debilitating neurological disorders.

Parts of this chapter are reprinted with permission from Kaufmann, K.; Romaine, I.; Days, E.; Pascual, C.; Malik, A.; Yang, L.; Zou, B.; Du, Y.; Sliwoski, G.; Morrison, R. D.; Denton, J.; Niswender, C. M.; Daniels, J. S.; Sulikowski, G. A.; Xie, X.; Lindsley, C. W.; Weaver, C. D., ML297 (VU0456810), the First Potent and Selective Activator of the GIRK Potassium Channel, Displays Antiepileptic Properties in Mice. *ACS Chem. Neurosci.* **2013**, *4*, 1278-1286.

**CHAPTER 2**  
**DISCOVERY AND SAR OF A NOVEL SERIES OF GIRK1/2 AND GIRK1/4**  
**ACTIVATORS:**  
**“SULFONAMIDE SERIES”**

**2.1 Introduction**

The G protein-gated Inwardly Rectifying Potassium ( $K^+$ ) (GIRK) channels are a family of inward-rectifying potassium channels also known as the Kir3 family, whose physiological role is to modulate the excitability of the various cell types in which they are expressed<sup>29</sup>. Four GIRK channel subunits are expressed, as either homo- or heterodimers, in mammals: GIRK1 (Kir3.1), GIRK2 (Kir3.2), GIRK3 (Kir3.3) and GIRK4 (Kir3.4). GIRK1–GIRK3 are the predominant subunits in the CNS, with GIRK4 expressed at low levels. Multiple lines of evidence support important roles for GIRK in a variety of physiological processes including the control of heart rate and electrical excitability in a variety of neuronal populations, leading to postulates that GIRK channel modulation as a potential therapeutic approach to indications including pain, epilepsy, and reward/addiction. However, a complete lack of selective and effective GIRK small molecule activators has prevented further validation for GIRK channel modulation as a therapeutic strategy. Prior to the work described here the only compounds known to activate GIRK channels were ethanol and >100 millimolar concentrations and more recently naringin has been identified as a GIRK activator; however, the reported  $EC_{50}$  is in excess of 100  $\mu M$ <sup>30</sup>.

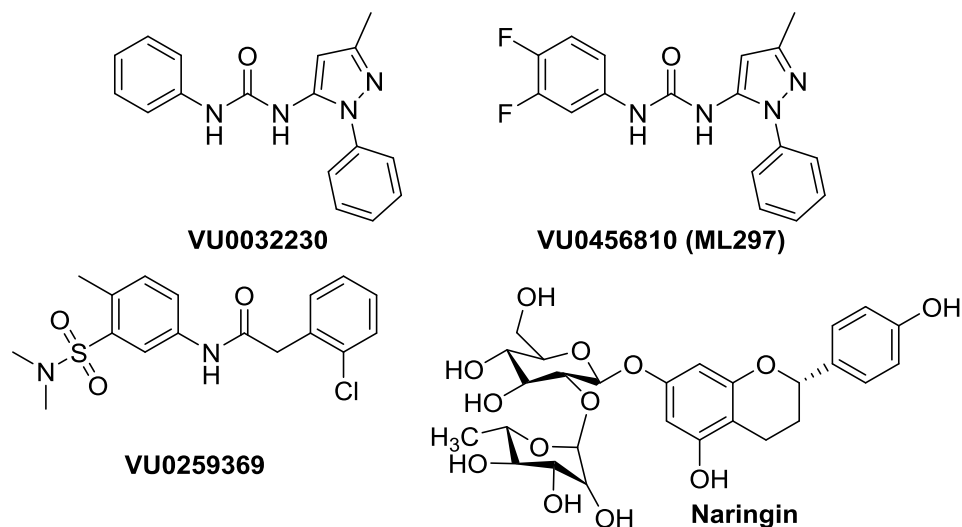


**Figure 2.1** GIRK1 containing GPCR ion channel modulators, original screening hit VU0032230, SAR study probe, VU0456810 (ML297), “sulfonamide” scaffold modification to amide, VU0259369, and Naringin a known GIRK activator (>100  $\mu$ M).

Based on the lack of useful chemical matter in the field, Weaver and co-workers sought to develop a suite of channel selective small molecule GIRK modulators. Lead compounds were identified by mining high-throughput screening data from an mGlu8 (Metabotropic glutamate receptor 8) screening project. In this screen, mGlu8 modulators were identified via a  $\text{TI}^+$  flux-based readout of GIRK1/GIRK2.11 channels. Once hits for mGlu8 were identified, multiple hits that remained were assumed GIRK activators with potencies ranging from  $\sim 1$   $\mu\text{M}$  to 10  $\mu\text{M}$ . Two of the most promising leads based on activity and chemical tractability were urea VU0032230 and sulfonamide VU0259369 (Figure 2.1). We recently reported on optimization of the urea series starting from VU0032230, leading to the first selective ( $\sim 10$ -fold vs GIRK1/4, inactive on non-GIRK1 containing GIRKS and inactive on other  $\text{K}^+$  channels) GIRK1/2 activator VU0456810 (aka ML297). Importantly, ML297 was centrally penetrant and demonstrated anti-epileptic properties in mice via GIRK1/2 activation.



## 2.2 Identification and Synthesis of Sulfonamide Analogs

Sulfonamide VU0259369 proved to act as a dual GIRK1/2 and GIRK1/4 activator showing potency of  $EC_{50}$  1.1  $\mu$ M on GIRK1/2, efficacy (100%) and  $EC_{50}$  1.1  $\mu$ M on GIRK1/4, efficacy (104%). Activity against other GIRK channels was  $>10$   $\mu$ M, respectively<sup>31</sup>. A generalized optimization strategy for sulfonamide '369 is shown in Figure 2.1. Our medicinal chemistry plan was to vary the Eastern arylsulfonamide and Western aryl groups. The resulting SAR would then be combined with modifications of the amide linker with the overall objective of increasing potency, selectivity and favorable *in vivo* properties.<sup>32</sup>.

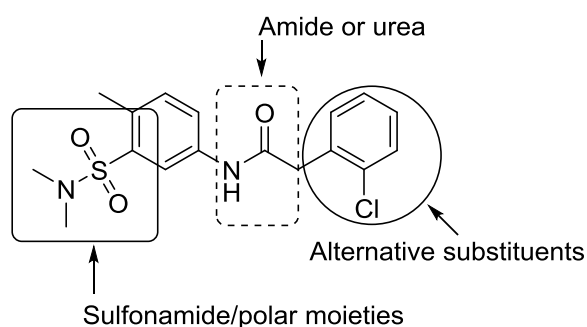
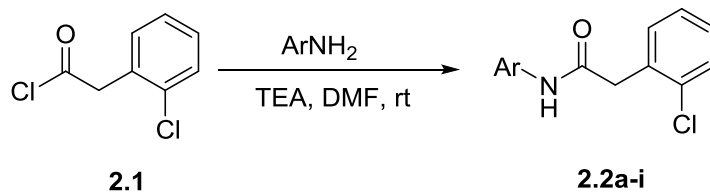


**Figure 2.2** Optimization plan for synthesis of amide and urea derivatives.

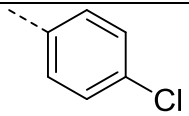
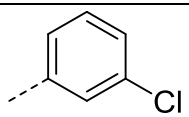
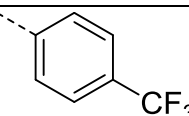
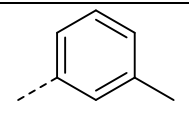
In short order, over 100 analogs were synthesized and analyzed using  $TI^+$  flux assays on GIRK1/2 and GIRK1/4 expressing cells. A series of analogs of VU '369 where the Western arylsulfonamide was varied is summarized in Table 2.1. Within this series the SAR proved to be shallow with  $>50\%$  of the analogs displaying no GIRK activity. The iterative parallel synthesis effort, surveying modifications to the parent VU '369, afforded few actives. Of the actives, bromine effectively replaced the chlorine atom, in contrast deletion of the methyl group, maintained activity but with diminished potency on GIRK1/4 compared with GIRK1/2. Moving

the halogen of **2.4b** from the 2- to the 4-position, also led to a diminution in potency at both GIRK1/2 and GIRK1/4. Figure 2.3 highlights the GIRK1/2 and GIRK1/4 concentration response curves for **2.4b** and **2.4a**. All attempts to replace or modify the N,N-dimethyl sulfonamide group, incorporation of heterocycles or modification of the linker moiety led to a complete loss of GIRK activity. Fortunately, the fragment libraries proved more productive (Table 2.2).

**Tables 2.1** GIRK activity of VU0259369 analogs varied within the Western arylsulfonamide

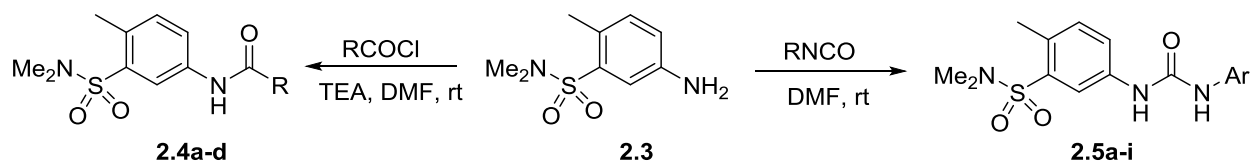


Compound	Ar	GIRK1/2 EC <sub>50</sub> ( $\mu\text{M}$ )	GIRK1/4 EC <sub>50</sub> ( $\mu\text{M}$ )
<b>2.2a</b>		>10	>10
<b>2.2b</b>		5.9	2.7
<b>2.2c</b>		>10	7.8
<b>2.2d</b>		>10	>10
<b>2.2e</b>		>10	0.24

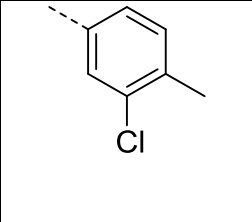
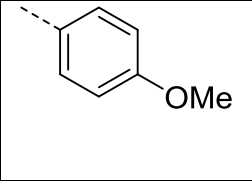
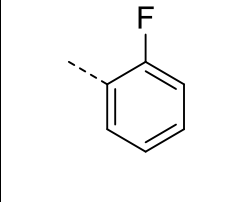
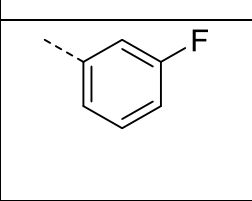
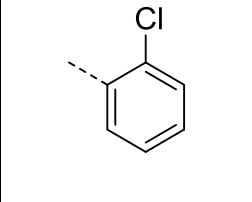
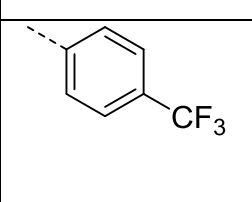
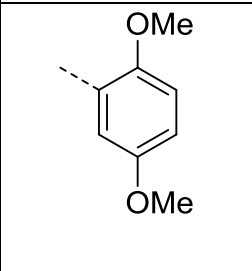
<b>2.2f</b>		>10	>10
<b>2.2g</b>		>10	1.8
<b>2.2h</b>		>10	2.1
<b>2.2i</b>		>10	>10

As summarized in Table 2.2 we held the required 5-(N,N-dimethylsulfonamide)-4-methylphenyl group constant, and prepared libraries of amide **2.4** and urea congeners **2.5**.

**Tables 2.2.** GIRK activity of VU0259369 analogs varied within the Eastern arylsulfonamide.



Compound	R/Ar	GIRK1/2 EC <sub>50</sub> (μM)	GIRK1/4 EC <sub>50</sub> (μM)
<b>2.4a</b>		1.4	1.6
<b>2.4b</b>		3.3	1.6
<b>2.4c</b>		2.3	2.2
<b>2.4d</b>		3.6	5.2
<b>2.5a</b>		1.4	3.9
<b>2.5b</b>		3.3	2.8

<b>2.5c</b>		2.9	6.2
<b>2.5d</b>		1.7	5.6
<b>2.5e</b>		3.9	7.8
<b>2.5f</b>		1.1	1.8
<b>2.5g</b>		2.7	6.8
<b>2.5h</b>		1.5	>10
<b>2.5i</b>		>10	>10

### 2.3 GIRK Activator CRCs Measuring TI<sup>+</sup> Flux

The amide congeners **2.4a-d** proved to be uniformly inactive, with the exception of a few C4- to C8-aliphatic amide congeners; however, the GIRK1/2 EC<sub>50</sub>s were in the 4–10 μM range with modest efficacies (23–91%, if ML297 = 100% activity). In contrast, the urea congeners **2.5a-j** possessed robust SAR, low micromolar potencies, high efficacy (71–120%) and engendered a slight preference for GIRK1/2 (Table 2.2). This effort provided dual GIRK1/2 and GIRK1/4 activators such as **2.5b**, **2.5f** and **2.5j**, with a range of full to partial efficacies. This is an important finding, as it is not yet clear if a full or partial GIRK activator will be more ideal in terms of *in vivo* efficacy, safety and tolerability, and having a range of chemical tools will enable these issues to be addressed. Analogs such as **2.5h**, with a 4-CF<sub>3</sub> moiety, proved to be selective for GIRK1/2 (EC<sub>50</sub> = 1.5 μM) over GIRK1/4 (EC<sub>50</sub> >10 μM), but with low efficacy (26%). Electron rich congeners, such as **2.5i**, were uniformly inactive at both GIRK1/2 and GIRK1/4.

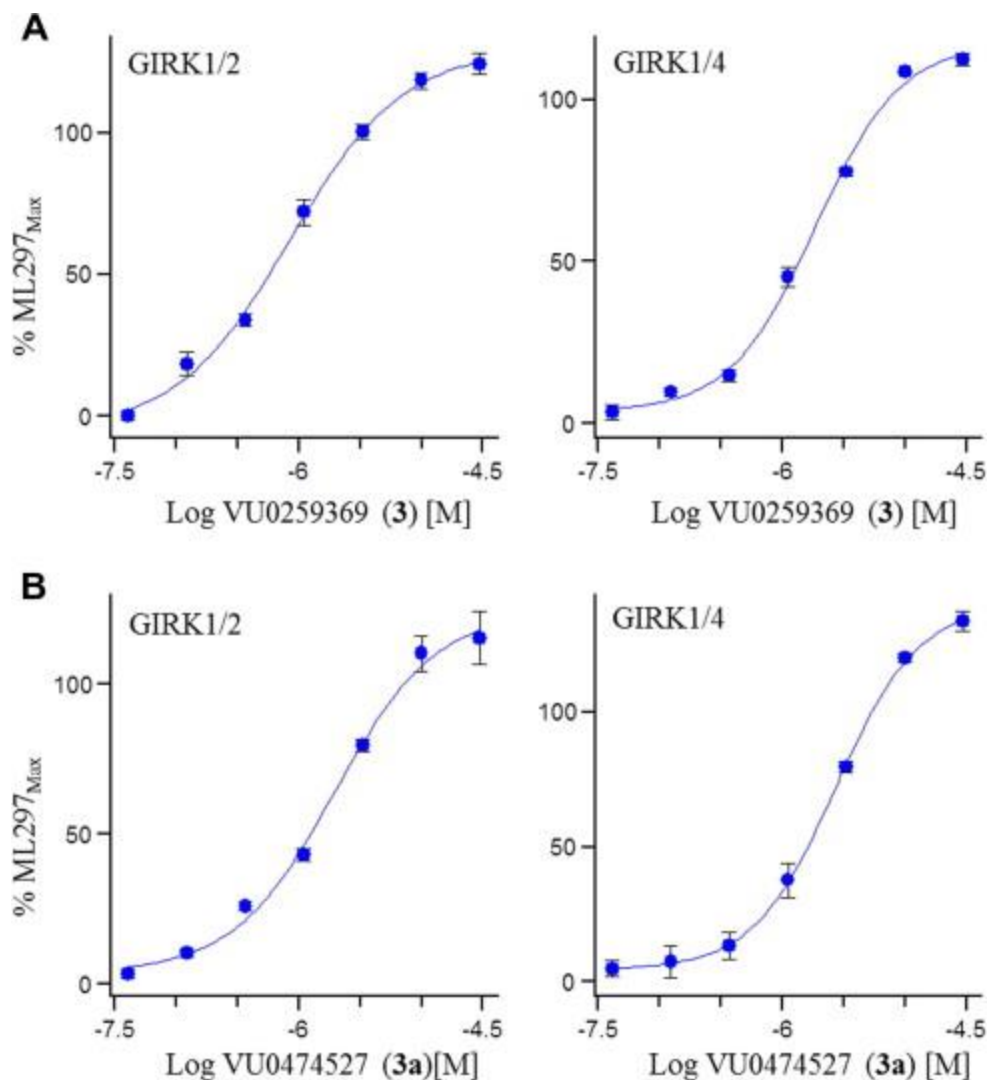


**Figure 2.3.** GIRK activator concentration response curves (CRC) measuring  $\text{Ti}^+$  flux. (A) GIRK1/2 ( $\text{EC}_{50} = 1.1$   $\mu\text{M}$ , 110%) and GIRK1/4 ( $\text{EC}_{50} = 1.1$   $\mu\text{M}$ , 104%) CRCs for the HTS hit **2.4b** (Shown as **3**); (B) GIRK1/2 ( $\text{EC}_{50} = 1.4$   $\mu\text{M}$ , 108%) and GIRK1/4 ( $\text{EC}_{50} = 1.6$   $\mu\text{M}$ , 114%) CRC for related analog **2.4a** (Shown as **3a**).

In analogs **2.2a-i**, where the eastern 2-(2-chlorophenyl)acetamide portion was held constant and diverse anilines were surveyed, interesting SAR emerged (Table 2.1). SAR was very shallow, and unlike analogs **2.5**, all analogs **2.2** were devoid of activity at GIRK1/2, affording GIRK1/4 preferring activators. A 4-Cl,3-CF<sub>3</sub>phenyl amide derivative **2.2e**, was a very potent GIRK1/4 activator ( $\text{EC}_{50} = 0.24$   $\mu\text{M}$ ), but displayed weak, partial activation (17%) and was inactive on GIRK1/2. Other electron withdrawing substituents in the 3-position, such as Cl (**2.2g**)



or CF<sub>3</sub> (**2.2h**), were selective, partial GIRK1/4 activators; interestingly, electron donating substituents in the 3-position, such as **2.2i**, were inactive at both GIRK1/2 and GIRK1/4. None of the analogs **2.2** or **2.5** were active at non-GIRK1 containing GIRK channels, further enabling them as valuable tool compounds to better understand selective GIRK channel activation (see Fig. 2.4).

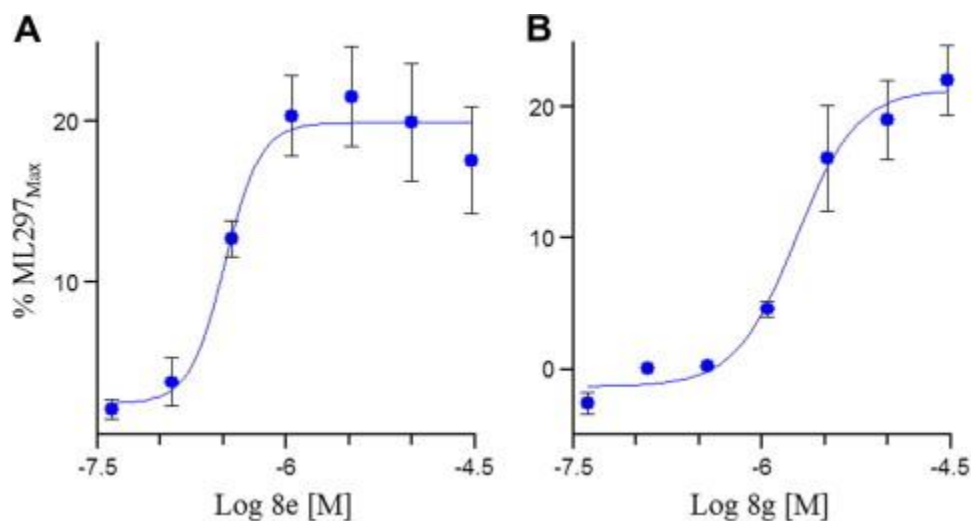


**Figure 2.4.** GIRK activator concentration response curves (CRC) measuring TI<sup>+</sup> flux. (A) GIRK1/4 (EC<sub>50</sub> = 0.24 μM, 17%) CRC for **2.2e** (Shown as **8e**); (B) GIRK1/4 (EC<sub>50</sub> = 1.8 μM, 22%) CRCs for **2.2g** (Shown as **8g**).

## 2.4 Conclusion

In summary, we have described the synthesis and one of the first accounts of SAR for a novel series of rarely described GIRK activators, indicating that GIRK activators can be identified from HTS campaigns and optimize their scaffold to improve activity. SAR proved shallow, and an iterative parallel synthesis approach provided little improvement in terms of potency or efficacy at GIRK1/2 or GIRK1/4. Instead a fragment library approach afforded a diverse array of GIRK activators that included dual GIRK1/2 and GIRK1/4 activators, GIRK1/2 preferring activators and GIRK1/4 selective activators possessing a wide range of efficacy (from weak partial to full activation), and devoid of activity at non-GIRK1-containing GIRK channels. Additional characterization and refinements are in progress and will be reported in due course

## 2.5 Experimental

### *General Experimental*

All glassware used for reactions was flame dried under vacuum. All reagents and solvents were commercial grade and purified prior to use when necessary. All reactions were performed under argon atmosphere unless otherwise stated. Diethyl ether (Et<sub>2</sub>O) and dichloromethane (CH<sub>2</sub>Cl<sub>2</sub>) were dried by passage through a column of activated alumina using an MBraun MB-SPS dry solvent system. Tetrahydrofuran (THF) was distilled from sodium with benzophenone as indicator prior to use.

Reactions were monitored by analytical thin-layer chromatography performed on Analtech silica gel GF 250 micron plates. The plates were visualized with UV light (254 nm) and either potassium permanganate, ceric ammonium molybdate, or p-anisaldehyde followed by charring on a hot-plate. Flash chromatography utilized 230-400 mesh silica gel (SiO<sub>2</sub>) from Sorbent Technologies or Silica RediSep Rf flash columns on a CombiFlash Rf automated flash chromatography system. Solvents for extraction, washing and chromatography were HPLC grade.

Nuclear magnetic resonance (NMR) spectra were acquired on either a 300 MHz Bruker DPX-300 FT-NMR, a 400 MHz Bruker AV-400 FT-NMR, or 500 MHz Bruker DRX-500 FT-NMR Spectrometer at ambient temperature. <sup>1</sup>H and <sup>13</sup>C NMR data are reported as values relative to CDCl<sub>3</sub>. <sup>1</sup>H chemical shifts are reported in δ values in ppm. Data are reported as follows: chemical shift, multiplicity (s = singlet, d = doublet, t = triplet, q = quartet, br = broad, m = multiplet), integration, coupling constant (Hz). <sup>13</sup>C chemical shifts are reported in δ values in ppm. Low resolution mass spectra were obtained on an Agilent 1200 series 6130 mass spectrometer with electrospray ionization. High resolution mass spectra were recorded on a Waters Q-TOF API-US. Analytical HPLC was performed on an Agilent 1200 series with UV detection at 214 nm and 254

nm along with ELSD detection. Preparative HPLC was conducted on a Gilson 215 Liquid Handler HPLC system using Gemini-NX 50 x 20 mm column.

### ***Synthesis of Urea Library***

To a solution of 5-amino-N,N,2-trimethylbenzenesulfonamide (**2.3**) (15 mg, 0.07 mmol, 1.0 equiv) in DMF (1.0 mL) was added an isocyanate (0.07 mmol, 1.0 equiv) at rt. After 12 h, the reaction was purified by reverse phase HPLC to afford the desired urea.

### ***Synthesis of Amide Library***

To a solution of 5-amino-N,N,2-trimethylbenzenesulfonamide (**2.3**) (15 mg, 0.07 mmol, 1.0 equiv) in DMF and TEA (4:1, 1.0 mL) was added the acid chloride (0.084 mmol, 1.1 equiv) at rt. Once the reaction was complete by LCMS, the reaction was filtered and purified by reverse phase HPLC to afford the desired amide.

### ***TI<sup>+</sup> Flux Assay Protocol***

Compounds were dissolved in DMSO, transferred to 384-well polypropylene plates, and serially diluted in DMSO using an Agilent Bravo (11-points, threefold dilutions). Serially diluted plates were dispensed to daughter plates using a Labcyte Echo555 and diluted to twofold over their target assay concentration with 20 mM HEPES-buffered (pH 7.4) Hanks Balanced Salt Solution (HBSS), hereafter referred to as Assay Buffer, using a Thermo Fisher Combi. Twenty-thousand HEK-293 cells/well stably transfected with the ion channel subunits of interest (e.g., GIRK1/GIRK2, GIRK1/GIRK4) were plated into 384-well, black-walled, clear-bottom, amine-coated coated plates in 20  $\mu$ L/well alpha-minimal essential medium (MEM) supplemented with 10% (v/v) fetal

bovine serum and incubated overnight in a 5% CO<sub>2</sub> incubator at 37 °C. Cell culture medium was removed from cell plates and replaced with 20 µL/well Assay Buffer. Twenty microliters/well of 0.5 µM of the Tl<sup>+</sup>-sensitive dye, Thallo<sup>TM</sup>-AM (TEFlabs, Austin TX) in Assay Buffer was added to cell plates. Cell plates were incubated for ~60 min at room temperature and then dye-loading solution was removed from cell plates and replaced with 20 µL/well Assay Buffer. Dye loaded and washed cell plates were transferred to a Hamamatsu FDSS 6000 and a double-addition protocol was initiated. After 10s, 20 µL/well of 20 µM test compound in 0.2% DMSO and Assay Buffer was added. After 4 min 10 µL/well of a 5× sodium bicarbonate-based Tl<sup>+</sup> stimulus buffer (20 mM HEPES pH 7.4, 135 mM NaHCO<sub>3</sub>, 2 mM CaSO<sub>4</sub>, 1 mM MgSO<sub>4</sub>, 5 mM glucose, 12 mM Tl<sub>2</sub>SO<sub>4</sub>) was added and 2 more minutes of data collection followed. Fluorescence data were collected at 1 Hz.

### ***Data Analysis***

Waveform signals (fluorescence intensity vs time normalized by dividing each fluorescence value (F) by the initial fluorescence value for each trace (F<sub>0</sub>)) were reduced to single values by subtracting the average normalized waveform from vehicle control wells from each wave on the plate followed by obtaining the slope of the change in fluorescence immediately after the addition of the Tl<sup>+</sup> stimulus. Slope values were normalized as a percentage of the slope obtained by the addition of a maximally effective concentration of the GIRK activator, ML297 (e.g., an efficacy value of 100% means that the compound's maximum apparent efficacy equals that of ML297). Curve fits for normalized slope values were obtained using a four-parameter logistic equation in the Excel add-in, XLfit.

Parts of this chapter are reprinted with permission from Ramos-Hunter, S. J.; Engers, D. W.; Kaufmann, K.; Du, Y.; Lindsley, C. W.; Weaver, C. D.; Sulikowski, G. A., Discovery and SAR of a novel series of GIRK1/2 and GIRK1/4 activators. *Bioorg. Med. Chem. Lett.* **2013**, *23*, 5195-5198.

## CHAPTER 3

### DISCOVERY OF A STEREO-SPECIFIC MODULATION OF GIRK1/2 AND GIRK1/4 CHANNELS:

### SYNTHESIS AND EVALUATION OF 2-METHYLCYCLOPROPYL ENANTIOMERS

#### 3.1 Introduction

G protein-gated inwardly rectifying potassium (GIRK) channels are part of a larger family of inwardly rectifying potassium channels ( $K_{ir}$ s) that regulate diverse biological processes.  $K_{ir}$ s regulate solute balance in the kidneys, cardiac rates and rhythms, and neuronal excitability. Specifically, dysfunction in GIRKs expressed throughout the central nervous system (CNS) have been linked to schizophrenia, pain perception, drug addiction, and epilepsy. Research into GIRK channels has been limited due to lack of selective and potent small molecule probes. Recently, a high throughput screen followed by SAR studies has led to the identification of a GIRK activator, VU810 (aka ML297) found to selectively activate GIRK1 containing channels. During the course of SAR studies, it was discovered that one enantiomer of unknown absolute configuration of a chiral analog of ML297 displayed high GIRK1/2 selectivity. This compound's ability to discriminate between the major brain (GIRK1/2) and cardiac (GIRK1/4) GIRK ion channels is significant in determining the therapeutic potential of these ion channel targets. In this chapter we describe the asymmetric synthesis of the GIRK1/2 selective enantiomer leading to the assignment of its absolute stereochemistry as *S,S*. Several single enantiomer probes were prepared around the core scaffold and found to act as selective GIRK1/2 activators and GIRK1/4 inhibitors. Our understanding of function and regulation of GIRK channels continues to improve with the identification of new potent and channel selective probes to guide the therapeutic potential of modulating GIRK channels.

### 3.2 Background

Potassium channels are key regulators of excitability in numerous excitable tissues including neurons, cardiomyocytes, and hormone-secreting endocrine cells. In particular, the G-protein-gated inward rectifying potassium channel (GIRK) is believed to play an important role in setting cellular membrane potential and in doing so effect neuron firing, heart rate, and hormone secretion<sup>1</sup>. GIRK activity can be regulated, as its name suggest by the activity of G-protein-coupled receptors (GPCR). The  $G_{i/o}$  coupled G-protein-coupled receptors (GPCR) class of receptors can mediate activation of GIRK via the  $\beta/\gamma$ -subunits<sup>3</sup> of the heterotrimeric G-protein and thus activation of the GPCR is able to affect GIRK's ability to modulate cellular excitability. In addition to GIRK activation by  $G_{i/o}$  GPCRs, the channel can also be modulated by changes in plasma membrane phosphatidylinositol 4,5-bisphosphate levels, by phosphorylation, and by small molecules. The GIRK family is comprised of four members, Kir3.1-Kir3.4 (aka GIRK1-GIRK4)<sup>5</sup>. These four family members can assemble into a variety of homo and heterotetrameric configurations to yield channels with different biophysical properties and different tissue distributions<sup>1</sup>. In the central nervous system the predominant subunit conformation is the GIRK1/2 heterotetramer while GIRK1/4 in atrial cardiomyocytes, in L-cells of the gut, in the adrenal gland, and in other tissues. Non-GIRK1-containing GIRKs have more limited expression in localized brain regions such as the ventral tegmental area<sup>28</sup>. Genetic manipulation of GIRK expression in mice has revealed a number of potential functions of GIRK in physiological/pathophysiological processes including epilepsy, anxiety, pain, and drug addiction. In addition, numerous studies point GIRK's involvement in a range of disorders such as epilepsy, Down's syndrome, alcoholism,

schizophrenia, hyperaldosteronism, atrial fibrillation, responsiveness to opioid analgesics, and others. A full review of GIRK's involvement can be found in reference<sup>1</sup>.

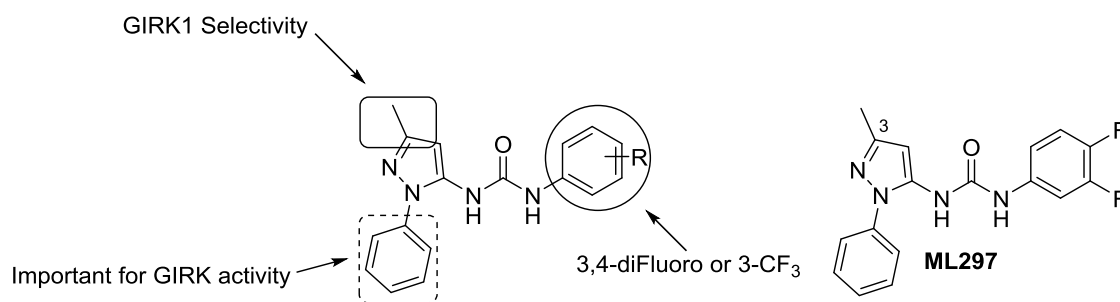


**Figure 3.1.** Functionalization around ML297 (left). Initially, 3,4-diFluoro was found to be an excellent activator of GIRK1 containing GIRK channels. Recently, selectivity studies have probed the C3 position on the pyrazole to determine GIRK1 containing selectivity and pursued a diversifying SAR (right).

Recently we demonstrated for the first time that it was possible to modulate the activity of GIRKs through the direct action of small molecule activators and inhibitors. Lead optimization led to the development of the GIRK1 selective activator ML297 (GIRK1/2  $EC_{50}$  = 0.16  $\mu$ M, Figure 3.1)<sup>9</sup>. ML297 and analogs possess the peculiar property of only changing the activity of GIRK1-containing GIRKs. We have discovered two key amino acids in GIRK1 that appear to be responsible for this exquisite subunit selectivity<sup>33</sup>. When our small molecule modulators of GIRK1-containing GIRKs have been tested *in vivo* we have observed concentration-dependent effects in murine models of epilepsy<sup>9</sup>, stress induce hyperthermia, and elevated plus maze<sup>34</sup>. These data suggest a potential role for pharmacological modulation of GIRK for the treatment of a number of disorders. Although molecules like ML297 are useful molecular tools, there are issues with them that limit their utility as pharmacological tools. Most notably ML297 is ~6-10f fold more selective for GIRK1/2 which limits ability to evaluate the therapeutic potential of GIRK1 containing GIRK channels as GIRK1/4 is expressed in cardiac and other peripheral tissues. During the course of SAR studies of ML297 we observed the pyrazole C3 position to be a “hot spot” as

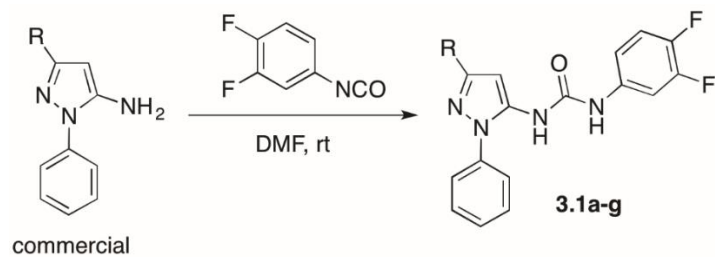


variation of substituents at this position led to significant changes in functional activity as well as potency (vide infra).

### ***GIRK1/2 Verses GIRK1/4 Selectivity Studies***

Wen and coworkers<sup>35</sup> proceeded to identify additional GIRK activators and “molecular switches” which were found to be the first examples of selective GIRK inhibitors. Holding the 3-methyl pyrazole and the 3,4-difluorophenyl aryl group constant, the N-Ph alternatives were explored. Here they uncovered one of the most potent GIRK1 activator, the N-benzyl derivative (GIRK1/2  $EC_{50}$  = 0.07  $\mu$ M, GIRK1/4  $EC_{50}$  = 0.11  $\mu$ M).

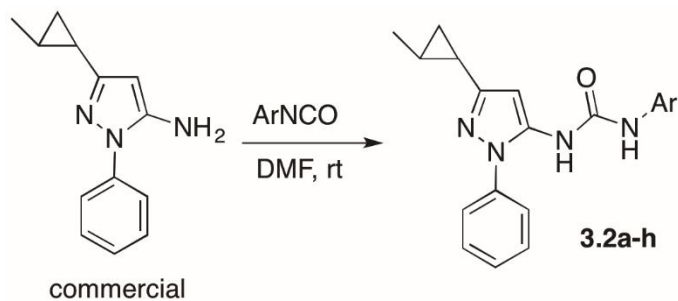
**Table 3.1** Structures and activity of GIRK probe analogs on GIRK1/2 and GIRK1/4. Potency values reported as  $\mu\text{M}$  and obtained from triplicate determinations. NA = not determined.



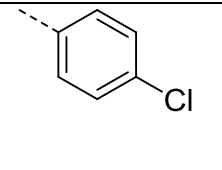
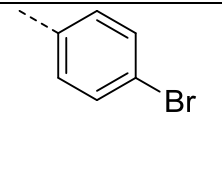
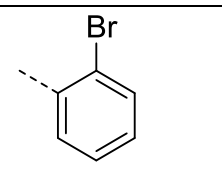
Compound	R group	GIRK1/2	GIRK1/2	GIRK1/4	GIRK1/4
		EC <sub>50</sub> ( $\mu\text{M}$ )	IC <sub>50</sub> ( $\mu\text{M}$ )	EC <sub>50</sub> ( $\mu\text{M}$ )	IC <sub>50</sub> ( $\mu\text{M}$ )
<b>3.1a</b>		>30	30	30	30
<b>3.1b</b>		0.41	NA	30	NA
<b>3.1c</b>		NA	2.0	NA	1.4
<b>3.1d</b>		30	30	30	30
<b>3.1e</b>		NA	5.1	NA	4.1
<b>3.1f</b>		30	30	30	30
<b>3.1g</b>		NA	0.65	NA	0.56

Changes in the pyrazole C3 substitution starting from commercial N-phenyl pyrazoles provided an equally rich span of activity and selectivity (Table 3.1). Unique to this series was the uncovering of the “molecular switch” of a cyclopropyl group as a GIRK1/2 activator derivative (GIRK1/2  $EC_{50}$  = 0.41  $\mu$ M, GIRK1/4  $EC_{50}$  = 30  $\mu$ M) and an *iso*-propyl GIRK1 inhibitor (GIRK1/2  $IC_{50}$  = 2.0  $\mu$ M, GIRK1/4  $IC_{50}$  = 1.4  $\mu$ M). Surprisingly, the cyclobutyl substitution was inactive on both GIRK1/2 and GIRK1/4, leading to the consideration that slight structural modification can determine GIRK1 selectivity in the pyrazole region. The SAR was further explored with a variety of isocyanate coupling partners for N-phenyl or benzyl pyrazoles bearing an *iso*-propyl, cyclopropyl or cyclobutyl. A wide range of selectivity and activity emerged, but most notably, the *iso*-propyl were exclusively inhibitors and active with a preference for GIRK1/4. Based on the previous report, the C3 position on the pyrazole had eluded to some degree of GIRK1 selectivity. We have described a series of compounds based on the ML297 structure that display a strong preference for activation of GIRK1/2 over GIRK1/4. Among these molecules are a family of substituted cyclopropanes. Coupling with a commercially provided 2-methyl cyclopropyl pyrazole, probe derivatives were synthesized and surveyed with a variety of aryl pendant groups (Table 3.2). Switching the methyl from 1-methyl cyclopropyl to 2-methyl cyclopropyl analogs displayed activator activity as opposite to inhibitor, suggesting a high degree of selectivity around the C3 position on the pyrazole.

**Table 3.2** Structures and activity of GIRK probe analogs on GIRK1/2 and GIRK1/4. Potency values reported as  $\mu\text{M}$  and obtained from triplicate determinations. NA = not determined.



Compound	R group	GIRK1/2	GIRK1/2	GIRK1/4	GIRK1/4
		EC <sub>50</sub> ( $\mu\text{M}$ )	IC <sub>50</sub> ( $\mu\text{M}$ )	EC <sub>50</sub> ( $\mu\text{M}$ )	IC <sub>50</sub> ( $\mu\text{M}$ )
3.2a		0.44	NA	0.89	NA
3.2b		0.46	NA	>10	NA
3.2c		0.85	NA	2.2	NA
3.2d		0.89	NA	>30	NA
3.2e		1.3	NA	2.3	NA

<b>3.2f</b>		1.9	NA	>30	NA
<b>3.2g</b>		3.0	NA	>30	NA
<b>3.2h</b>		>30	NA	>30	NA

Because some of the molecules in question possess chiral centers and because the samples we tested were a racemic mixture, we were interested in determining whether there might be a stereochemical bias for their GIRK1/2 vs GIRK1/4 selectivity. After assaying a racemic mixture of 2-methyl cyclopropyl analogue **3.2a** (presumed to possess trans relative stereochemistry about the cyclopropyl ring), those data suggested a higher selectivity for GIRK1/2 ( $EC_{50} = 0.440 \mu\text{M}$ ) channels when compared to GIRK1/4 ( $EC_{50} = 0.890 \mu\text{M}$ ). The mixture was resolved by chiral LC and one enantiomer proved to be significantly more potent in activating GIRK 1/4 channels relative to the second. In order to assign the absolute configuration of the GIRK1/4 selective enantiomer we set out to prepare optically pure isomers of **3.2a** using a well-defined synthetic route. The individual enantiomers were then assayed using for GIRK channel selectivity using HEK-293 cells expressing either GIRK1/2 or GIRK1/4 using the  $\text{TI}^+$  flux assay.

### 3.3 Synthesis of *trans* 2-Methyl Cyclopropyl Enantiomer Probes

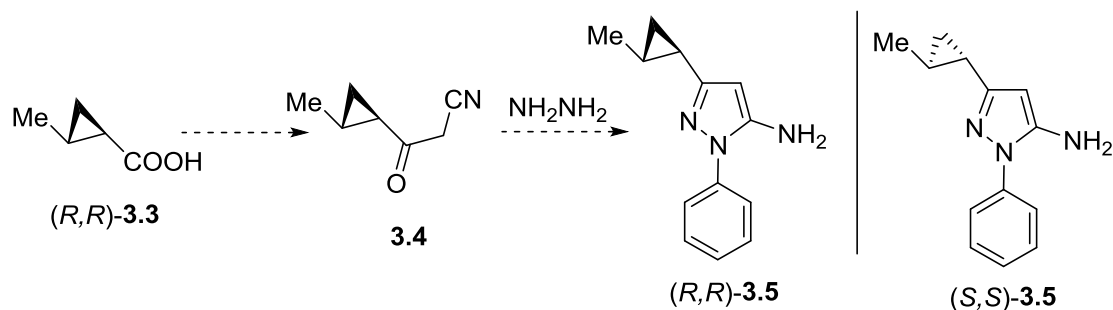
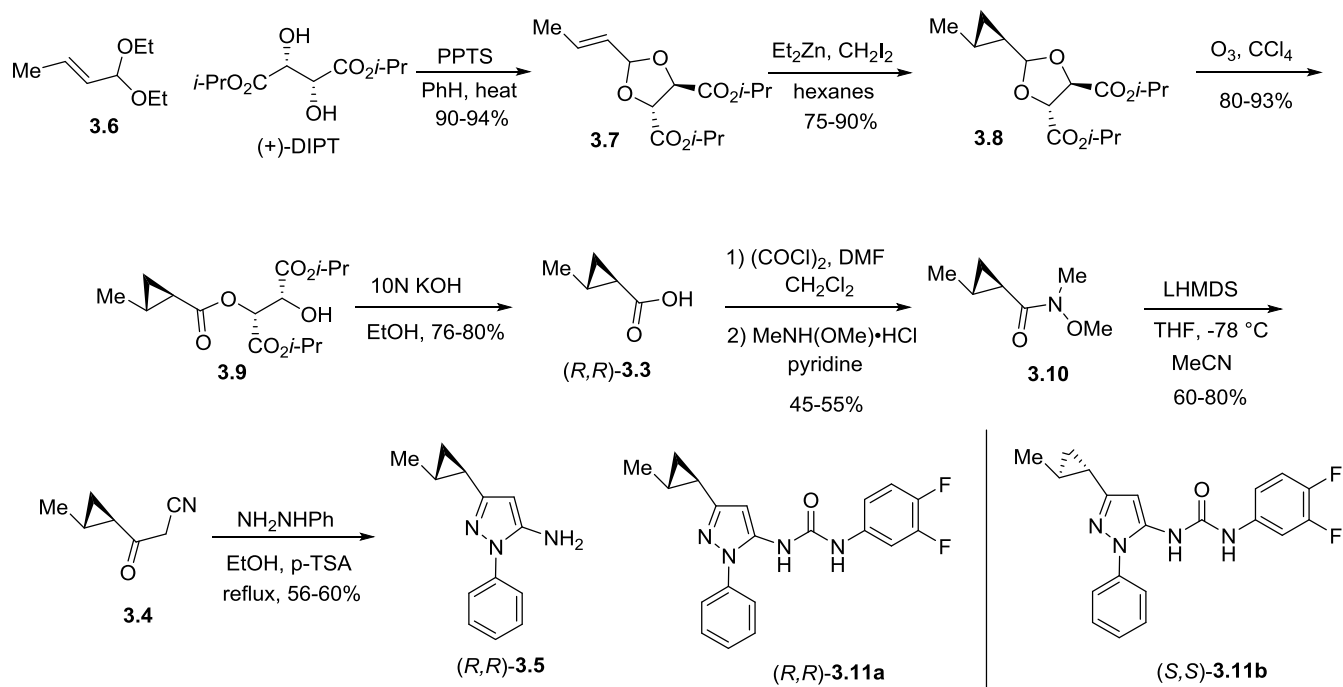


**Figure 3.2.** Preparation of single enantiomer methylcyclopropanes.

The most common synthesis of aminopyrazoles is the condensation of beta-ketonitriles with hydrazines. For the preparation of aminopyrazoles **(R,R)-3.5** this requires beta-ketonitrile **3.4**. The latter would be readily derived from cyclopropanecarboxylic acid **(R,R)-3.3**. Conversely, aminopyrazole **(S,S)-3.5** will be derived from **(S,S)-3.3**. Our first objective became the asymmetric synthesis of **(R,R)-3.3** and **(S,S)-3.3**. Examination of the literature immediately identified the Mori method<sup>36</sup> for the preparation of the two enantiomeric cyclopropanecarboxylic acids as the optimal preparation of optically active material<sup>37</sup>.

The Mori procedure starts with the *trans* acetalization of crotonaldehyde diethyl acetal with readily available (+)- or (-)-diisopropyl tartrate leading to optically active carboxylic acid **3.3** of either absolute configuration depending on the starting tartrate ester. The reaction sequence is illustrated for **(R,R)-3.3** starting from (+)-DIPT. The key Simon-Smiths cyclopropanation occurred in high yields (70-85%) and >95% diastereoselectivity based on NMR analysis<sup>36</sup>. Oxidation of the acetal **3.8** with ozone provided ester **3.9** which upon saponification gave cyclopropane carboxylic acid **(R,R)-3.3**<sup>37</sup>. The latter was converted to Weinreb amide **3.10** and reacted with the anion derived from acetonitrile to provide beta-ketonitrile **3.4**. Condensation of **3.4** with phenylhydrazine gave aminopyrazole **(R,R)-3.5** as a single enantiomer product ( $[\alpha]_D^{20} -25.2$  (c 2.50 ethanol)). Following the identical synthetic route starting from (-)-DIPT afforded the enantiomeric aminopyrazole **(S,S)-3.5** ( $[\alpha]_D^{20} +22.8$  (c 1.25, ethanol)).

Aminopyrazoles (*S,S*)- and (*R,R*)-**3.5** were individually condensed with 3,4-difluorophenyl isocyanate to give (*S,S*)- and (*R,R*)-**3.2a** which were subsequently evaluated in the TI<sup>+</sup> flux assay.



**Scheme 3.1.** Synthesis of 2-methylcyclopropyl (*R,R*) or (*S,S*) enantiomers. *Trans* 2-methyl cyclopropyl carbocyclic acid enantiomers were prepared following the work of Mori and coworkers<sup>39</sup>

### 3.4 Cyclopropyl Enantiomer CRCs Measuring TI<sup>+</sup> Flux

Using the Panoptic kinetic imaging plate reader in the Vanderbilt University High-Throughput Screening facility, Human Embryonic Kidney (HEK-293) cells expressing GIRK1/2 or GIRK1/4 channels were assayed using serial dilutions of the urea enantiomers and ML297 as a standard (Detailed procedure found in Experimental). The raw traces for compound efficacy (normalized to %ML297Max, Figure 3.4) over time showed an enantiomer (1*R*,2*R*) preference for GIRK1/2 over GIRK1/4. Not surprisingly, the enantiomers were all active on GIRK1/2 but an interesting relationship developed with GIRK1/4. Those channels show activator selectivity preference for (3,4-difluoro) VU0657405 **3.11a** (GIRK1/2 = 0.79 μM, GIRK1/4 = 1.1 μM) versus VU0657424 **3.11b** (GIRK1/2 = 0.63 μM, GIRK1/4 inactive) enantiomers. We now have a GIRK1 selective probe that is preferentially active for GIRK1/2 to use in our molecular toolbox. To our astonishment, we also identified isomers with inhibitor selectivity

VU0657532 **3.12b** (GIRK1/2 = 1.8 $\mu$ M, GIRK1/4 inhibitor = 2.0 $\mu$ M) versus VU0659392 **3.12a** (GIRK1/2 = 0.87 $\mu$ M, GIRK1/4 inactive) enantiomer. Just as we had seen with the racemic data, activity for a single enantiomer dropped off dramatically with GIRK1/4 channels. This “molecular switch” probe **3.12b** would act to inhibit GIRK1/4 and activate GIRK1/2 (See Figure 3.3).

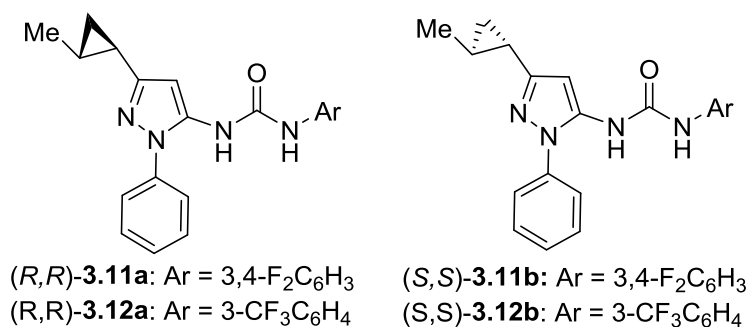


**Figure 3.3.** Single enantiomer ureas: VU0659392(**3.12a**), VU0657532(**3.12b**), VU0657405(**3.11a**), and VU0657424(**3.11b**).



To further validate these results from  $\text{TI}^+$  flux assay, electrophysiology was recorded for the 2-methylcyclopropyl enantiomers on GIRK1/2 and GIRK1/4 channels. Using (1*S*,2*S*), VU0657532 demonstrated selectivity preference for GIRK1/2 as an activator and GIRK/14 as an inhibitor.

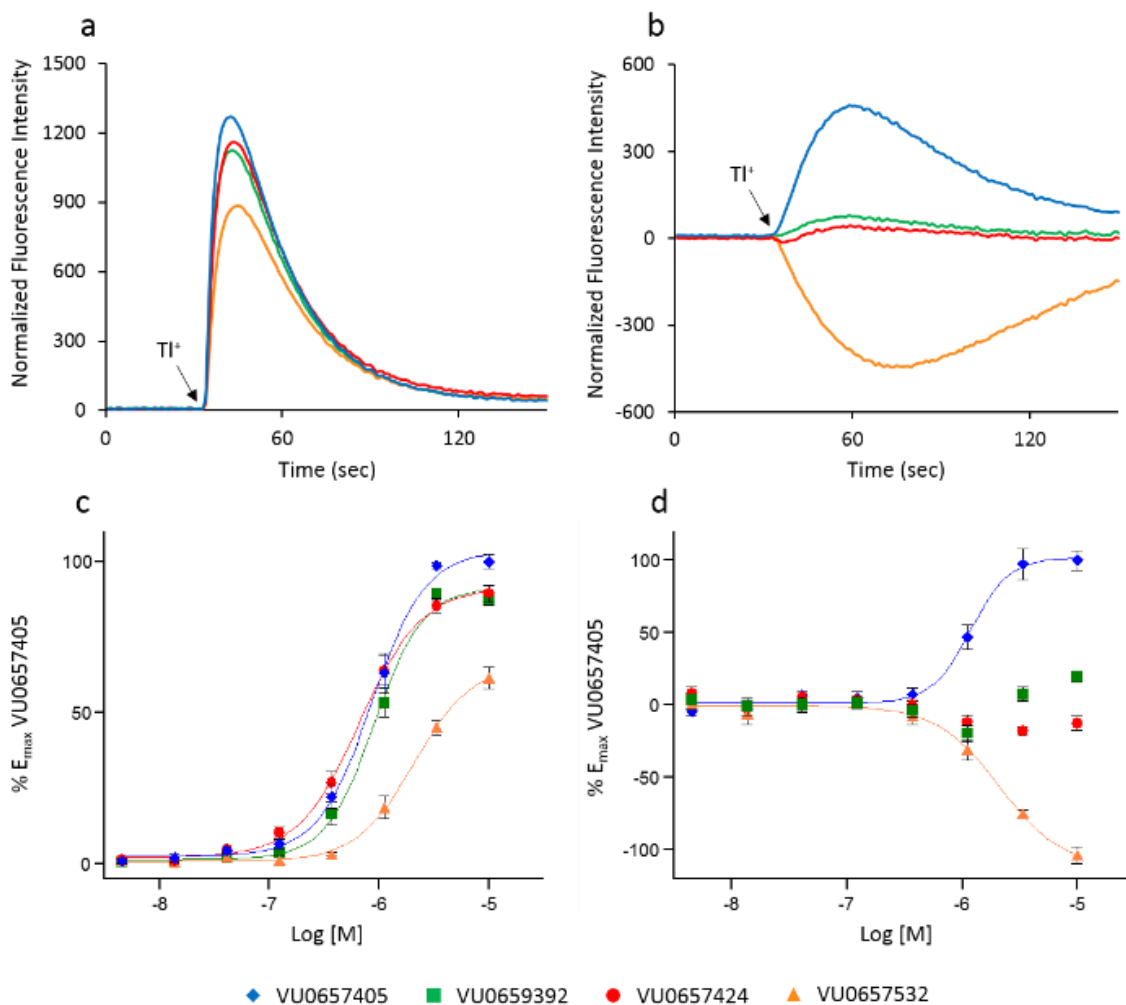


**Figure 3.4.**  $\text{TI}^+$  flux of GIRK1/2 (left) and GIRK1/4 (right) with compounds 3.11a-3.12b, standardized to ML297 fluorescence intensity. A) Raw  $\text{TI}^+$  activity trace of GIRK1/2 channels demonstrating activation by MCP enantiomers. B) Raw  $\text{TI}^+$  activity trace of GIRK1/4 channels. One enantiomer (VU0657532) acts as an inhibitor. C) Concentration Response Curve (CRC) of MCP enantiomers on GIRK1/2 channels. D) CRC of MCP enantiomers on GIRK1/4 channels

**Table 3.3.** EC<sub>50</sub> and IC<sub>50</sub> (μM) of MCP Isomers on GIRK1/2 and GIRK1/4 channels.

Compound	VU Number	Isomer	GIRK1/2 EC <sub>50</sub> (μM)	GIRK1/2 IC <sub>50</sub> (μM)	GIRK1/4 EC <sub>50</sub> (μM)	GIRK1/4 IC <sub>50</sub> (μM)
	VU0456810  (ML297)		0.16	NA	1.8	NA
<b>3.12a</b>	VU0659392	( <i>R,R</i> )	0.87	NA	NA	NA
<b>3.12b</b>	VU0657532	( <i>S,S</i> )	1.8	NA	NA	2.0
<b>3.11a</b>	VU0657405	( <i>R,R</i> )	0.79	NA	1.1	NA
<b>3.11b</b>	VU0657424	( <i>S,S</i> )	0.63	NA	NA	NA

### 3.5 Conclusion

Research into GIRK channels has been limited due to lack of selective and potent small molecule probes. During the course of SAR studies a highly GIRK1/2 selective enantiomer was discovered following chiral LC resolution. Preparation of single enantiomers of known configuration and results of channel selective activation and inhibition are shown. These enantiomer probes were found to all act as GIRK1/2 activators but with varying activity on GIRK1/4. One enantiomer, VU0657532 (3.12a) was found to contain a configuration “molecular switch”, acting as an activator on GIRK1/2 and inhibitor on GIRK1/4. These results from TI<sup>+</sup> flux assay were validated using (electrophysiology). The ability to preference GIRK1 selectivity has been generously driven in the correct direction with MCP probes from the initial non-selective GIRK1 activator, ML297. To capture both GIRK1 selectivity and potency, further

SAR studies should be conducted on the MCP scaffold, such as investigating the *cis* geometry or additional chiral pendant groups. Our understanding of function and regulation of GIRK channels will improve with better chemically-synthesized products; potent and selective small molecules will guide the therapeutic potential of modulating GIRK channels. On-going work in this area will define our understanding of GIRK1 containing GIRK channels through selective activation. We could potentially use the scaffold of these probes as GIRK1 active pharmaceutical lead compounds.

### 3.6 Experimental

#### *General Experimental*

All glassware used for reactions was flame dried under vacuum. All reagents and solvents were commercial grade and purified prior to use when necessary. All reactions were performed under argon atmosphere unless otherwise stated. Diethyl ether (Et<sub>2</sub>O) and dichloromethane (CH<sub>2</sub>Cl<sub>2</sub>) were dried by passage through a column of activated alumina using an MBraun MB-SPS dry solvent system. Tetrahydrofuran (THF) was distilled from sodium with benzophenone as indicator prior to use.

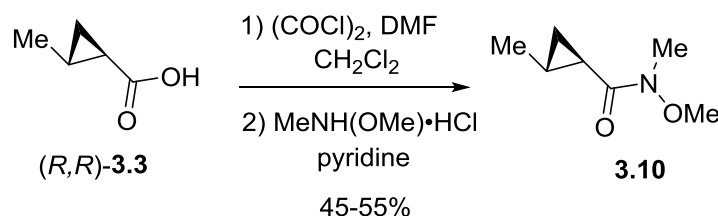
Reactions were monitored by analytical thin-layer chromatography performed on Analtech silica gel GF 250 micron plates. The plates were visualized with UV light (254 nm) and either potassium permanganate, ceric ammonium molybdate, or p-anisaldehyde followed by charring on a hot-plate. Flash chromatography utilized 230-400 mesh silica gel (SiO<sub>2</sub>) from Sorbent Technologies or Silica RediSep Rf flash columns on a CombiFlash Rf automated flash chromatography system. Solvents for extraction, washing and chromatography were HPLC grade.

Nuclear magnetic resonance (NMR) spectra were acquired on either a 300 MHz Bruker DPX-300 FT-NMR, a 400 MHz Bruker AV-400 FT-NMR, or 500 MHz Bruker DRX-500 FT-NMR Spectrometer at ambient temperature. <sup>1</sup>H and <sup>13</sup>C NMR data are reported as values relative to CDCl<sub>3</sub>. <sup>1</sup>H chemical shifts are reported in δ values in ppm. Data are reported as follows: chemical shift, multiplicity (s = singlet, d = doublet, t = triplet, q = quartet, br = broad, m = multiplet), integration, coupling constant (Hz). <sup>13</sup>C

chemical shifts are reported in  $\delta$  values in ppm. Low resolution mass spectra were obtained on an Agilent 1200 series 6130 mass spectrometer with electrospray ionization. High resolution mass spectra were recorded on a Waters Q-TOF API-US. Analytical HPLC was performed on an Agilent 1200 series with UV detection at 214 nm and 254 nm along with ELSD detection. Preparative HPLC was conducted on a Gilson 215 Liquid Handler HPLC system using Gemini-NX 50 x 20 mm column.

### Synthesis of (*R,R*) and (*S,S*) *trans* 2-methyl Cyclopropyl Phenyl Pyrazole Urea Enantiomers

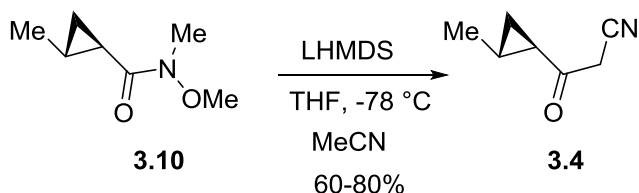
Note: *Trans* 2-methyl cyclopropyl carbocyclic acid enantiomers were prepared following the work of Mori and coworkers<sup>36</sup>.



**(1*R*,2*R*)-N-methoxy-N,2-dimethylcyclopropanecarboxamide.** To a solution of **3.3**<sup>37</sup> (1.6 g, 15.99 mmol) in DCM (10 mL) were added freshly distilled oxalyl chloride (1.65 mL, 19.19 mmol) and a catalytic amount of dimethylformamide. The mixture was stirred until gaseous bubbles ceased evolving and excess oxalyl chloride was removed *in vacuo*. The residue was dissolved in DCM (10 mL). To the solution was added N,O-dimethylhydroxylamine hydrochloride (2.34 g, 24.0 mmol) followed by pyridine (5.16 mL). The mixture was stirred until judged complete by TLC (1:1 hex/EtOAc). When complete, reaction was quenched with 2M HCl (20 mL) and extracted with EtOAc (3X50mL). Organic layer was combined, dried over MgSO<sub>4</sub>, and concentrated *in vacuo* to yield a crude yellow oil. The residue was purified by vacuum distillation (b.p. 35-40°C at 10 Torr ) to yield 700 mg (30% over two steps) of Weinreb amide **3.10** as a colorless oil:  $[\alpha]_D^{20}$  -38.2 (*c* 1.31, ethanol); <sup>1</sup>H NMR (400 MHz, CDCl<sub>3</sub>):  $\delta$  3.73 (s, 3H), 3.19 (s, 3H), 1.83 (m, 1H), 1.34 (m, 1H), 1.65 (q, *J* = 5.1 Hz, 1H), 1.12 (d, *J* = 6.0 Hz, 3H), 0.63 (m, 1H). <sup>13</sup>C NMR (400 MHz, CDCl<sub>3</sub>):  $\delta$  16.2, 16.6, 17.9, 18.5, 32.5, 61.4, 174.4.

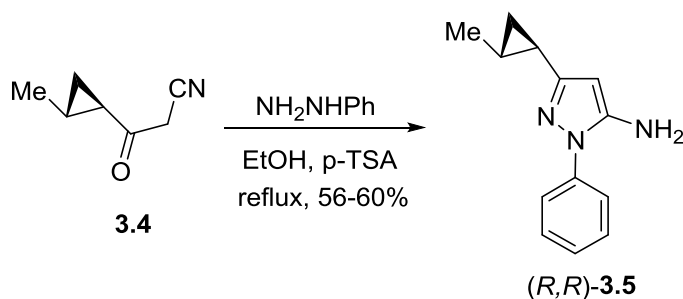
**(1S,2S)-N-methoxy-N,2-dimethylcyclopropanecarboxamide.** Following the above procedure.

The residue was purified by vacuum distillation (b.p. 35-40°C at 10 Torr ) to yield 615mg (30% over two steps) of the Weinreb amide as a colorless oil identical to R,R isomer except for optical rotation:  $[\alpha]^{20}_D$  +32.7 (*c* 1.13, ethanol).



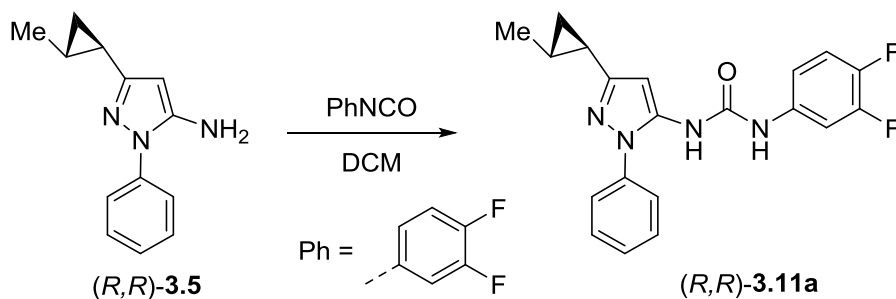
**3-((1R,2R)-2-methylcyclopropyl)-3-oxopropanenitrile.** To a solution of acetonitrile (0.24 mL, 4.54 mmol) and THF (2.3 mL) cooled to -78 °C was added dropwise 12.2 mL of 1M lithium bis(trimethylsilyl)amide in THF. The reaction mixture was stirred at -78 °C for 1h and a solution of 0.500 g (3.49 mmol) of Weinreb amide **3.10** in THF (2.5 mL) was added drop wise. The solution was stirred for an additional 1 h at -78 °C and allowed to warm to room temperature. The reaction mixture was quenched with Sat. NH<sub>4</sub>Cl (5.0 mL) and the mixture extracted with EtOAc (3X25 mL). The combined organic extracts were dried over MgSO<sub>4</sub>, and concentrated *in vacuo* to yield a crude brown oil. The residue was purified by column chromatography with hexane/ethyl acetate (10% to 30%) to yield 342.5 mg (80%) of  $\beta$ -keto nitrile **3.4** as a colorless oil:  $[\alpha]^{20}_D$  -126.0 (*c* 1.50, ethanol); <sup>1</sup>H NMR (400 MHz, CDCl<sub>3</sub>):  $\delta$ 3.55 (s, 2H), 1.85 (quintet, *J* = 4.05 Hz, 1H), 1.59 (m, 1H), 1.42 (m, 1H), 1.17 (d, *J* = 6.20 Hz, 3H), 0.94 (m, 1H). <sup>13</sup>C NMR (400 MHz, CDCl<sub>3</sub>):  $\delta$ 17.8, 21.2, 22.7, 28.9, 32.6, 114.0, 196.9.

**3-((1S,2S)-2-methylcyclopropyl)-3-oxopropanenitrile.** Following the above procedure. The residue was purified by column chromatography with hexane/ethyl acetate (10% to 30%) to yield 100.1 mg (60%) of  $\beta$ -keto nitrile as a colorless oil identical to RR isomer except for optical rotation:  $[\alpha]^{20}_D$  +122.0 (*c* 1.50, ethanol).



**3-((1R,2R)-2-methylcyclopropyl)-1-phenyl-1H-pyrazol-5-amine.** To a solution of **3.4** (100.0 mg, 0.81 mmol), p-TsOH (0.1 mmol) and phenylhydrazine (0.11 mL, 0.81 mmol) in ethanol (1M) was heated to reflux until determined judged complete by TLC (1:1 hex/EtOAc). The mixture was concentrated *in vacuo*, washed with saturated NaHCO<sub>3</sub> (15 mL) solution and extracted with EtOAc. (3X25 mL). The organic layers were combined, dried over MgSO<sub>4</sub> and concentrated to yield a crude orange oil. The residue was purified by column chromatography with hexane/ethyl acetate (20% to 50%) to yield 100.5 mg (60%) of 2-methyl cyclopropyl pyrazole **3.5** as an orange solid:  $[\alpha]^{20}_{\text{D}} -25.2$  (*c* 2.50 ethanol); <sup>1</sup>H NMR (400 MHz, CDCl<sub>3</sub>): δ 7.53 (m, 2H), 7.43 (t, *J* = 7.46 Hz, 2H), 7.29 (t, *J* = 7.46 Hz, 1H), 5.24 (s, 1H), 3.71, (s, 2H), 1.58 (sextet, *J* = 4.42 Hz, 1H), 1.14 (d, *J* = 5.25 Hz, 3H) 1.08 (m, 1H), 0.880 (m, 1H), 0.663 (m, 1H). <sup>13</sup>C NMR (400 MHz, CDCl<sub>3</sub>): δ 16.1, 16.3, 18.1, 18.7, 86.9, 123.8, 126.9, 129.4, 138.7, 145.0, 155.8. LCMS calculated for C<sub>13</sub>H<sub>15</sub>N<sub>3</sub> (M+H)<sup>+</sup> *m/z*: 213.3, Measured 214.7 *m/z*.

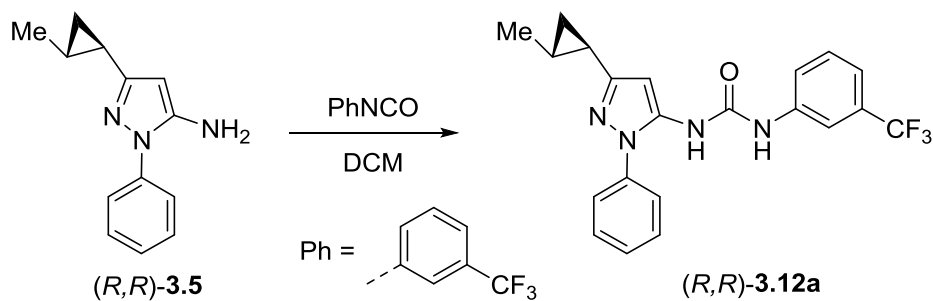
**3-((1S,2S)-2-methylcyclopropyl)-1-phenyl-1H-pyrazol-5-amine.** Following the above procedure. The residue was purified by column chromatography with hexane/ethyl acetate (20% to 50%) to yield 35.5 mg (40%) of the 2-methyl cyclopropyl pyrazole as an orange solid identical to RR isomer except for optical rotation:  $[\alpha]^{20}_{\text{D}} +22.8$  (*c* 1.25, ethanol).



**1-(3,4-difluorophenyl)-3-(3-((1R,2R)-2-methylcyclopropyl)-1-phenyl-1H-pyrazol-5-yl)urea.** To a solution of **3.5** (100.0mg, 0.47 mmol) in 1.56 mL of dichloromethane was added 3,4-difluorophenyl isocyanate (0.11 mL, 0.94 mmol) and allowed to stir overnight. The mixture was concentrated *in vacuo* to yield an off-white solid. The solid urea was purified by column chromatography with hexane/ethyl acetate (20% to 50%) to yield 103.0 mg (60%) of the 2-methylcyclopropyl pyrazole urea **3.11a** as a white solid, mp 175-176°C.  $[\alpha]_{\text{D}}^{20}$  -30.7 (*c* 1.30, ethanol);  $^1\text{H}$  NMR (400 MHz, DMSO):  $\delta$ 9.17 (s, 1H), 8.46 (s, 1H), 7.60 (ddd, *J* = 7.56, 6.55, 6.00 Hz, 1H), 7.49 (m, 4H), 7.39 (m, 1H), 7.31 (q, *J* = 9.03, 10.42 Hz, 1H), 7.06 (m, 1H), 6.13 (s, 1H), 1.59 (qu, *J* = 4.00, 4.84 Hz, 1H), 1.13 (d, *J* = 5.57 Hz, 3H), 0.873 (m, 1H), 0.697 (m, 1H).  $^{13}\text{C}$  NMR (400 MHz, DMSO):  $\delta$ 16.2, 16.3, 18.1, 18.9, 96.4, 107.4-107.6, 114.8, 117.7-117.9, 124.5, 127.6, 129.6, 136.8-136.9, 137.4, 138.8, 143.7-143.8, 146.1, 148.2- 148.3, 150.7, 152.1, 154.6. LCMS calculated for  $\text{C}_{20}\text{H}_{18}\text{F}_2\text{N}_4\text{O}$  (M+H)<sup>+</sup> *m/z*: 368.4, Measured 369.1 *m/z*.

**1-(3,4-difluorophenyl)-3-(3-((1S,2S)-2-methylcyclopropyl)-1-phenyl-1H-pyrazol-5-yl)urea.**

Following the above procedure The solid urea was purified by column chromatography with hexane/ethyl acetate (20% to 50%) to yield 41.0mg (80%) of the 2-methylcyclopropyl pyrazole urea as a white solid identical to RR isomer except for optical rotation:  $[\alpha]_{\text{D}}^{20}$  +39.0 (*c* 1.10, ethanol).



**1-(3-((1R,2R)-2-methylcyclopropyl)-1-phenyl-1H-pyrazol-5-yl)-3-(4-(trifluoromethyl)phenyl)urea.**

To a solution of **3.5** (25.0mg, 0.12 mmol) in 0.40 mL of dichloromethane was added 3,4-difluorophenyl isocyanate (0.03 mL, 0.24 mmol) and allowed to stir overnight. The mixture was concentrated *in vacuo* to yield an off-white solid. The solid urea was purified by column chromatography with hexane/ethyl acetate (20% to 50%) to yield 43.0 mg (86%) of the 2-methylcyclopropyl pyrazole urea **3.12a** as a white solid, mp 160-163°C:  $[\alpha]_{\text{D}}^{20} -17.3$  (*c* 3.00, ethanol);  $^1\text{H NMR}$  (400 MHz, DMSO):  $\delta$  9.33 (s, 1H), 8.51 (s, 1H), 7.95 (s, 1H) 7.52 (m, 6H), 7.40 (m, 1H), 7.31 (d, *J* = 8.00 Hz, 1H), 6.16 (s, 1H), 1.59 (qu, *J* = 4.00, 4.84 Hz, 1H), 1.13 (d, *J* = 5.57 Hz, 3H), 0.873 (m, 1H), 0.697 (m, 1H).  $^{13}\text{C NMR}$  (400 MHz, DMSO):  $\delta$  16.2, 16.3, 18.2, 18.9, 96.4, 114.5-114.6, 118.8, 121.9- 127.3, 122.2, 124.6, 127.7, 129.6, 129.8, 130.4, 137.40, 138.8, 140.7, 152.2, 154.7. LCMS calculated for  $\text{C}_{21}\text{H}_{19}\text{F}_3\text{N}_4\text{O}$  ( $\text{M}+\text{H}$ ) $^+$  *m/z*: 400.2, Measured 401.2 *m/z*.

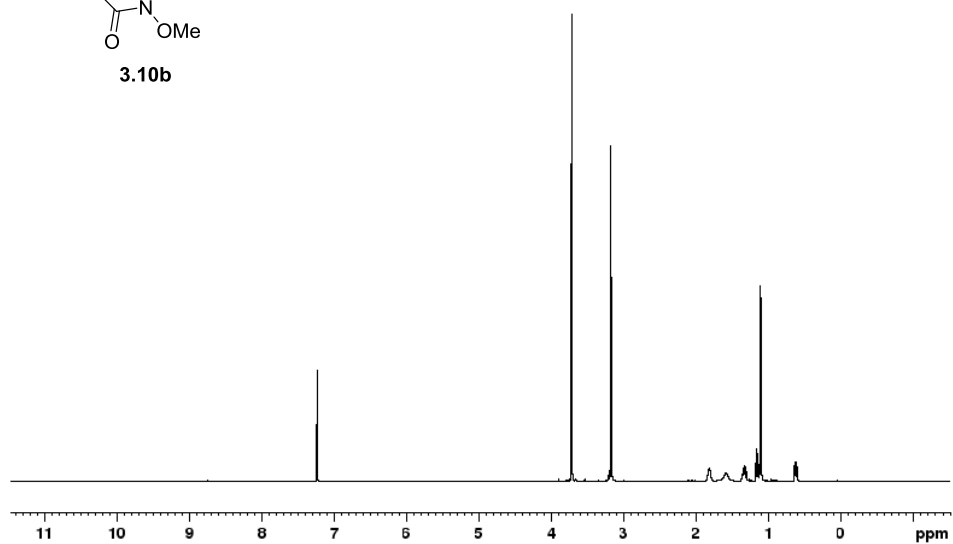
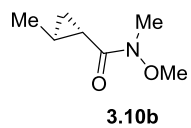
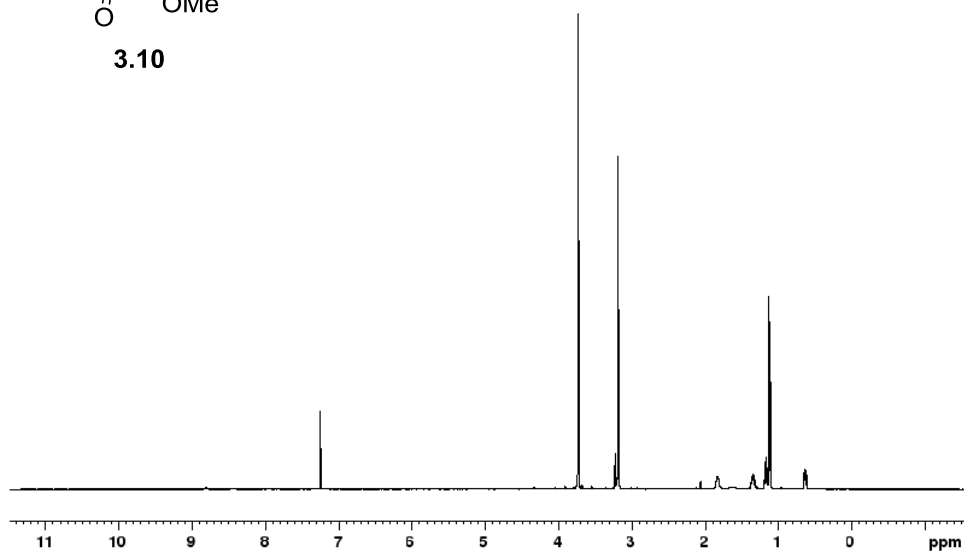
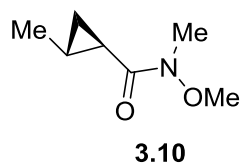
**1-(3-((1S,2S)-2-methylcyclopropyl)-1-phenyl-1H-pyrazol-5-yl)-3-(3-(trifluoromethyl)phenyl)urea.**

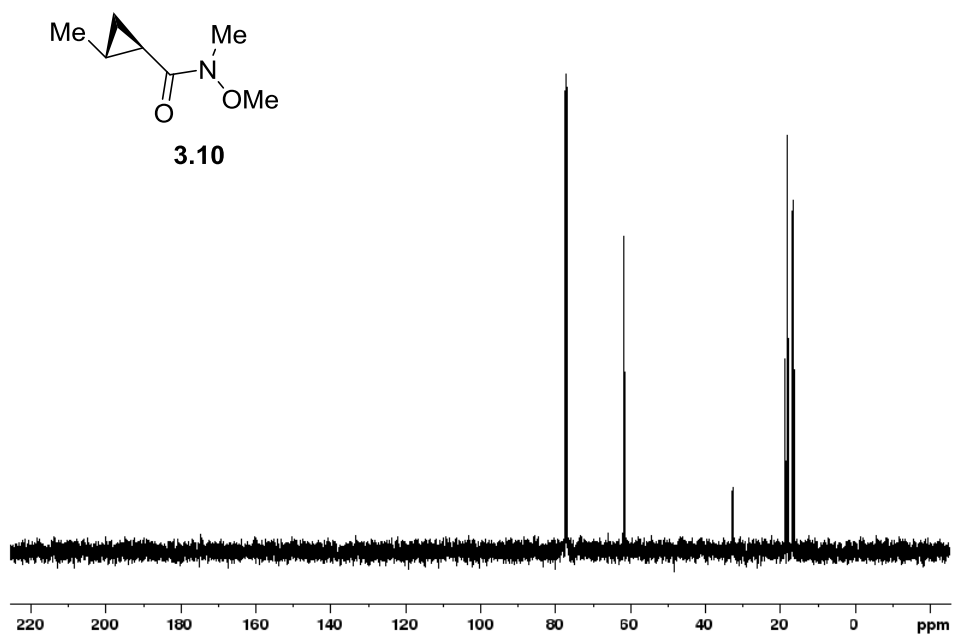
Following the above procedure The solid urea was purified by column chromatography with hexane/ethyl acetate (20% to 50%) to yield 71.0 mg (63%) of the 2-methylcyclopropyl pyrazole urea as a white solid identical to RR isomer except for optical rotation:  $[\alpha]_{\text{D}}^{20} +18.0$  (*c* 1.10, ethanol)



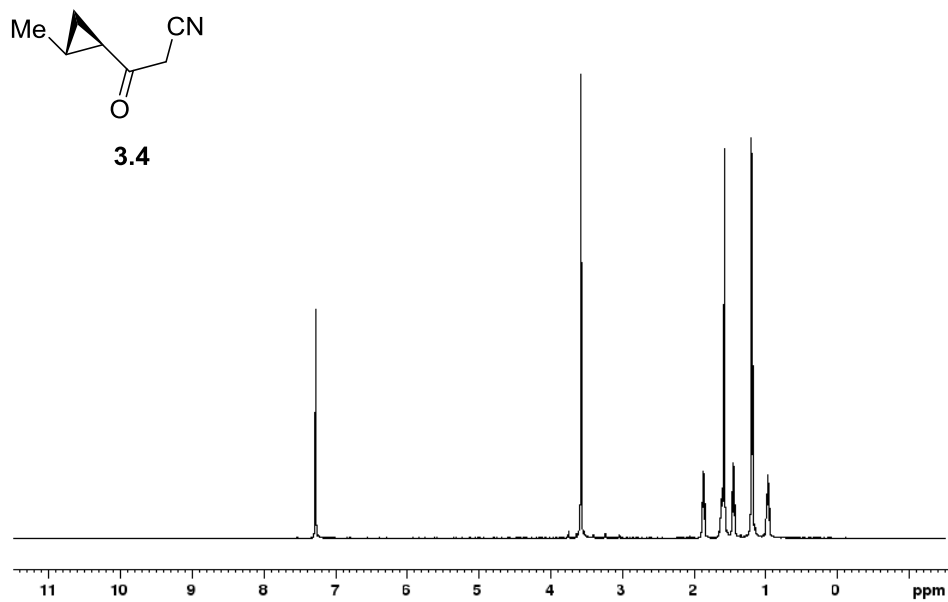
# APPENDIX

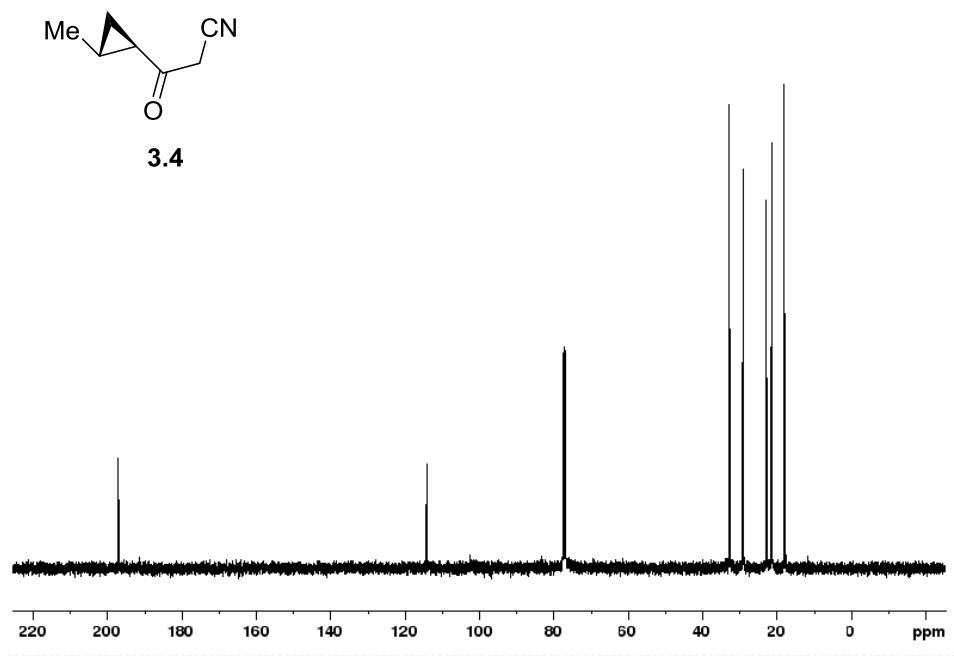
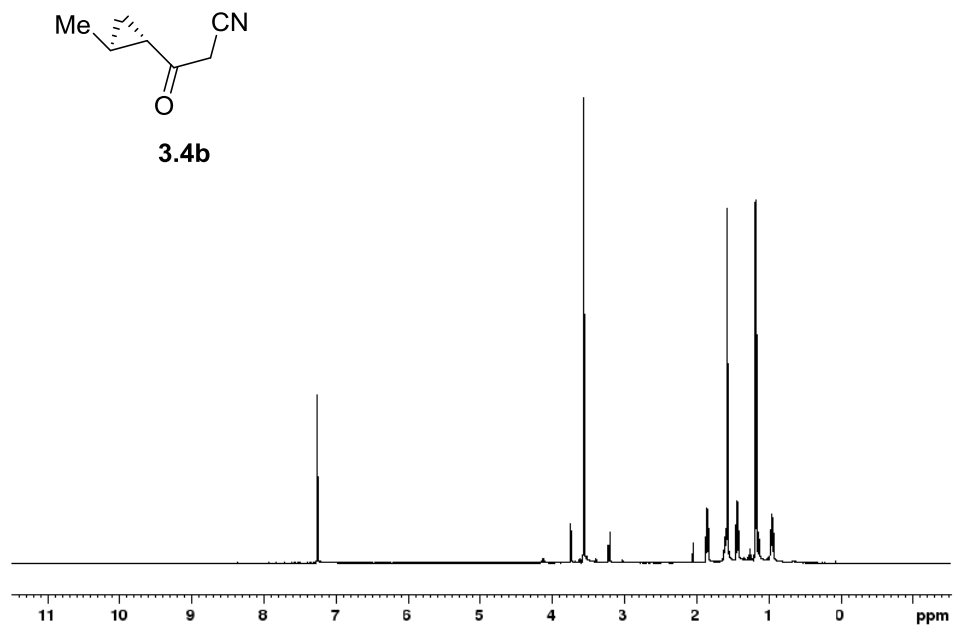
## NMRS FOR CHAPTER 3



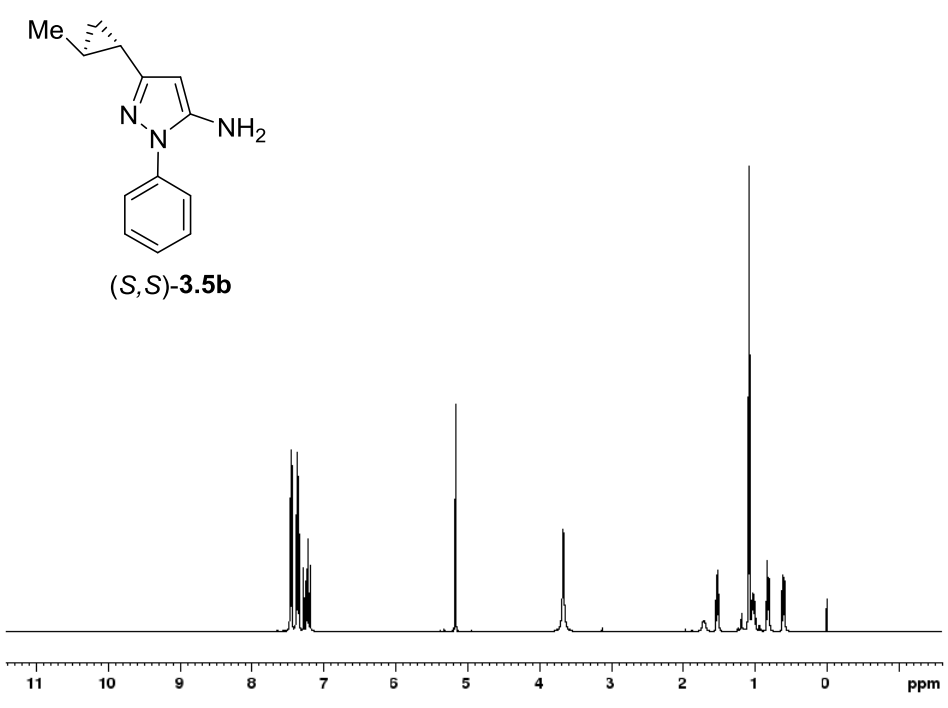
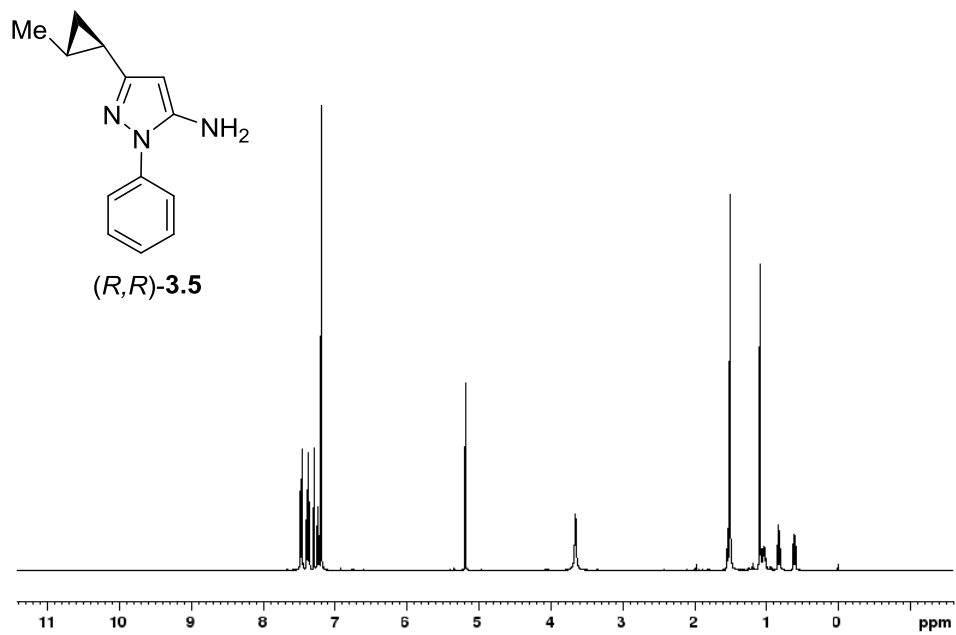


**Figure 3.5.** <sup>1</sup>H-NMR spectrum (400 MHz, CDCl<sub>3</sub>) of 1*R*,2*R* **3.10**, <sup>1</sup>H-NMR spectrum (400 MHz, CDCl<sub>3</sub>) of 1*S*,2*S* **3.10b** and <sup>13</sup>C-NMR spectrum (400 MHz, CDCl<sub>3</sub>) of 1*R*,2*R* **3.10**.





**Figure 3.6.** <sup>1</sup>H-NMR spectrum (400 MHz, CDCl<sub>3</sub>) of 1*R*,2*R* **3.4**, <sup>1</sup>H-NMR spectrum (400 MHz, CDCl<sub>3</sub>) of 1*S*,2*S* **3.4b** and <sup>13</sup>C-NMR spectrum (400 MHz, CDCl<sub>3</sub>) of 1*R*,2*R* **3.4**.



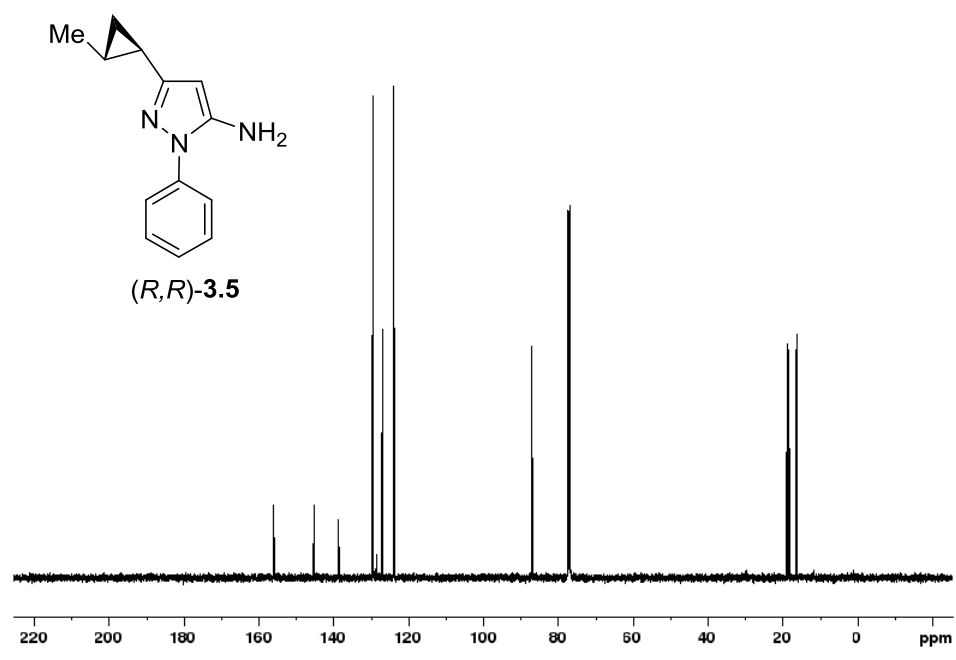
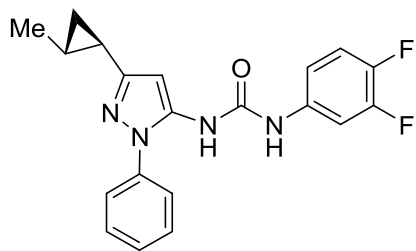
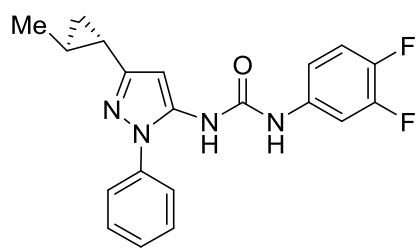
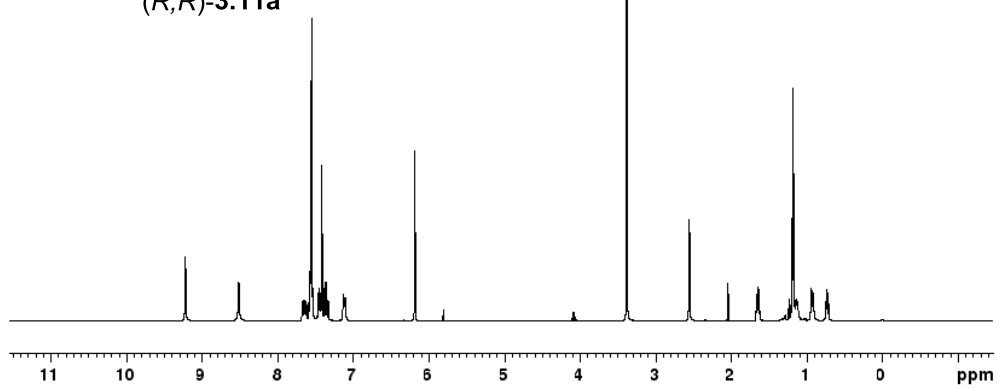


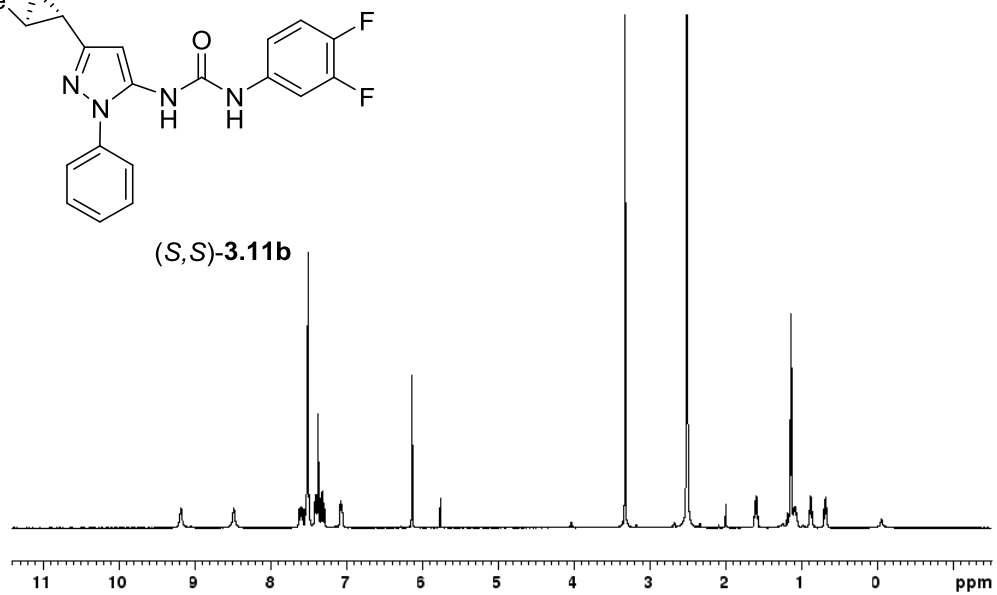
**Figure 3.7.** <sup>1</sup>H-NMR spectrum (400 MHz, CDCl<sub>3</sub>) of 1*R*,2*R* **3.5**, <sup>1</sup>H-NMR spectrum (400 MHz, CDCl<sub>3</sub>) of 1*S*,2*S* **3.5b** and <sup>13</sup>C-NMR spectrum (600 MHz, CDCl<sub>3</sub>) of 1*R*,2*R* **3.5**.

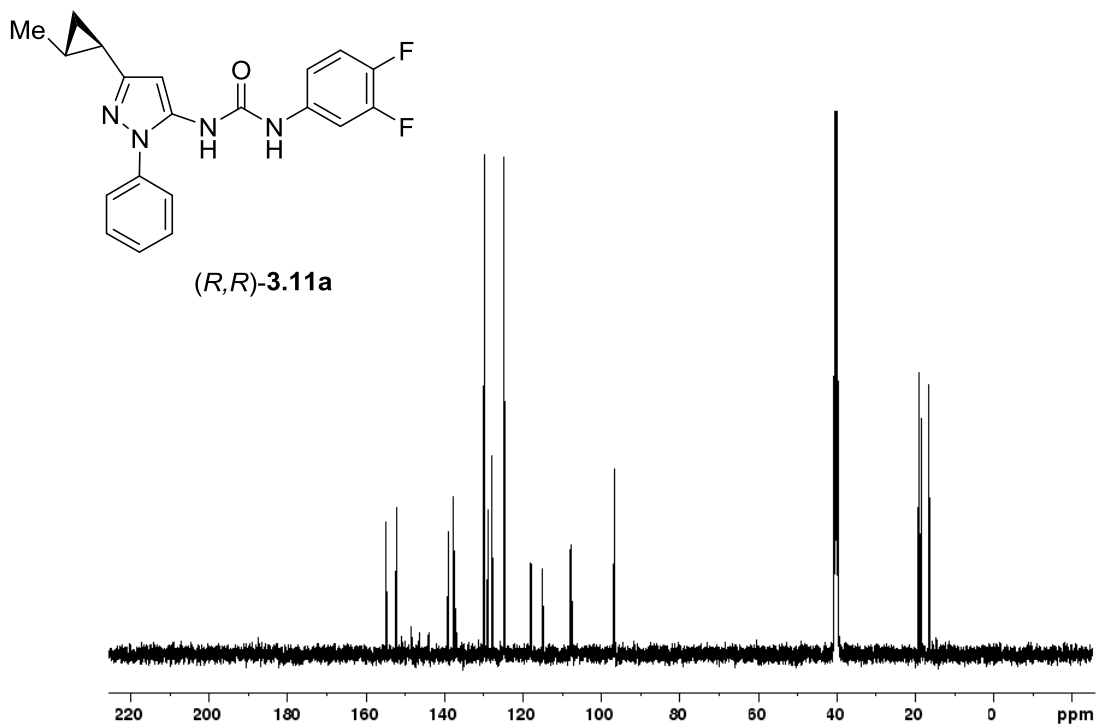


(R,R)-3.11a

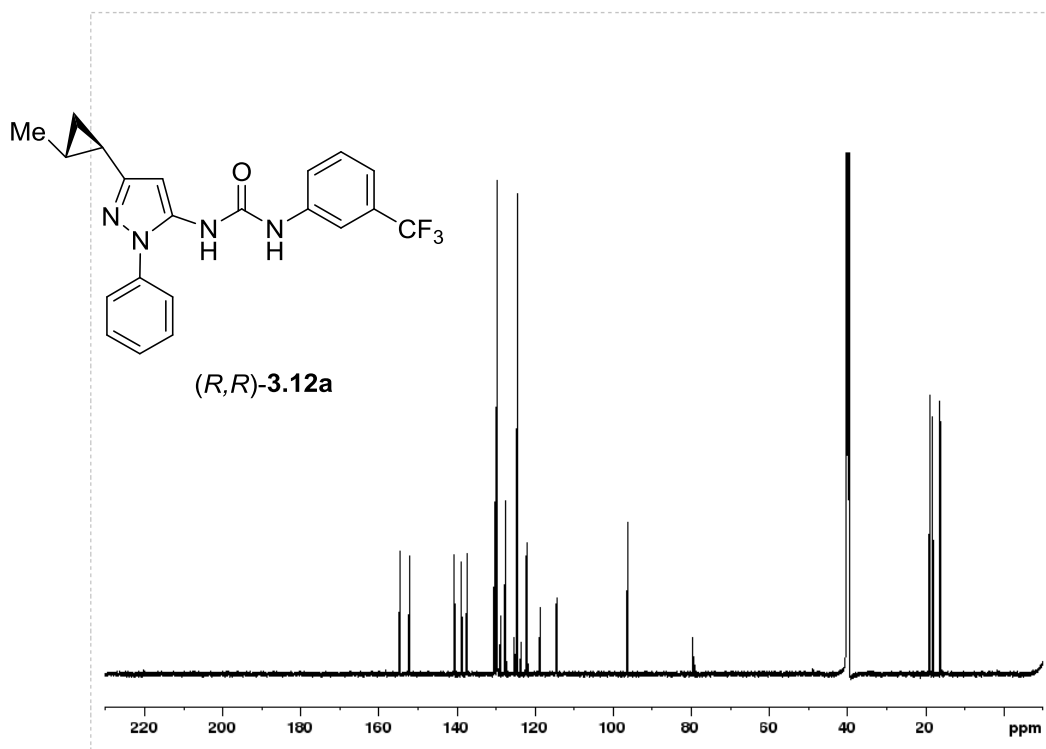
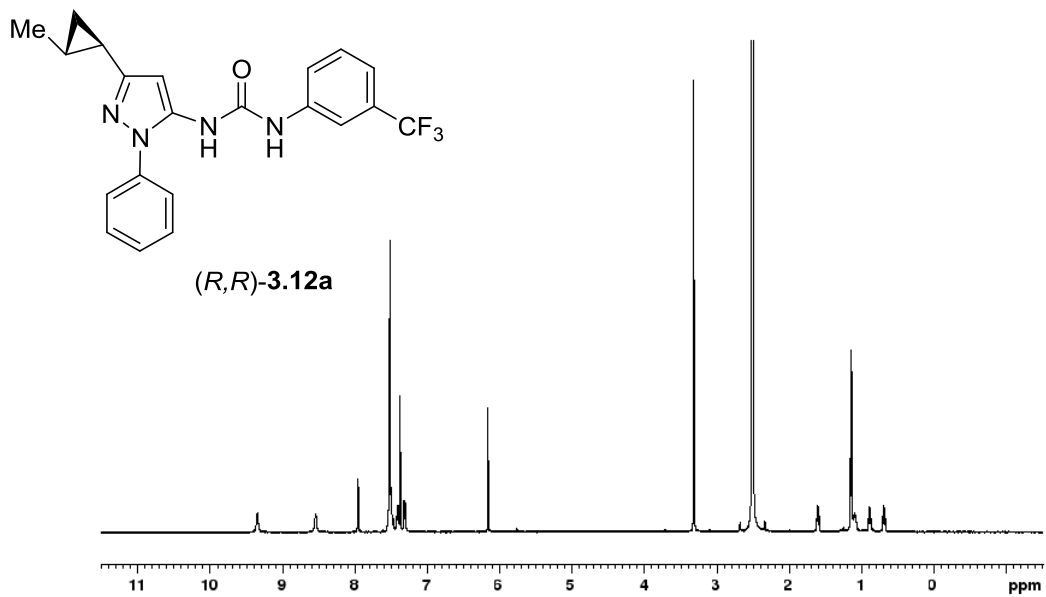


(S,S)-3.11b





**Figure 3.8.** <sup>1</sup>H-NMR spectrum (400 MHz, DMSO) of 1*R*,2*R* **3.11a**, <sup>1</sup>H-NMR spectrum (400 MHz, DMSO) of 1*S*,2*S* **3.11b** and <sup>13</sup>C-NMR spectrum (600 MHz, DMSO) of 1*R*,2*R* **3.11a**.





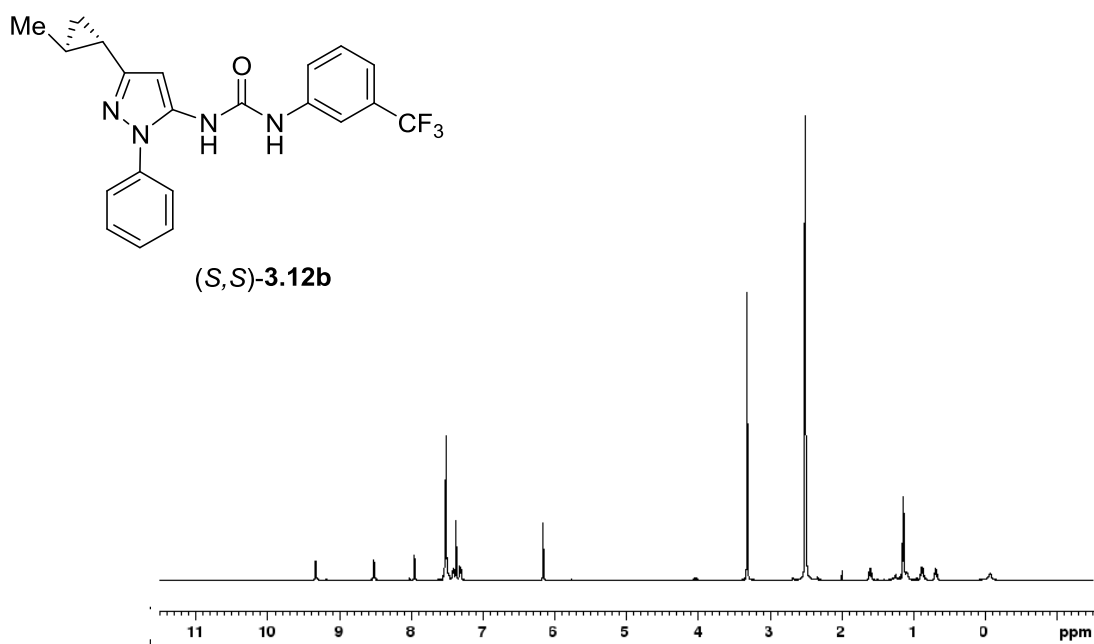


**Figure 3.9.** <sup>1</sup>H-NMR spectrum (400 MHz, DMSO) of 1*R*,2*R* **3.12a**, <sup>1</sup>H-NMR spectrum (400 MHz, DMSO) of 1*S*,2*S* **3.12b** and <sup>13</sup>C-NMR spectrum (600 MHz, DMSO) of 1*R*,2*R* **3.12a**.

## CHAPTER 4

### SELECTIVE RHODAMINE PRO-DYE/ENZYME RELEASING PAIR: MITOCHONDRION MEMBRANE POTENTIAL SENSORS

#### 4.1 Introduction

A powerful molecular tool used in biological assays has been organic fluorophores. Fluorogenic molecules have shown broad utility as reporter tags, sensors and cellular dyes<sup>14</sup>. A comprehensive collection of fluorogenic core scaffolds include fluorescein, which was first synthesized in 1871 spanning to the recently developed boron dipyrromethene (BODIPY) dyes, where all scaffolds have varying optical and physical properties. A variety of fluorogenic molecules that emit in the ultra-violet to near infra-red spectrum and offer varying scaffolds for useful applications such as organelle localization (i.e. rhodamines localizing to the mitochondria)<sup>38</sup>. The most common fluorogenic scaffold is xanthene-based, also known as fluorescein. Fluorescein spirolactones have a unique pH sensitive on-off equilibrium, shifting between a closed non-fluorescent lactone and an open fluorescent carboxylate-quinoid structure<sup>14</sup>. The introduction of electron withdrawing groups on the phenol containing rings, such as halogenation can lower the phenolic pKa and drive the equilibrium towards the fluorescent quinoid<sup>16</sup>. The non-fluorescent spirolactone can be “locked” by phenol protection such as acetylation.

A recent renaissance of dye synthesis and application has extended to the unique properties of xanthene scaffolds. Examples include replacing the oxygen on the xanthene scaffold with a dimethyl silyl group and effectively red-shifted the emission of the fluorescent molecule (2-Me, ToykoMagenta (TM)). Also, upon replacement of the carboxylic acid with a methyl, dubbed ToykoGreen, further red-shifts the emission wavelength<sup>8</sup>. In addition to changing spectral properties of dyes, modifications to the core scaffold have resulted in chemical on “switches” and reversible photo switching. These dyes have been used as enzymatic sensors by indicating specific cellular activities with increasing fluorescence through the selective “unmasking” or removal of a protection group on the phenol or aniline group. Previous

examples have focused in protein specific, light or pH dependent activation to real-time imaging, the spatial exploration of cellular machinery and high resolution imaging of live cells. This study explores the potential of engineering cells for pro-dye/enzyme selectivity pairing, (e.g. caged dyes) to overcome issues of non-selective fluorescence that currently impairs our cellular assays.

## 4.2 Background

### *Metal Ion Sensor Dyes*

Notably, one of the most popular and well defined metal ion probes were  $\text{Ca}^{2+}$  sensors developed by Tsien<sup>24</sup>. Using the novel chelator, 1,2-bis(2-aminophenoxy)ethane-*N,N,N',N'*-tetraacetic acid (BAPTA, Figure 4.1), improved previously known chelators by modifying the  $\text{pK}_a$  of the amine moieties<sup>39</sup> and allowed  $\text{Ca}^{2+}$  to chelate at physiological pH. Fluorescent probes with the BAPTA chelator then were developed, markedly Oregon Green 488 BAPTA-1 for dendritic  $\text{Ca}^{2+}$  detection<sup>40</sup>. Metal sensors for  $\text{K}^+$  and  $\text{Na}^+$  have also been developed, such as potassium-binding benzofuran isophthalate (PBFI) which contains a 18-crown-6 chelator but suffers from low quantum yield and poor selectivity for  $\text{K}^+$  over  $\text{Na}^+$ . To address this, a rhodamine scaffold (Figure 4.1) was tied to a modified 18-crown-6 scaffold, known as 2-triazacryptand[2,2,3]-1-(2-methoxyethoxy)benzene (TAC)<sup>41</sup> which offers improved selectivity and quantum yield. After first exploring with the chelating abilities of coumarin benzothiazole (BTC), FluoZin, originally a  $\text{Zn}^{2+}$  dye, presented dequenching metal sensing upon the addition of  $\text{Tl}^+$  with the *N*-(2-methoxyphenyl)iminodiacetate chelation subunit. The addition of  $\text{Tl}^+$  dequenched the fluorescence and presented a brighter form of the dye.

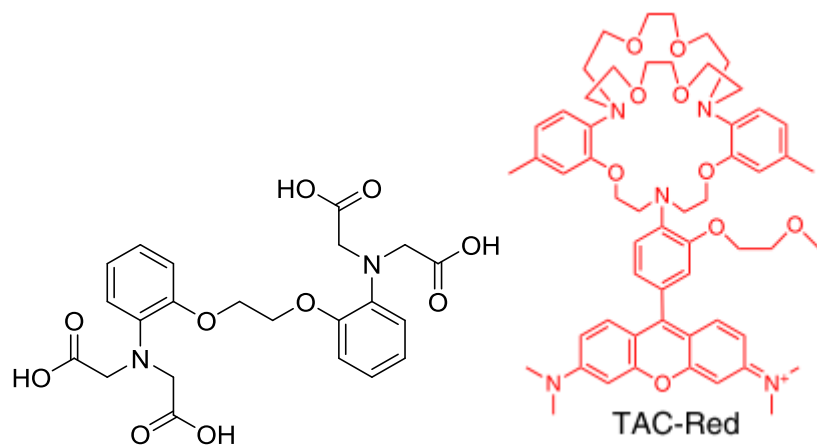


**Figure 4.1.** (Left) 1,2-bis(2-aminophenoxy)ethane-*N,N,N',N'*-tetraacetic acid (BAPTA) developed by Tsien chelates  $\text{Ca}^{2+}$ . (Right) 2-triazacryptand[2,2,3]-1-(2-methoxyethoxy)benzene (TAC-RED) are selective for  $\text{K}^+$ .

The requirement of a metal sensor that permitted a brighter fluorophore with  $\text{Tl}^+$  drove towards the development of Thallo<sup>TM</sup> <sup>13</sup>, a BAPTA-AM hybrid linked to a xanthene fluorophore.

### ***“Protected” Dyes Used For Enzymatic Studies***

Using fluorogenic substrates to measure catalytic efficiency of enzymes has been well established in the latter half of the 21<sup>st</sup> century. Coumarin, a benzopyrone dye scaffold commonly emitting in the blue-green spectrum (>450 nm) is an early example of a modified peptide substrate used to measure enzymatic properties. The activity of trypsin, chymotrypsin and elastase were elucidated by coupling 7-amino-4-methylcoumarin with peptide chains specific to their respective enzyme substrate<sup>42</sup>. Fluorescein and rhodamine dyes have also been previously utilized in enzyme activity assays. Fluorescein, when acetylated, produces the readily hydrolyzed ester by cellular esterases. Rhodamine amide protecting groups are not easily hydrolyzed and provide a resistant alternative with similar xanthene fluorescent properties. Previously, Lavis and coworkers had identified Porcine Liver Esterase (PLE) as a promiscuous hydrolase to activate their “trimethyl lock” (Figure 4.2) and release their modified rhodamine<sup>43</sup>. Originally, the trimethyl lock moiety had been installed to combat spontaneous hydrolysis

in aqueous solutions. Their substrate was well tolerated by PLE ( $K_{cat}/K_M = 8.2 \times 10^5 \text{ M}^{-1}\text{s}^{-1}$ ) and suggested that it may accommodate a variety of amide functionalities. Pig or Porcine Liver Esterase (PLE) is a carboxyl esterase that has had previous applications as a biocatalyst<sup>44</sup>. The heteromeric enzyme is composed of three subunits ( $\alpha$ ,  $\beta$ ,  $\gamma$ ) and exists as a trimeric form. Utilization of this exogenous enzyme allowed the cleavage of the sterically congested trimethyl lock to release the rhodamine. We considered this caged rhodamine example and thought we could apply a similar principle to provide us with a rhodamine 110 pro-dye.

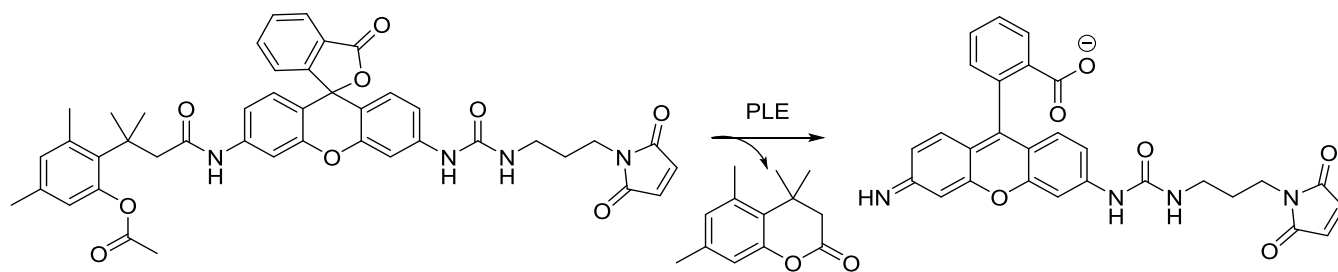


**Figure 4.2.** Trimethyl lock scheme using PLE activated rhodamine protecting group<sup>43</sup>.

Rhodamine 110, protected as a diamide, emits very weak fluorescence but when substituted with a peptide sequence specific to proteases, will then emit strong fluorescence when one of those amide bonds are cleaved<sup>45</sup>. The rate of increase in fluorescence<sup>45</sup> can then be detected to find the enzyme's catalytic efficiency ( $K_{cat}/K_M$ ). We explored the idea of a protected dye that would demonstrate weak fluorescence as a diamide but when in the presence of an enzyme engineered into the cell line, would then act as rhodamine 110. This concept had been also utilized to allow the passage of dye into cells as the open quinoid form with rhodamine 123, which would then be deesterified by endogenous esterases, and act as rhodamine 110 (Figure 4.3, route A) based on reported literature<sup>38</sup>. Conversely, we would prepare diamide protected rhodamines in the closed, spiro-lactone conformation and cells expressing the enzyme of interest would release the fluorophore into the fluorescent rhodamine 110 (Figure 4.3, route B). The preparation of amide protected rhodamines offered a unique and relatively simple way of caging the dye

without too much scaffold modification or a complicated release mechanism. We set forward with initial synthesis of PLE selective rhodamine dyes.

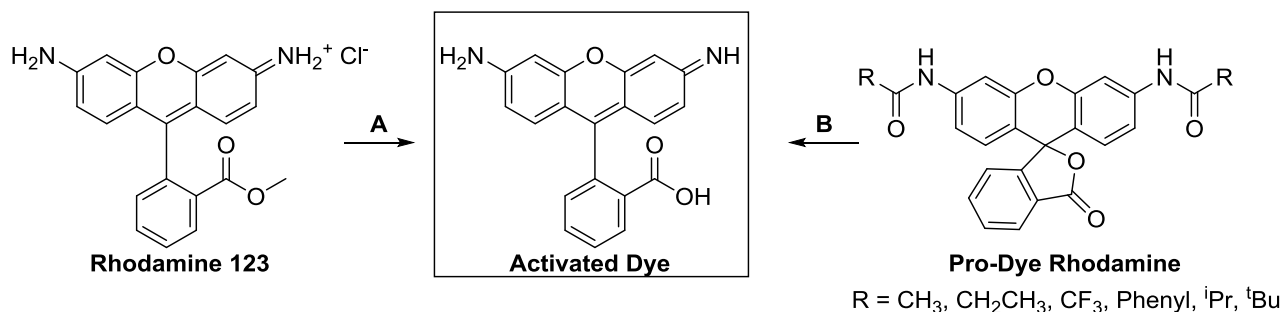
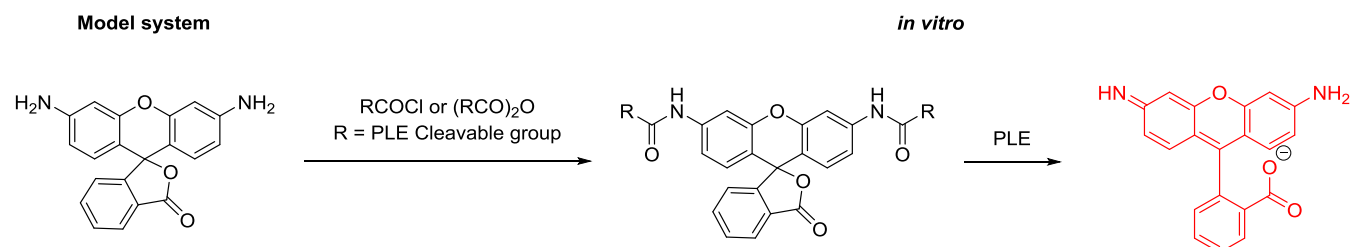


**Figure 4.3.** Activated dye from A (Intracellular esterases<sup>38</sup>) or B (Exogenous hydrolase/amidase)

### 4.3 Synthesis of PLE-Selective Rhodamine Dyes

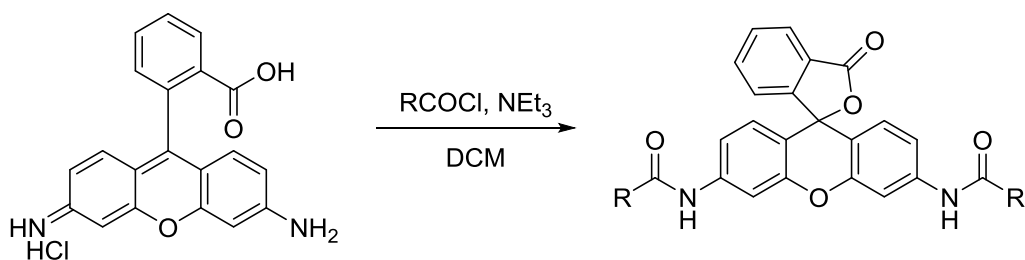
The salt form of rhodamine 110 is commercially available in large quantities. Formation of the diamide protection groups proceeded through either preparation or purchase of the acid chloride derivative



**Scheme 4.2.** Synthesizing and evaluating PLE-Pro Dye Rhodamines. R = CH<sub>3</sub>, CH<sub>2</sub>CH<sub>3</sub>, CF<sub>3</sub>, Phenyl, <sup>i</sup>Pr, <sup>t</sup>Bu.

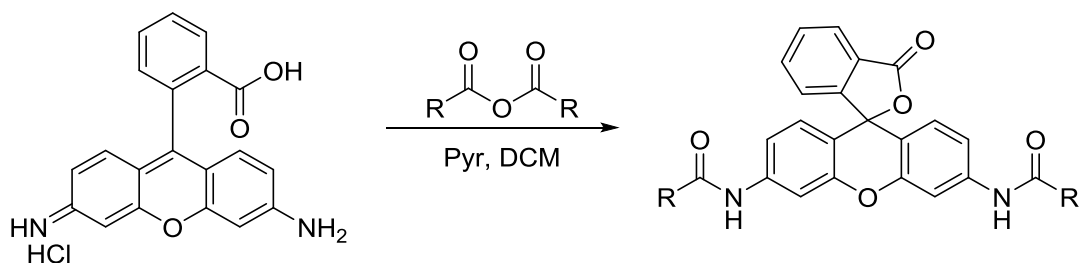
or the respective anhydride (Table 4.1). Deprotection would then be detected (through change in fluorescence) by introduction of dyes to a solution of PLE in assay buffer. Due to the nature of the xanthene scaffold, once the rhodamine nitrogens had been acetylated, isolation on silica proceeded smoothly. Yields varied from 42-91%, mostly recovering unreacted and/or mono-protected rhodamine species. Products were crystalline solids often colorless or faintly orange.

**Table 4.1.** Synthesis of pro-dye rhodamines with ID/VU number, derivative type and yield of reactions. Reaction conditions: [a] 2.2 eq acetic or propionic anhydride, 2.1 eq. pyridine and 0.4M DCM. [b] 2.2 eq RCOCl, where R = <sup>t</sup>Pr, <sup>t</sup>Bu or Ar, 5.0 eq. NEt<sub>3</sub>, and 0.1M DCM. [c] 4.0 eq. (CF<sub>3</sub>CO)<sub>2</sub>O, 4.0 eq. NaH, 0.7 M DMF.



Compound	ID Number	R =	Reaction	% Yield
<b>4.1a</b>	0000024HO	<sup>t</sup> Bu	b	91
<b>4.1b</b>	0000024HF	<sup>i</sup> Pr	b	83
<b>4.1c</b>	0000024HD	Ar	d	42

**Table 4.1 cont.** Synthesis of pro-dye rhodamines with ID/VU number, derivative type and yield of reactions. Reaction conditions: [a] 2.2 eq acetic or propionic anhydride, 2.1 eq. pyridine and 0.4M DCM. [b] 2.2 eq RCOCl, where R = <sup>i</sup>Pr, <sup>t</sup>Bu or Ar, 5.0 eq. NEt<sub>3</sub>, and 0.1M DCM. [c] 4.0 eq. (CF<sub>3</sub>CO)<sub>2</sub>O, 4.0 eq. NaH, 0.7 M DMF.



Compound	ID Number	R =	Reaction	%Yield
<b>4.1d</b>	VU0806840	CH <sub>3</sub>	a	89
<b>4.1e</b>	0000024HQ	CH <sub>3</sub> CH <sub>2</sub>	a	83
<b>4.1f</b>	VU0806841	CF <sub>3</sub>	c	76

Various protected rhodamine derivatives detailed preparation can be found in the experimental section (4.9 Experimental). The enzymatic reactivity of the protected rhodamine dyes were then explored with commercially available PLE substrate.

#### 4.4 Enzymatic Reactivity of PLE with Prepared Rhodamines

We first determined that no deprotection would occur in aqueous solutions before examining the stability of the fluorophore in non-transfected cells. All protected rhodamine dyes had no absorbance or emission near to the reported values of Rhodamine 110 ( $\lambda_{\text{max}} = 496 \text{ nm}$ ,  $\lambda_{\text{em}} = 517 \text{ nm}$ )<sup>43</sup>. This suggested that the fluorophores were locked into the spiro-lactone closed form and non-fluorescent. When mixed with a solution of PLE in assay buffer (See Experimental), increase in fluorescence was recorded as the



rhodamine dyes were deprotected by the enzyme. We detected the immediate removal of the trifluoroacetamide group and learned that this is our most labile pro-dye. We were also pleased to see the deprotection of the other available pro-dyes, but noticed that there was a change in rate of fluorescence between the different pro-dye protecting groups. Initially, we had been transfecting PLE weekly for our assays, but these results encouraged us to generate a PLE expressing cell line and measure change in fluorescence. Fortunately, we had previous examples of cell lines expressing PLE through the publications of Lavis and coworkers<sup>18</sup>.

#### **4.5 Pro-Dye Selectivity With Transient and Stable PLE cell lines**

##### ***Transiently Transfected HEK-293 with PLE***

*In situ* experiments with PLE demonstrated that the esterase could deprotect the pro-dye as an active rhodamine dye. Previous authors had reported expressing PLE in a stable cell line but before producing the PLE cell-line, we transiently transfected PLE into readily available HEK-293 and incubated with the pro-dyes. The results of these early transfections were encouraging (Figure 4.3) with excellent selectivity for dye fluorescence in +PLE transfected cells. When compared to the standard bis-acetylated fluorescein dye (de-esterified by endogenous esterases), we noted an absence of cellular fluorescence at the same exposure times. These results were encouraging and led to the development of PLE expressing cell line. We transiently transfected HEK-293 cells expressing GIRK1/2 and under selective pressure, were able to show fluorescent activity on cells that had been positively transfected with PLE. With these results, we then moved to a stable cell line expressing PLE.

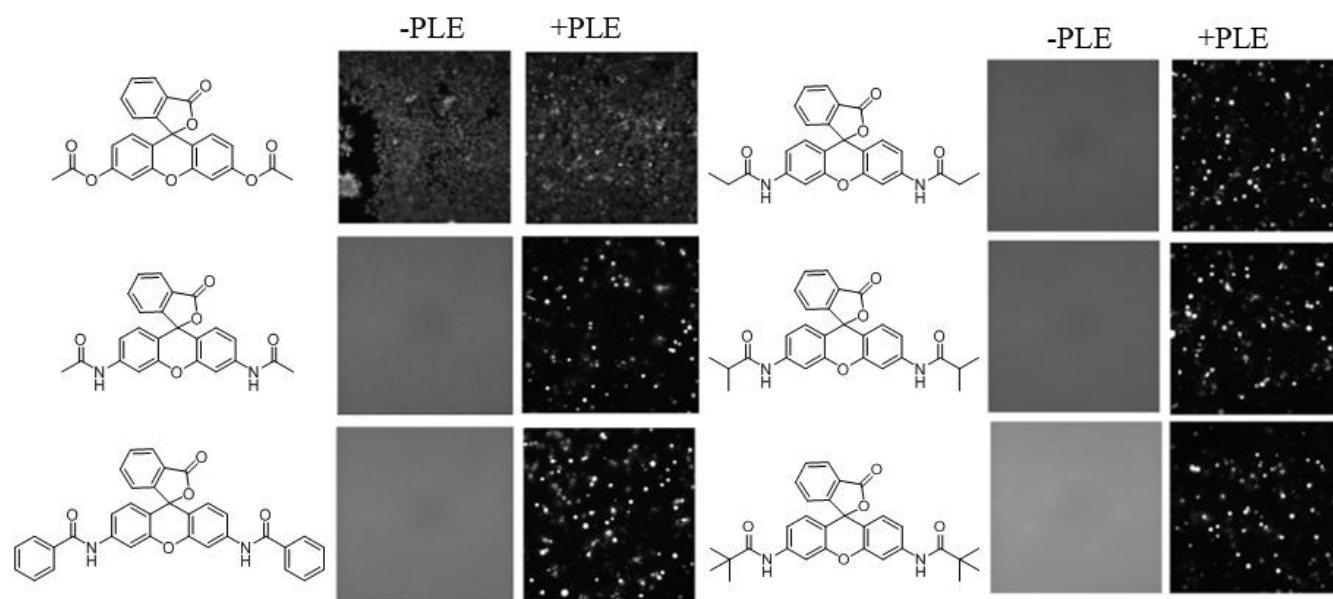


**Figure 4.4.** +/-PLE transiently transfected HEK-293 incubated (1h) with pro-dyes [10 $\mu$ M]. PLE expressing cells showed fluorescence (0.1ms) when excited at 490nm.

### *Stable PLE Expressing HEK-293 Cell Line*

Previous publications had provided us with a place to begin, first by subcloning PLE into pcDNA3.1/Zeo vector (See Experimental). This work had been performed by Kristopher K. Abney of the Weaver laboratory. Production of the PLE expressing cell line has been explained in detail in the experimental section. We could quickly determine expression by fluorescence of PLE expressing cells when incubated in the pro-dye. This compared to our bisacetylated fluorescein standard, there was an absence of fluorescence detected in cells that did not express PLE. Compared to the transiently transfected PLE cells, the stable expressing PLE cell line was brighter in fluorescence. To verify our observation of variable deprotection rates, we compared the rate of fluorescence using the Panoptic kinetic plate reader.

#### 4. 6 Rate of Pro-Dye Deprotection Using Kinetic Plate Reader (Panoptic)

With the stable PLE producing cell line now accessible, the rate of deprotection with the enzyme *in vitro* can now be determined. First, we desired to repeat our *in situ* findings with by modifying the assay to our needs. Serial dilutions of the pro-dyes would need to be added at a zero time point to generate a best fit ( $v^{-1}/[S]^{-1}$  and  $K_m$ ) of the rate of fluorescence with the cells. Panoptic, a kinetic plate reader used for assay screening was utilized. Cells expressing PLE were plated and pro-dyes were added in three-fold serial dilutions, starting with [40 $\mu$ M] and change in fluorescence was observed (Figure 4.5).

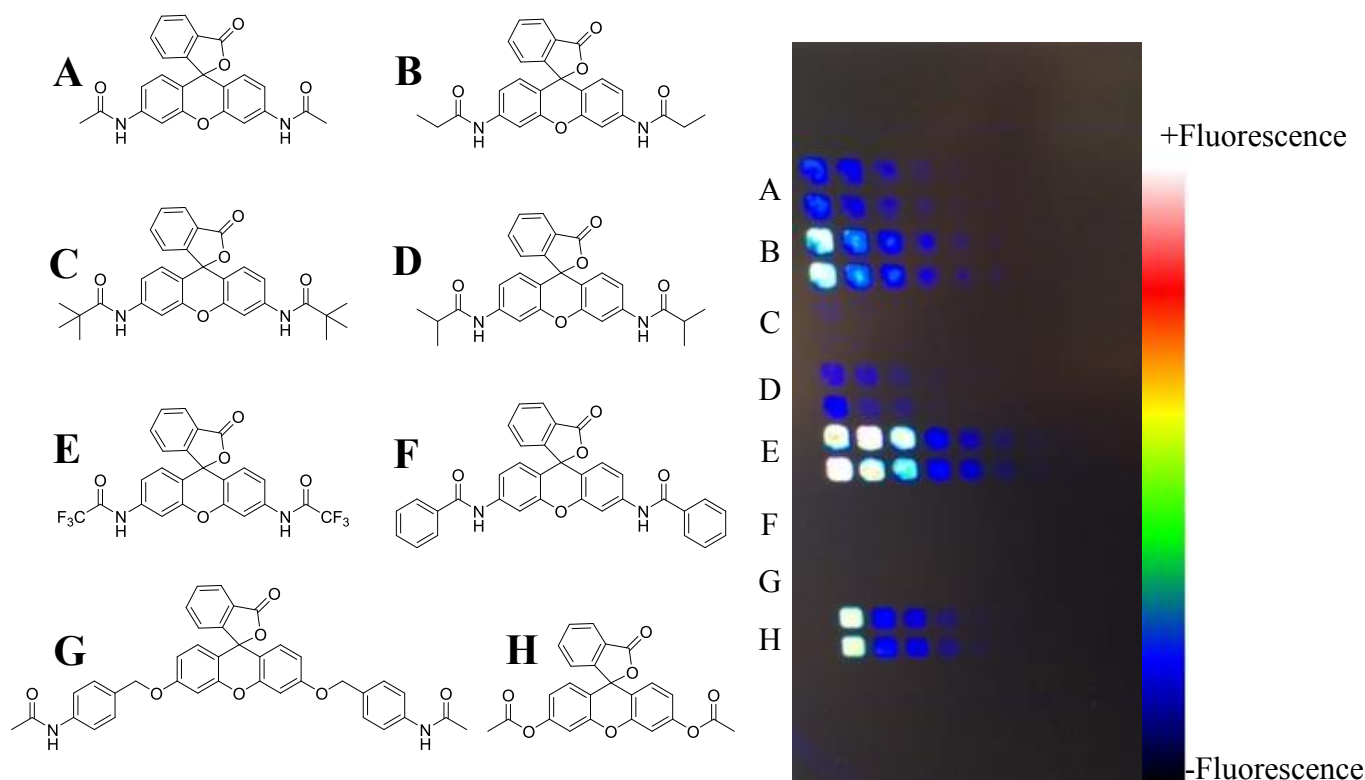
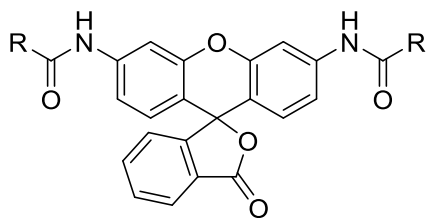


**Figure 4.5.** +PLE stable cell line generated by K. Abney (Weaver). Raw activity data: Rate of fluorescence detected by kinetic plate reader on HEK-293 +PLE when exposed to pro-dye serial dilutions. Fluorescence (+) indicated by white and absence of fluorescence as black. Pro-Dye G was developed based on previously reported methods<sup>46</sup>.

We were able to record the change in fluorescence based on concentration of our dyes when exposed to cells expressing PLE. As expected, the deprotection of trifluoromethyl acetamide was our most labile

protecting group and rapidly fluoresced upon addition to the PLE expressing cells. We were interested to see if the rate of deprotection with PLE *in situ* was comparable to diffusion and deprotection inside of our PLE expressing cell line. First, we wanted to verify if there would be a difference between diffusion of the dye into the cells and rate of deprotection. This suggested that the possible difference in derivative deprotection was substrate/enzyme related and not permeability into the cell. The relative rates of deprotection were generated based on concentration response series. We did not generally detect a major increase or decrease in time of onset onto fluorescence, in fact, we were pleased to see the similar trends of high activity with the trifluoroacetamide when compared *in situ* PLE activity and cells expressing PLE. When the slope (concentration/activity) was plotted over time, we uncovered comparable trends in activity of the enzyme alone or cells expressing PLE (Table 4.2).

**Table 4.2.**  $K_m$  of Pro-dye rhodamine derivatives rate of deprotection by PLE reported as [dye] of PLE expressing cells compared to *in situ*.



Compound	R Group	Cell (M)	<i>In situ</i> (M)
<b>4.1d</b>	CH <sub>3</sub>	1.90 X10 <sup>-4</sup>	1.63 X10 <sup>-4</sup>
<b>4.1e</b>	CH <sub>2</sub> CH <sub>3</sub>	1.85 X10 <sup>-4</sup>	1.65 X10 <sup>-4</sup>
<b>4.1b</b>	<sup>i</sup> Pr	2.17 X10 <sup>-4</sup>	2.40 X10 <sup>-4</sup>
<b>4.1a</b>	<sup>t</sup> Bu	1.81 X10 <sup>-4</sup>	2.30 X10 <sup>-4</sup>
<b>4.1f</b>	CF <sub>3</sub>	1.92 X10 <sup>-4</sup>	2.67 X10 <sup>-4</sup>
<b>4.1c</b>	Aryl	3.87 X10 <sup>-4</sup>	4.76 X10 <sup>-5</sup>

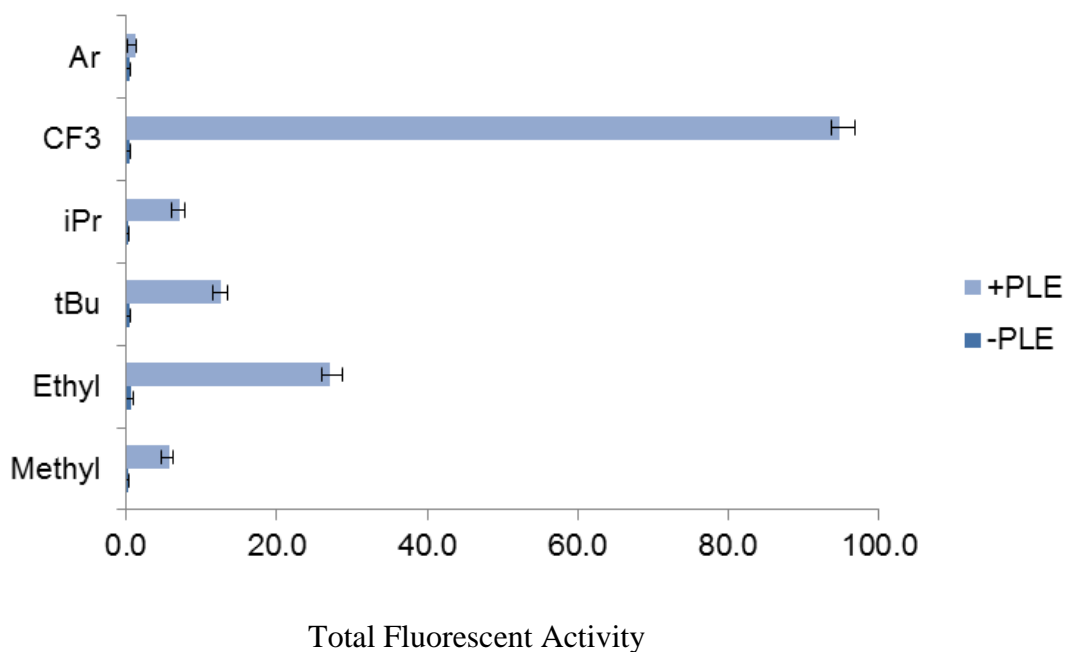


**Figure 4.6.** Histogram representing activity (total fluorescence normalized to rhodamine control) of PLE substrate rhodamines in +/-PLE cells. 100% equals total fluorescent activity of the control standard. The  $-CF_3$  protected acetamide rhodamines were the most active compared to aryl or methyl, but surpassed by “ethyl” protected acetamide (propionamide).

Rates of deprotection of pro-dyes varied based on amide groups (Figure 4.5). The strongly electron withdrawing group trifluoromethyl acetamide had the highest rate of fluorescence increase compared to the other pro-dyes, suggesting that this group was incredibly liable for rhodamine deprotection. Next, the propionamide seemed to offer more of the properties we were looking for, both being reasonable liable but offering some chemical stability. We decided to move forward with the propionamide “ethyl” protected rhodamines as our PLE pro-dye for use in selectivity assays.

#### 4.7 Applying Pro-Dyes in Selectivity Assays

We originally desired to have a selective dye, that only under the correct conditions, would fluoresce and give us an advantage by reducing background noise typically experienced by other fluorescent dyes. Our first thought was to use the pro-dye/enzyme pair as a screening tool, first in cells that selectively expressed our enzyme of interest, and then primary cultures of tissue, which would then

repress any tissue that did not contain the correct factors. Unfortunately, when screening for possible aryl-amide substrates of PLE (NIH Clinical Collection I and II ~760 compounds), we identified a number of “inhibitors” of PLE in the assay (~25% showed inhibitor activity). This would lead to false positives, or ineffective dye activity if we were to continue use of this pro-dye/enzyme pair in experimental compound conditions. A variety of these test compounds had a scaffold that contained an aryl amide. Due to these uncertainties, we would need to use the pro-dye with substrates that would not inhibit PLE.

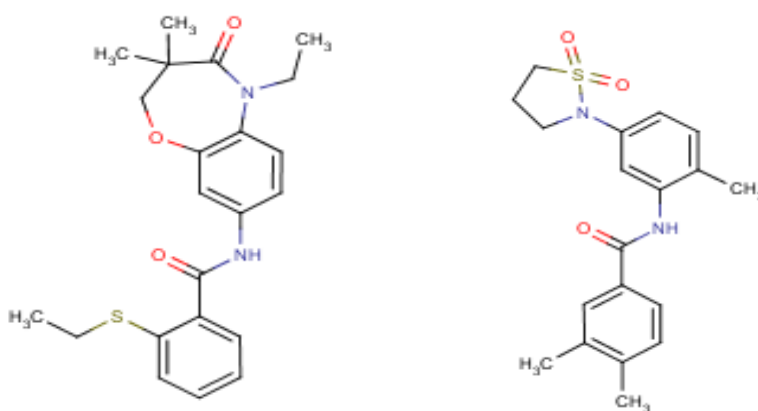


**Figure 4.7.** (Left) VU0523039 and (right) VU0496934 positive hits for PLE “inhibition”.

### ***Rhodamine Pro-Dyes to Study Mitochondria***

Early studies of mitochondria have showed that they play an important role in the generation of energy essential for a cell. It is no surprise that morphology of a mitochondria influenced by differing states of a cell, including cell cycle and pathological states. Much work has been done in the area of dye staining of mitochondria in living cells, commonly used in fluorescence microscopy, flow cytometry and spectroscopy. Rhodamine 123, the methyl ester version of rhodamine 110 (Figure 4.8) with the locked “open quinoid” form, is specifically taken up by mitochondria (as a substrate or passively diffused<sup>38</sup>) with little to no staining of the nucleus and presents low cytotoxic effects<sup>47</sup>.

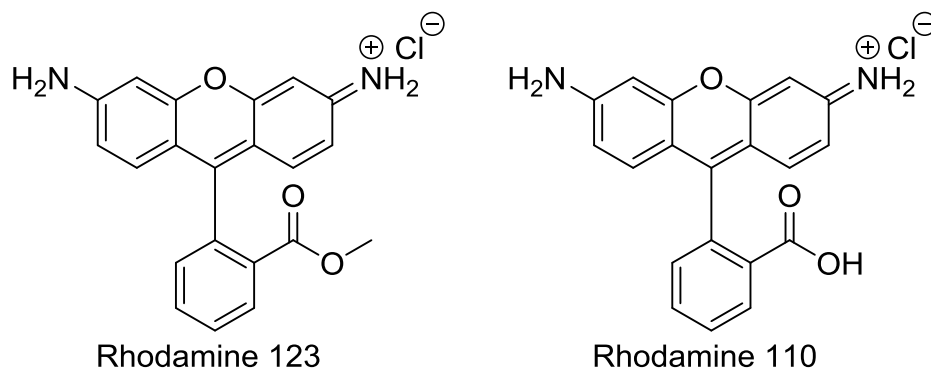


**Figure 4.8.** Rhodamine 123 and 110 cellular dyes

Rhodamine 123 is metabolized into rhodamine 110 by intracellular esterases<sup>38</sup> which has different fluorogenic properties and glucuronidated<sup>48</sup> as a substrate for MRP2<sup>49</sup>. Based on earlier assumptions that rhodamine 123 is converted into rhodamine 110, we expected that our pro-dye rhodamines would also be taken up by the mitochondria in a similar manner.

### ***Rhodamine Pro-Dyes Cellular Staining***

Based on previous work exploring the metabolism of rhodamine 123 to rhodamine 110, we expected a similar route with the pro-dye as a PLE substrate. Due to this assumption, we anticipated that rhodamine 110 was the active form of the dye that stained mitochondria and expected this to occur with the pro-dye substrates. Inversely, this was not the case as shown in Figure 4.8. In +PLE expressing cells, we compared our “ethyl” pro-dye, rhodamine 123 and rhodamine 110. Rhodamine 123 performed as expected but with a relative lower fluorescent signal than rhodamine 110 or the pro-dye. Cytosolic staining was observed with rhodamine 110 and the pro-dye. We reasoned this could be due to the “overloading” of the cells with dye and visually blocking any potential mitochondrial signal. Mechanistically, we expected that rhodamine 123 would be converted into rhodamine 110, but there is a disconnection between when and where this occurs. Additional evidence suggests at least one metabolic pathways for rhodamine 123 (as it has been used for tumor identification in murine studies<sup>48</sup>), a glucuronidated



metabolite that returns to the parent rhodamine 123 upon incubation with  $\beta$ -glucuronidase. These results were initially disappointing but suggested an additional line of thought. The mechanism for rhodamine 123 to rhodamine 110 had been well established but we could not conclude that was the case with the conversion of our pro-dyes into rhodamine 110. We were approaching the mechanism of deesterification in a linear way: rhodamine 123 is deesterified into rhodamine 110. It is not entirely impossible that rhodamine 123 metabolites are formed. In addition to metabolites, we had not even begun to address how a dianion fluorophore will accumulate in different regions of the cell than a zwitterion or even a neutral fluorophore. The most basic pH assumption is that positively charged rhodamine species accumulate in the mitochondria due to the negative membrane potential. I offer some approaches to answer these questions in Chapter 5 – though superficial as a mitochondrial membrane sensor, we can begin to explore what may actually be happening to rhodamine 123 and our pro-dyes.

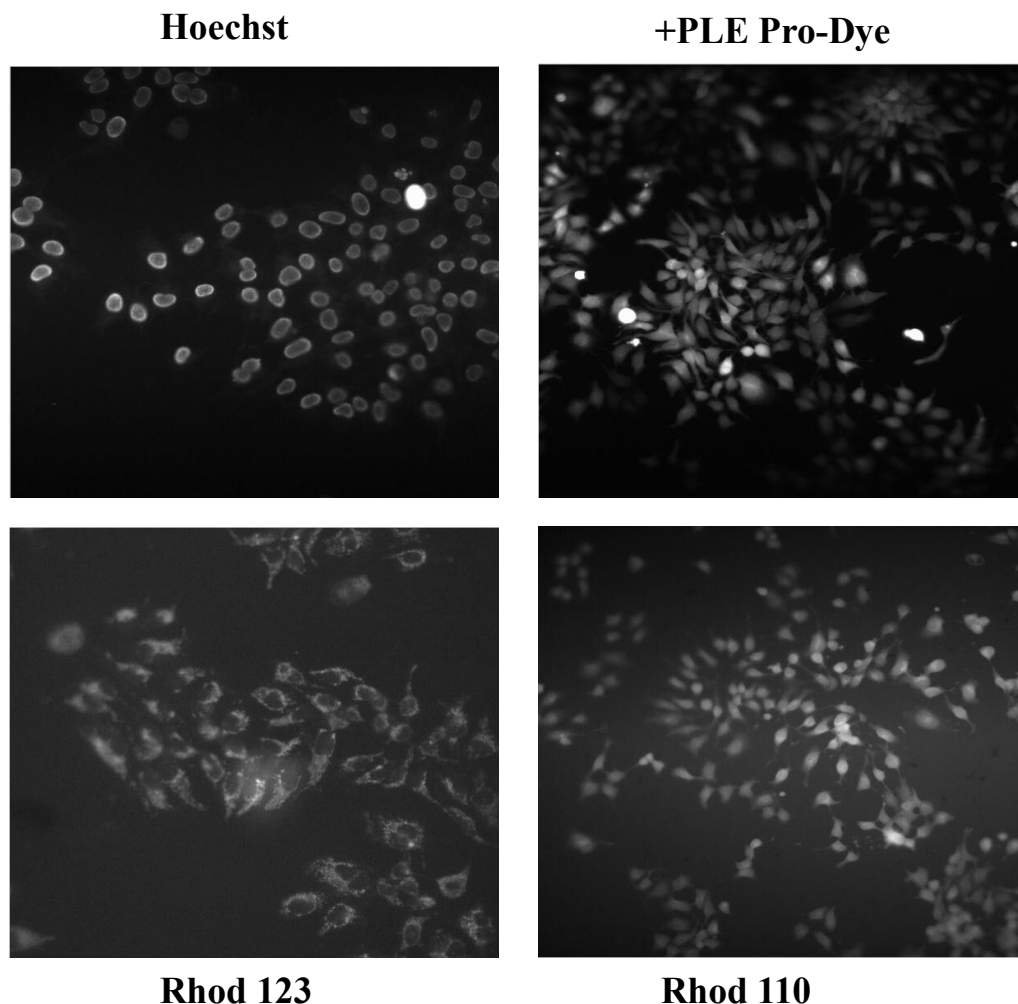


**Figure 4.9.** Cellular staining of HEK-293 cells expressing PLE. All dyes incubated at [10 $\mu$ M] for 30 minutes. Images obtained at 350 or 490nm excitation at respective exposure times. (Top Left) Hoechst nuclear stain 0.01ms (Top Right) "Ethyl" pro-dye selectively fluoresces with +PLE expressing cells. Note cytosolic accumulation 0.01ms (Bottom Left) Rhodamine 123 mitochondrial dye 0.2ms. (Bottom Right) Rhodamine 110 accumulates in the cytosol similar to the activated pro-dye 0.01ms.

#### 4.8 Conclusion and Future Directions

In this chapter, we successfully demonstrated pro-dye/enzyme selectivity with PLE expressing cells with a variety of pro-dye rhodamine derivatives. Additionally, we were able to identify our best pro-dye substrates using PanOptic kinetic plate reader assay by reporting the increase in fluorescence over time with varying concentrations (R= CF<sub>3</sub>, CH<sub>2</sub>CH<sub>3</sub>). Previously reported by Lavis, caged compounds have the ability to be selectively activated but this work was the first demonstration of a variety of similar

substrates that had been evaluated for their enzymatic affinity and selectively activated. The utility of producing a number of similar dyes and assaying with an exogenous enzyme offers a high potential for future use in cellular assays. We suggested the use of the dyes as mitochondrial membrane potential sensors and still potentially could be used for that purpose. Additional important questions have formed based on cellular staining results, perhaps examining our understanding of the endogenous conversion of rhodamine 123 to rhodamine 110, which now will be explored in Chapter 5.

## 4.9 Experimental

### *General Experimental*

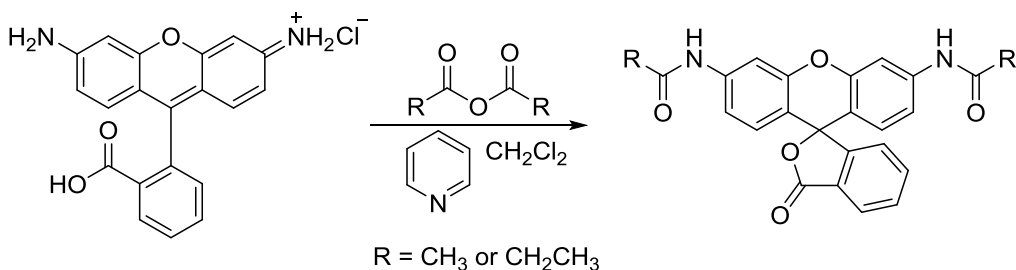
All glassware used for reactions was flame dried under vacuum. All reagents and solvents were commercial grade and purified prior to use when necessary. All reactions were performed under argon atmosphere unless otherwise stated. Diethyl ether (Et<sub>2</sub>O) and dichloromethane (CH<sub>2</sub>Cl<sub>2</sub>) were dried by passage through a column of activated alumina using an MBraun MB-SPS dry solvent system. Tetrahydrofuran (THF) was distilled from sodium with benzophenone as indicator prior to use.

Reactions were monitored by analytical thin-layer chromatography performed on Analtech silica gel GF 250 micron plates. The plates were visualized with UV light (254 nm) and either potassium permanganate, ceric ammonium molybdate, or p-anisaldehyde followed by charring on a hot-plate. Flash chromatography utilized 230-400 mesh silica gel (SiO<sub>2</sub>) from Sorbent Technologies or Silica RediSep Rf flash columns on a CombiFlash Rf automated flash chromatography system. Solvents for extraction, washing and chromatography were HPLC grade.

Nuclear magnetic resonance (NMR) spectra were acquired on either a 300 MHz Bruker DPX-300 FT-NMR, a 400 MHz Bruker AV-400 FT-NMR, or 500 MHz Bruker DRX-500 FT-NMR Spectrometer at ambient temperature. <sup>1</sup>H and <sup>13</sup>C NMR data are reported as values relative to CDCl<sub>3</sub>. <sup>1</sup>H chemical shifts are reported in δ values in ppm. Data are reported as follows: chemical shift, multiplicity (s = singlet, d = doublet, t = triplet, q = quartet, br = broad, m = multiplet), integration, coupling constant (Hz). <sup>13</sup>C chemical shifts are reported in δ values in ppm. Low resolution mass spectra were obtained on an Agilent 1200 series 6130 mass spectrometer with electrospray ionization. High resolution mass spectra were recorded on a Waters Q-TOF API-US. Analytical HPLC was performed on an Agilent 1200 series with UV detection at 214 nm and 254

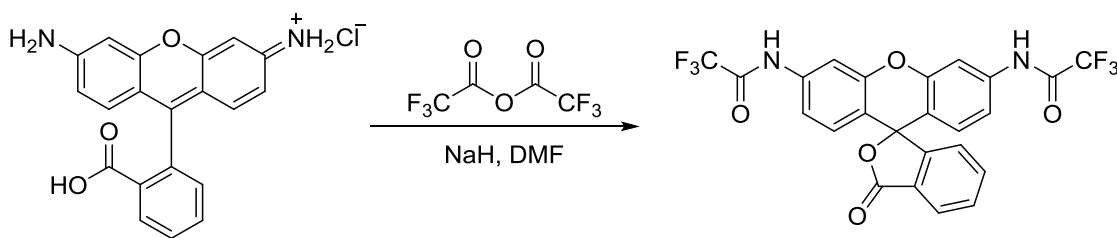
nm along with ELSD detection. Preparative HPLC was conducted on a Gilson 215 Liquid Handler HPLC system using Gemini-NX 50 x 20 mm column. Cellular imaging was done on a Zeiss Axiovert 200 microscope using 20X0.8 objective to collect fluorescence data.

### *Synthesis of Rhodamine Pro-dye PLE substrates*



**N,N'-(3-oxo-3H-spiro[isobenzofuran-1,9'-xanthene]-3',6'-diyl)diacetamide.** To a solution of Rhodamine 110 chloride (0.1g, 0.27 mmol) in dichloromethane (0.4M) were added acetic anhydride (0.06 mL, 0.6 mmol) and pyridine (0.1mL, 0.57 mmol). The mixture was stirred until judged complete by TLC (1:1 hex/EtoAc). When complete, reaction was washed with sodium carbonate (20 mL) and extracted with EtOAc (3X50mL). Organic layer was combined, dried over MgSO<sub>4</sub>, and concentrated *in vacuo* to yield a crude orange solid. The residue was purified by column chromatography with hexane/ethyl acetate (4:1 to 1:1) to yield 89 mg (90%) of N,N'-(3-oxo-3H-spiro[isobenzofuran-1,9'-xanthene]-3',6'-diyl)diacetamide **4.1d** as a white solid. <sup>1</sup>H NMR (400 MHz, CDCl<sub>3</sub>): δ7.92 (d, J = 7.6 Hz 1H), 7.79 (s, 2H), 7.57 (m, 2H), 7.37 (s, 2H), 7.07 (m, 3H), 6.61 (d, J = 8.6 Hz, 2H), 2.13 (s, 6H). LCMS calculated for C<sub>24</sub>H<sub>18</sub>N<sub>2</sub>O<sub>5</sub> (M+H)<sup>+</sup> *m/z*: 414.4, Measured 415.0 *m/z*.

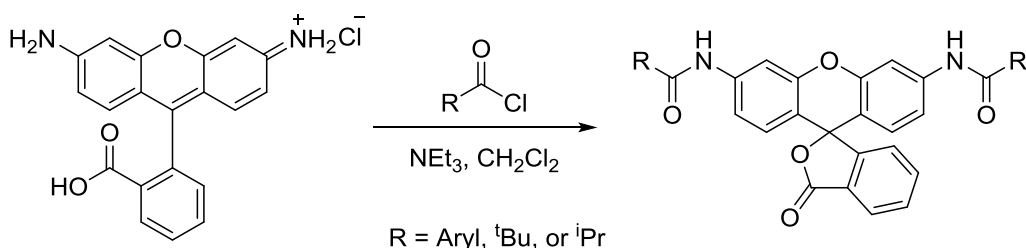
**N,N'-(3-oxo-3H-spiro[isobenzofuran-1,9'-xanthene]-3',6'-diyl)dipropionamide.** To a solution of Rhodamine 110 chloride (0.05g, 0.14 mmol) in dichloromethane (3.0mL, 0.4M) were added propionic anhydride (0.04 mL, 0.30 mmol) and pyridine (0.05mL, 0.286 mmol). The mixture was stirred until judged complete by TLC (1:1 hex/EtoAc). When complete, reaction was washed with sodium carbonate (20 mL) and extracted with EtOAc (3X50mL). Organic layer was combined, dried over MgSO<sub>4</sub>, and concentrated *in vacuo* to yield a crude orange solid. The residue was purified by column chromatography with hexane/ethyl acetate (1:1 to flush with EtOAc) to yield 50 mg (80%) of N,N'-(3-oxo-3H-spiro[isobenzofuran-1,9'-xanthene]-3',6'-diyl)dipropionamide **4.1e** as a white solid. <sup>1</sup>H NMR (400 MHz, MeOD): δ8.04 (d, J = 7.6 Hz, 1H), 7.81-7.71 (m, 4H), 7.23-7.16 (m, 3H), 6.72 (d, J = 8.8 Hz 2H), 2.42 (q, J = 7.6 Hz, 4H), 1.22 (t, J = 7.0 Hz, 6H). <sup>13</sup>C NMR (400 MHz, MeOD): δ8.53, 29.5, 82.8, 106.9, 113.6, 115.1, 123.6, 124.4, 126.1, 127.8, 129.8, 135.2, 141.0, 151.5, 152.9, 169.8, 174.1. LCMS calculated for C<sub>26</sub>H<sub>22</sub>N<sub>2</sub>O<sub>5</sub> (M+H)<sup>+</sup> *m/z*: 442.4, Measured 443.0 *m/z*.



**N,N'-(3-oxo-3H-spiro[isobenzofuran-1,9'-xanthene]-3',6'-diyl)bis(2,2,2-trifluoroacetamide)**

– To a solution of Rhodamine 110(100 mg, 0.3 mmol) in 5.0 mL of DMF added slowly NaH (60%, 50 mg, 1.2 mmol). This was then allowed to stir at R.T. for 1 h. At this time trifluoroacetic anhydride (170μL, 1.2 mmol) was added. This was then allowed to stir for 16 h. At this time AcOH (3 drops) was added and the organics were then concentrated. The crude product was then

purified by column chromatography with a gradient of 20-100% Hexane:EtOAc to afford 122 mg (76%) of the desired product **4.1f**.  $^1\text{H}$  NMR ( $\text{CDCl}_3$ )  $\delta$ 8.08 (d,  $J = 7.5$  Hz, 1H), 7.97 (bs, 2H), 7.79 (d,  $J = 2.0$  Hz, 2H), 7.74-7.66 (m, 2H), 7.19 (d,  $J = 2.0$  Hz, 1H), 7.17-7.15 (m, 2H), 6.89 (d,  $J = 8.6$  Hz, 2H);  $^{19}\text{F}$  NMR ( $\text{CDCl}_3$ )  $\delta$ -75.6; LCMS calculated for  $\text{C}_{24}\text{H}_{12}\text{F}_6\text{N}_2\text{O}_5$  ( $\text{M}+\text{H}$ ) $^+$  523.1  $m/z$ : Measured 522.9  $m/z$ . This compound had been graciously synthesized by Dr. Ian Romaine.



**N,N'-(3-oxo-3H-spiro[isobenzofuran-1,9'-xanthene]-3',6'-diyl)dibenzamide.** To a solution of Rhodamine 110 chloride (0.05g, 0.14 mmol) in dichloromethane (0.4M) and triethylamine (0.1mL, 0.682 mmol) were added benzoyl chloride dropwise (30 $\mu\text{L}$ , 0.30 mmol). The mixture was stirred until judged complete by TLC (1:1 hex/EtOAc). When complete, reaction was concentrated *in vacuo* to yield a crude orange solid. The residue was purified by column chromatography with hexane/ethyl acetate (1:1 to flush with EtOAc) to yield 30 mg (42%) of N,N'-(3-oxo-3H-spiro[isobenzofuran-1,9'-xanthene]-3',6'-diyl)dibenzamide **4.1c** as a white solid.  $^1\text{H}$  NMR (400 MHz,  $\text{CDCl}_3$ ):  $\delta$ 8.75 (s, 2H), 8.08 (d,  $J = 7.4$  Hz, 1H), 7.92 (d,  $J = 7.5$  Hz, 1H), 7.80 (d,  $J = 7.5$  Hz, 4H), 7.66-7.55 (m, 2H), 7.47-7.41 (m, 3H), 7.33-7.30 (m, 2H), 7.25-7.21 (m, 2H), 7.12 (d,  $J = 7.6$  Hz, 1H), 6.61 (d,  $J = 8.6$  Hz, 2H).  $^{13}\text{C}$  NMR (400 MHz,  $\text{CDCl}_3$ ):  $\delta$ 83.1, 108.4, 114.0, 116.2, 124.1, 124.9, 126.0, 127.2, 128.1, 128.3, 128.5, 129.8, 130.0, 131.9, 133.5, 134.1, 135.4, 140.2, 151.4, 152.9, 166.3, 169.9. LCMS calculated for  $\text{C}_{34}\text{H}_{22}\text{N}_2\text{O}_5$  ( $\text{M}+\text{H}$ ) $^+$   $m/z$ : 538.6, Measured 539.0  $m/z$ .

**N,N'-(3-oxo-3H-spiro[isobenzofuran-1,9'-xanthene]-3',6'-diyl)bis(2,2-**

**dimethylpropanamide)-** To a solution of Rhodamine 110 chloride (0.05g, 0.14 mmol) in dichloromethane (1.36mL, 0.4M) and triethylamine (0.1mL, 0.682 mmol) were added trimethylacetyl chloride dropwise (40 $\mu$ L, 0.30 mmol). The mixture was stirred until judged complete by TLC (1:1 hex/EtOAc). When complete, reaction was concentrated *in vacuo* to yield a crude orange solid. The residue was purified by column chromatography with hexane/ethyl acetate (1:1 to flush with EtOAc) to yield 55 mg (91%) of N,N'-(3-oxo-3H-spiro[isobenzofuran-1,9'-xanthene]-3',6'-diyl)bis(2,2-dimethylpropanamide) **4.1a** as a white solid. <sup>1</sup>H NMR (400 MHz, MeOD):  $\delta$ 8.03 (d, J = 7.6 Hz, 1H), 7.79-7.69 (m, 4H), 7.26-7.19 (m, 3H), 6.71 (d, J = 8.4 Hz, 2H), 1.31 (s, 18H). <sup>13</sup>C NMR (400 MHz, MeOD):  $\delta$ 26.2, 39.3, 83.2, 108.2, 113.9, 116.3, 123.6, 124.4, 126.2, 127.6, 129.8, 135.9, 140.9, 151.4, 153.0, 170.2, 178.6. LCMS calculated for C<sub>34</sub>H<sub>22</sub>N<sub>2</sub>O<sub>5</sub> (M+H)<sup>+</sup> *m/z*: 498.5, Measured 499.0 *m/z*.

**N,N'-(3-oxo-3H-spiro[isobenzofuran-1,9'-xanthene]-3',6'-diyl)bis(2-methylpropanamide)-**

To a solution of Rhodamine 110 chloride (0.05g, 0.14 mmol) in dichloromethane (3.0mL, 0.1M) and triethylamine (0.1mL, 0.682 mmol) were added isobutyryl chloride dropwise (10 $\mu$ L, 0.82 mmol). The mixture was stirred until judged complete by TLC (1:1 hex/EtOAc). When complete, reaction was concentrated *in vacuo* to yield a crude orange solid. The residue was purified by column chromatography with hexane/ethyl acetate (1:1 to flush with EtOAc) to yield 51 mg (83%) of N,N'-(3-oxo-3H-spiro[isobenzofuran-1,9'-xanthene]-3',6'-diyl)bis(2-methylpropanamide) **4.1b** as a white solid. <sup>1</sup>H NMR (400 MHz, MeOD)  $\delta$ 8.03(d, J = 7.4 Hz 1H), 7.81-7.70 (m, 4H), 7.22-7.17 (m, 3H), 6.71 (d, J = 8.6 Hz 2H), 2.65 (q, J = 6.8 Hz 2H), 1.21 (d, J = 6.8 Hz, 12H); <sup>13</sup>C NMR (400 MHz, MeOD)  $\delta$ 18.3, 35.6, 82.8, 107.1, 113.6, 115.3, 123.6, 124.4, 126.2, 127.8, 129.8, 135.3,



141.1, 151.5, 152.9, 169.8, 177.4; LCMS calculated for  $C_{23}H_{18}N_2O_4$  (M+H)<sup>+</sup> 470.5 m/z: Measured 471.0 m/z

## **Cellular Experimental**

### ***Cell Line Formation***

pCAG-PLE-IRES-mCherry (addgene, Lavis L) vector was taken and amplified using chemically competent DH5 $\alpha$  E.coli cells. The PLE-IRES-mCherry DNA was purified using QIAprep Spin Miniprep kit (Qiagen) and quantified on a NanoDrop ND-1000 spectrophotometer (Thermo Fisher). Using the protocols described by New England Biosciences, restriction endonuclease enzyme digestion used Not1-HF and Xho1 to cleave PLE-IRES-mCherry insert from the pCAG backbone. The digestion was purified by regular agarose gel electrophoresis using the QIAquick Gel Extraction kit (Qiagen). In order to confer selective pressure, the PLE-IRES-mCherry insert was cloned into pcDNA3.1/Zeo vector. The insert and vector were combined using T4 DNA ligase (Thermo Fisher). The pcDNA3.1/Zeo PLE-IRES-mCherry vector was introduced to HEK293 (ATCC) cells by means of cationic lipids (FuGENE HD Promega), and selected for by using Zeocin. Cells were maintained in cell culture medium, alpha MEM ( 10% vol/vol FBS (Thermo-Fisher) and 1% GlutaGro (Corning)) in a cell culture incubator at 37oC with 5% CO<sub>2</sub>.

### ***Kinetic Dye Assays***

For kinetic dye assays, we used PLE-IRES-mCherry expressing HEK293 cells (ATCC), referred to as PLE cells. PLE cells were dislodged from T-175 tissue culture flasks using TrypLE Express (Life Sciences, Carlsbad, CA), then transferred into a 50mL conical tube, and centrifuged at 500g for 2 min. The supernatant solution was aspirated and resuspended at a concentration of

~1000cell/ $\mu$ L in alpha MEM ( 10% vol/vol FBS (Thermo-Fisher) and 1% GlutaGro (Corning)) . Twenty  $\mu$ L of the cell suspension were plated into amine coated, clear-bottom, and black walled 384 well plate (cat# 354719, BD, Franklin Lakes, NJ) by an electronic multichannel pipette. Plates were then cultured overnight at 5% CO<sub>2</sub> in a cell culture incubator at 37°C. Following overnight incubation, cell culture medium was removed and replaced with dye-loading assay buffer (Hank's Balanced salt solution, 20mM HEPES). The dyes: R= CH<sub>3</sub>, CH<sub>2</sub>CH<sub>3</sub>, iPr, tBu, CF<sub>3</sub>, and Aryl were added into assay buffer with a final concentration of 0.01% DMSO. The plates were then loaded into a WaveFront Panoptic (Nashville, TN). The data were acquired at 1Hz (excitation 470 $\pm$  20nm and 540  $\pm$  30nm), then 20 $\mu$ L/well of the aforementioned dyes were added and incubated for 15 minutes. Fluorescence was measured following addition of dyes into cell wells and data collection continued for 15 total minutes. Data were analyzed using Microsoft Office as described in Kaufmann et al.<sup>9</sup> and slopes were collected. XLfit (IDBS, Surrey, UK) was utilized to create fits to a 4 parameter logistic equation. Test Dyes compounds were solubilized in DMSO to 50 $\mu$ M. A 7-point 3 fold serial dilution was achieved using an electronic pipette. All data represent at least 3 independent experiments per compound concentration and all DMSO concentration is 0.01% or less. Experiments involving FCCP, the cells were incubated with R= CH<sub>2</sub>CH<sub>3</sub> dye for 30 minutes. FCCP was then added to PLE cells and control cells in varying concentrations.

APPENDIX  
NMRS FOR CHAPTER 4

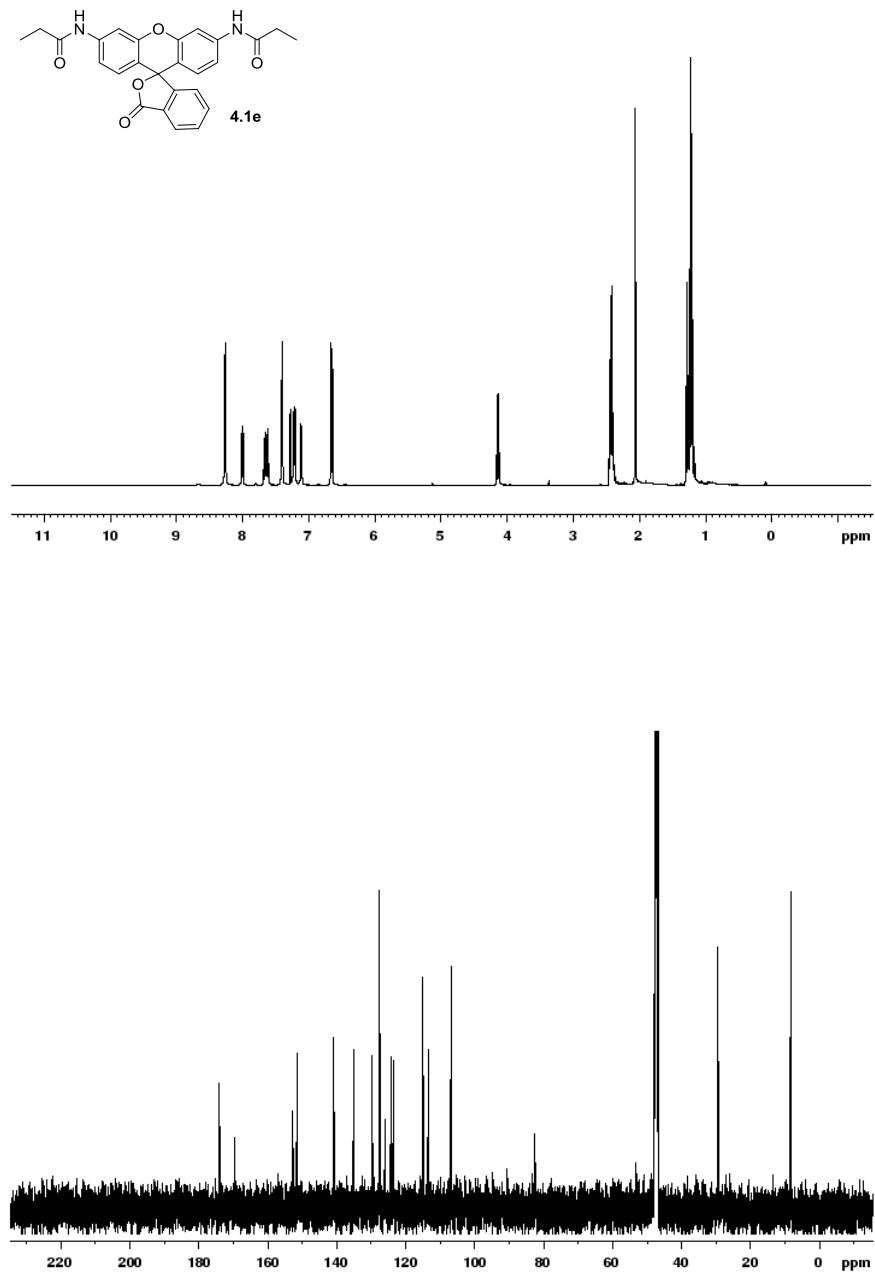


**Figure 4.9.** <sup>1</sup>H-NMR spectrum (400 MHz, MeOD) and <sup>13</sup>C-NMR spectrum (400 MHz, MeOD) of **4.1e**.

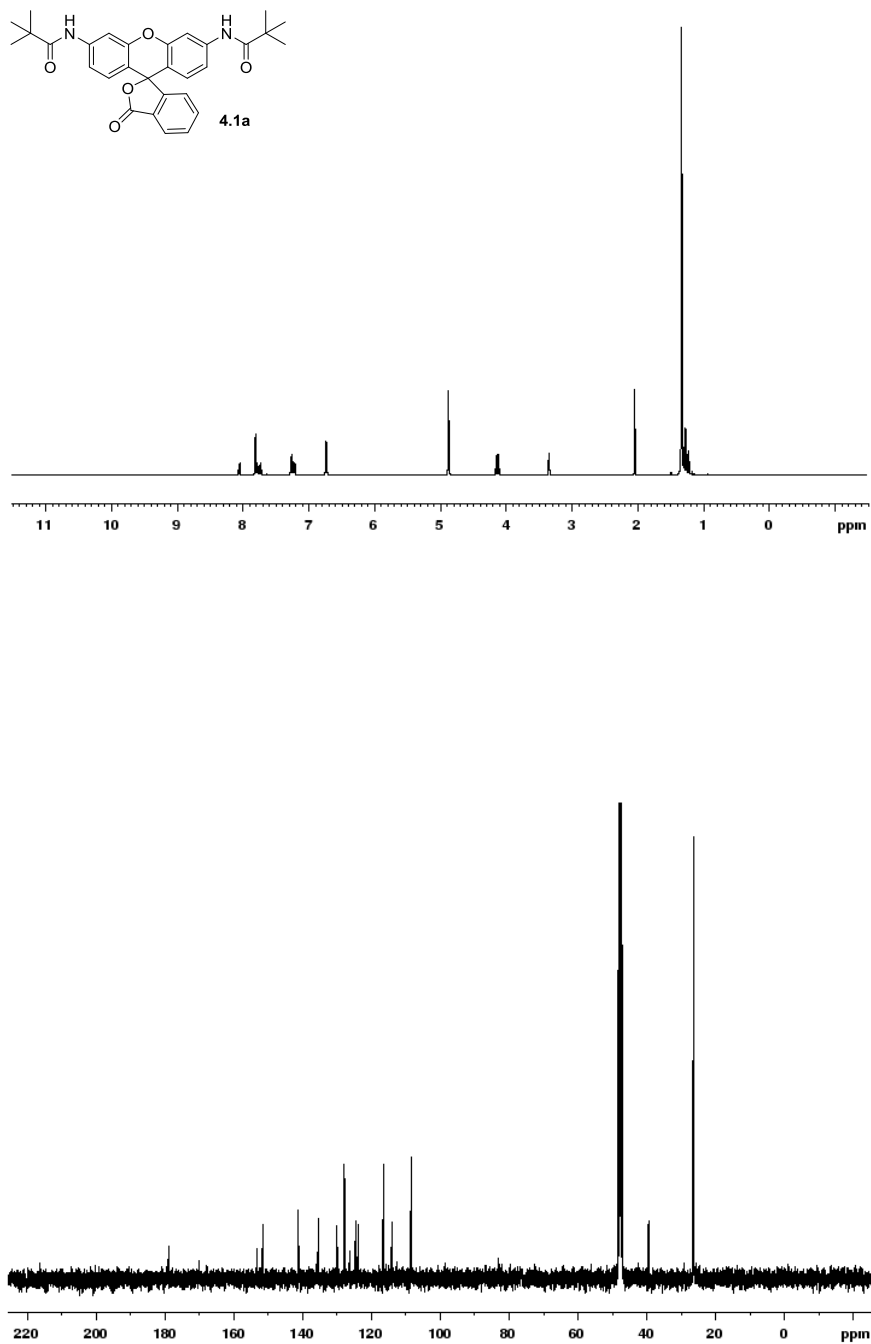


**Figure 4.10.** <sup>1</sup>H-NMR spectrum (400 MHz, MeOD) and <sup>13</sup>C-NMR spectrum (400 MHz, MeOD) of 4.1a.

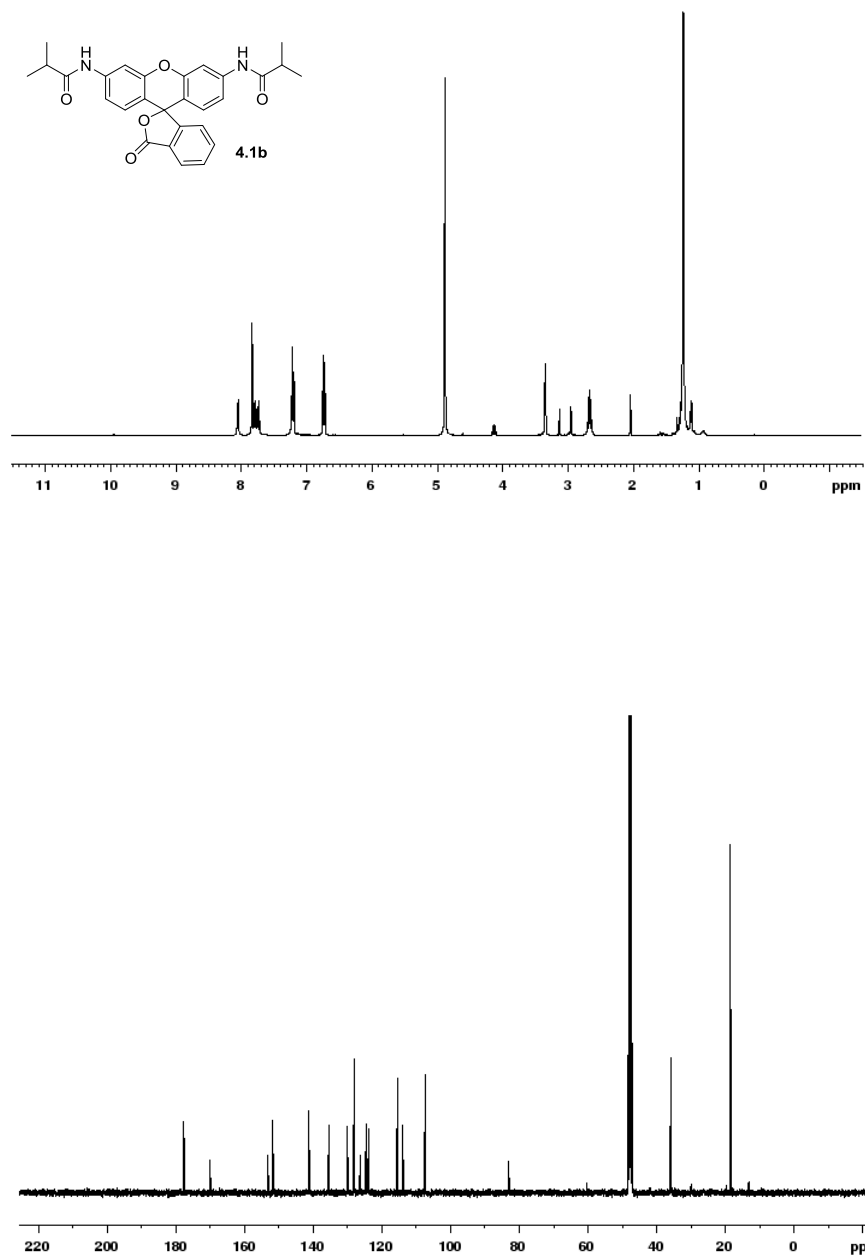


**Figure 4.11.**  $^1\text{H-NMR}$  spectrum (400 MHz, MeOD) and  $^{13}\text{C-NMR}$  spectrum (400 MHz, MeOD) of **4.1b**.

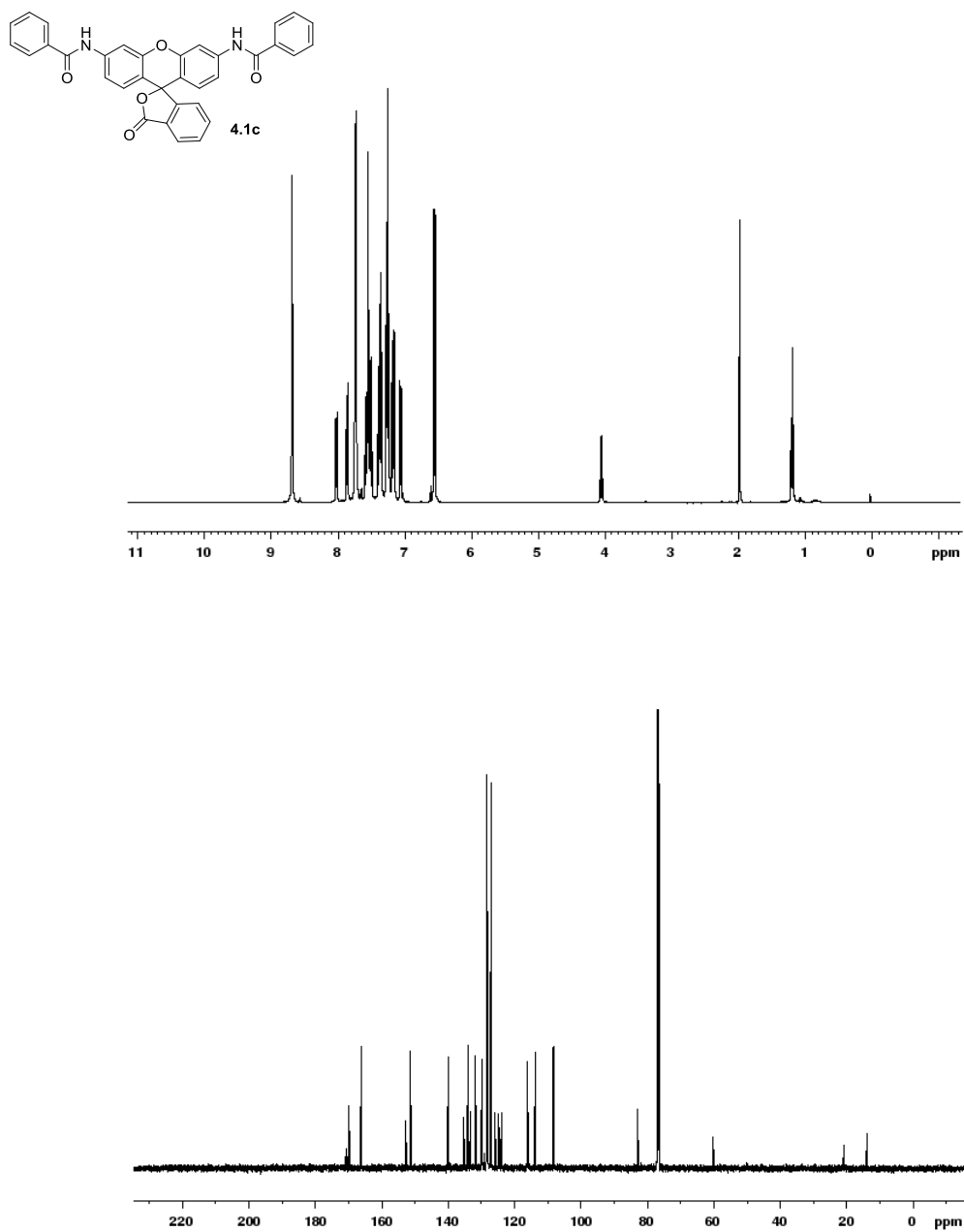


**Figure 4.12.**  $^1\text{H-NMR}$  spectrum (400 MHz, DMSO) and  $^{13}\text{C-NMR}$  spectrum (400 MHz, DMSO) of 4.1c.

## CHAPTER 5

### CONCLUSIONS AND FUTURE DIRECTIONS

#### 5.1 Introduction

This chapter serves as a place to expand upon ideas or questions we may have about the experiments previously described. In chapters 2 and 3, GIRK channels were heavily explored with an armory of molecular probe scaffolds. This opened up opportunities for other researchers to explore GIRK channels with their own probe design (Trauner, LOGOs) and propose some novel ideas for the exploration of binding pocket locations. Chapter 4 diverged from the GIRK probe theme but instead focused on fluorophore development for use in GIRK assays. Exploring selectively activated fluorophores provided a powerful platform for future discoveries with GIRK assays. Some questions have yet to be answers concerning the future use of pro-dye/enzyme pair but the following suggestions may lead a future researcher to the currently unsolved.

#### 5.2 Chapter 2 Conclusions and Future Directions of Discovery and SAR of a Novel Series of GIRK1/2 and GIRK1/4 Activators: “Sulfonamide Series”

The results of the work in chapter 2 helped to identify a novel scaffold that was still active on GIRK channels. Very recently published by the Trauner and Weaver<sup>50</sup>, light operated GIRK channel openers (LOGOs) were developed based on the sulfonamide scaffolds. Azo-benzenes are known to photo-switch or isomerize to a *cis* or *trans* geometry in the presence of light. The probe in figure 5.1 was synthesized and used to selectively activate GIRK1 containing GIRK channels at 440nm as the *trans*-isomer.

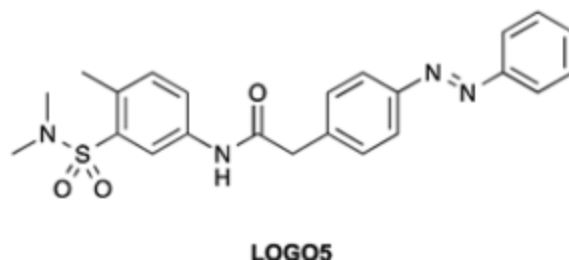


**Figure 5.1.** LOGO5 was found to selectively activate GIRK channels in the presence of 440nm.

Interestingly, LOGOs developed with the ML297 urea scaffold (not shown) were active as the *trans*-isomer but upon photolysis to the *cis*-isomer (360nm), only a small decrease of GIRK current was noted. Further attention then went to the development using the amide based scaffold, which then worked as an excellent photo-switch. Application of these probes were verified using electrophysiology and then incubated with zebrafish larvae. They compared the photolysis LOGO5 probe with results from ML297 and found comparable changes in swimming behavior.

The previous study was an example of how the results of these probes can be translated into higher order organisms or even primary cultures to investigate GIRK activation. With the LOGOs investigation, the ML297 like urea probe was found to activate GIRK channels regardless to the *cis* or *trans* isomer. This approaches the question of the binding pocket location on the GIRK channel and how residues associated with this region play a steric role. We had previously learned from Wydeven and coworkers<sup>51</sup> about the importance of two residues that seemed necessary for ML297 activity. Accessing GIRK mutants with point mutations and the power of LOGOs could help us understand the binding region if activity increases or decreases upon photolysis. Also, it was interesting to note how much the GIRK channels tolerated the extension of the aromatic system. Previously, we had discussed how sensitive the pyrazole C3 substituent was to selectivity



and GIRK1 activity. The LOGOs probes extend out with the azo-benzene past what we had originally assumed the channel binding region would “accommodate”.

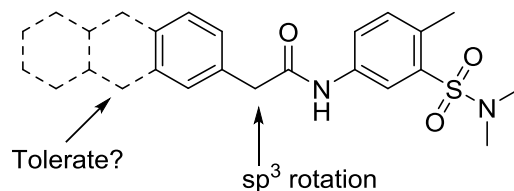


**Figure 5.2.** Implementing more sulfonamide probes based off of LOGOs results.

Additionally, ML297 suffers from its insolubility due to the urea scaffold. Modification to an amide scaffold with varying functional groups may provide improved solvation. Exploring around the sulfonamide may provide some useful SAR information, possibly leading to a better affinity probe for use in the LOGOs studies. One drawback highlighted was the inability to produce a red-shifted photo-switching probe. Longer wavelength probes first move the excitation wavelength away from cellular damaging UV light and offer deeper tissue penetration, perhaps translating these studies into primary cultures or *in vivo* murine models with fiber optics.

### **5.3 Chapter 3 Conclusions and Future Directions of Discovery of a Stereo-Specific Modulation of GIRK1/2 and GIRK1/4 Channels: Synthesis and Evaluation of 2-Methylcyclopropyl Enantiomers**

The findings in Chapter 3 with GIRK1 selectivity based on enantiomeric preference offers a more subtle look at how GIRK channels are activated (or inhibited). ML297 was 6-10 fold more active on GIRK1/2 channels but was still activate on GIRK1/4. Finding that the 2-methyl cyclopropyl probes were active on GIRK1/2 but inactive or inhibitory on GIRK1/4 suggests a

delicate selectivity for interaction with the channel. Adventitious in selectivity but not activity, the probes did not have the highest efficacy nor potency as ML297 ( $EC_{50} = 0.160 \mu\text{M}$ ) or derivatives, leading them to be a medocore candidate for anything other than selectivity studies. The 2-methyl cyclopropyl route to pure (1*R*, 2*R*) or (1*S*, 2*S*) enantiomers has been established, however, not trivial, may be repeated to generate the pyrazole coupling piece. This built in flexibly in the last step allows the potential to generate another small library of compounds.

Due to the convergent nature of building ureas, exploring areas of the molecule while holding the other constant is an excellent way to probe structure and activity relationships. Pyrazoles with a varying alkyl group in the C3 position lead to Wen and co-worker<sup>35</sup>'s molecular switch of an isopropyl inhibitor to a cyclopropyl activator, but the original ML297 screen held the methyl pyrazole constant. Holding the 3,4-difluorophenyl moiety constant to better explore the steric relationship with the pyrazole, we can then investigate the relevance of the bulk of that group. Also, the benzyl derivative of ML297 demonstrated potency on both GIRK1/2 and GIRK1/4 with high efficacy relative to ML297. A benzylic methylene is not planar and has free rotation to position the phenyl in a more favorable conformation in the GIRK binding pocket. Locking in a conformer with a phenylethyl enantiomer would set the direction of the phenyl and tease out any preference. Additionally, we can solidify this enantiomer preference by introducing the methyl cyclopropyl enantiomer to the pyrazole by looking to increase potency on GIRK channel preference. We would start with the GIRK enantiomer preference probe, (1*S*,2*S*) 2- methyl cyclopropyl.

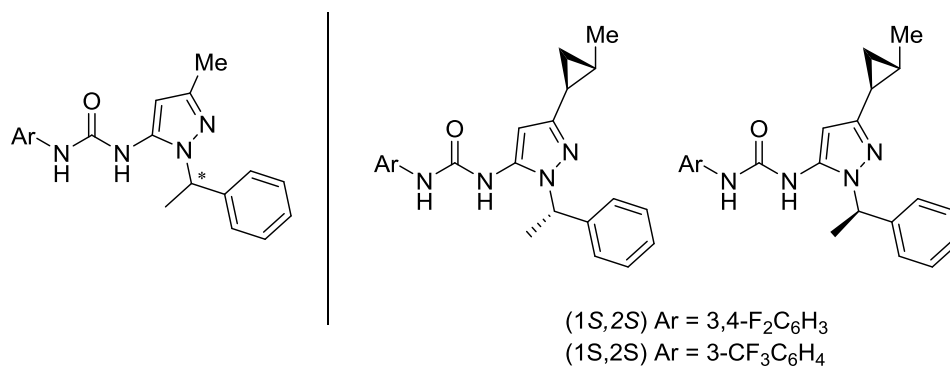


**Figure 5.3.** Examining enantiomer preference with (1*S*,2*S*) 2-methyl cyclopropyl probes and *R* or *S* phenylethyl pyrazole modification.

Considering how to go about synthesizing phenylethyl pyrazole enantiomers, we thought about how to construct the hydrazine needed for the condensation on the desired  $\beta$ -keto nitrile.  $S_n^2$  on a benzyl halide to a hydrazine potentially would cause enantiopurity issues so we thought to use a substrate with the stereocenter already in place. A solution to this problem are oxaziridines; an oxidant with two electronegative atoms, oxygen and nitrogen in a strained three member ring. Williamson and coworkers<sup>52</sup> recently reported on the usefulness of these oxidants through a variety of transformations, including electrophilic transfer of the nitrogen atom. Amination of a nitrogen to form the desired hydrazine was pioneered by Andreae and Schmitz<sup>53</sup>, offering a way to form peptide hydrazines with no racemization from the chiral amino acid. Vidal and coworkers prepared *N*-Moc and *N*-Boc protected hydrazines<sup>54</sup>, starting with 4-cyanobenzaldehyde reacted with aza-Wittig and oxidized to the oxaziridine using buffered Oxone (potassium peroxymonosulfate). The Boc-protected imine can also be isolated through a base catalyzed elimination of a sulfonyl from the benzyl carbamate<sup>55</sup>, and then oxidized using similar conditions. With the pyrazole stereoisomers in hand, we then may couple with an isocyanate to produce the urea small molecule probe. Once assayed, we then can determine our future directions with molecular modeling using these data.

## 5.4 Chapter 4 Conclusions and Future Directions of Selective Rhodamine Pro-dye/Enzyme Releasing Pair: Mitochondrion Membrane Potential Sensors

In Chapter 4, we had evaluated a series of rhodamine pro-dyes with an exogenously expressed enzyme PLE in cell lines. We had demonstrated exquisite activation and selectivity with the cells expressing PLE versus the cells that were not. This led to the potential of using the cell line expressing our enzyme as mitochondrial membrane potential sensors. Initial experiments were conducted on its use as a membrane potential sensor but until following up with cellular staining (Figure 4.9), we uncovered that our expectations of our pro-dye as a mitochondrial dye were not as anticipated. In fact, when compared to rhodamine 123 (a known mitochondrial dye), rhodamine 110 failed to perform similarly, despite the known conversion of rhodamine 123 to rhodamine 110 by endogenous enzymes. Seeing as we had pro-dyes that were protected and converted to rhodamine 110, this left a very large question: What was different about rhodamine 123 that allowed it to preferentially stain mitochondria despite its known metabolite rhodamine 110 being reported consistently? Thinking about this problem, especially considering what we have learned about our pro-dyes, we propose this substrate to evaluate in Figure 5.4.

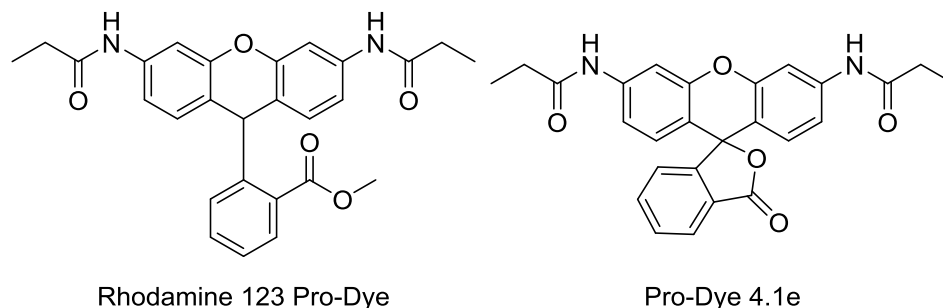


**Figure 5.4.** (Left) Proposed Rhodamine 123 based pro-dye off of (Right) Pro-dye **4.1e**.

Accessing the pro-dye derived from rhodamine 123 would require treatment in basic conditions<sup>56</sup> with either propionic acid or propionyl chloride. This pro-dye should then validate if mitochondrial staining occurs due to the methyl ester moiety. Unfortunately, we expect this pro-dye to be fluorescent due to the open conformation but we are unsure of the exact quantum yield with the acetylated nitrogens. In another approach, we could learn more about the metabolic profile of rhodamine 123 and our pro-dyes, and compare lysates of cells that have been treated with the pro-dye and those without. Similar to the glucuronidation studies, we could determine the metabolites present using mass spectrometry and comparing to the known compounds.

## **5.5 Concluding Remarks**

The utility of molecular tools for the investigation of complex biological system is only limited by our imagination. We have come to some solid conclusions on what may be happening with GIRK channels but many questions remain unanswered or not even conceived yet. The impact of these tools hopefully will begin to unravel the complexity of GIRK channels and may even one day offer us a solution to the host of disorders we currently do not have the cure for.

## REFERENCES

1. Luscher, C.; Slesinger, P. A., Emerging roles for G protein-gated inwardly rectifying potassium (GIRK) channels in health and disease. *Nature. Rev. Neurosci.* **2010**, *11*, 301-315.
2. Hille, B., *Ion Channels of Excitable Membranes*. Third ed.; Sinauer Associates, Inc.: Sunderland, MA, 2001.
3. Whorton, M. R.; MacKinnon, R., X-ray structure of the mammalian GIRK2-beta gamma G-protein complex. *Nature* **2013**, *498*, 190-197.
4. Kobayashi, T.; Ikeda, K.; Ichikawa, T.; Abe, S.; Togashi, S.; Kumanishi, T., Molecular Cloning of a Mouse G-Protein-Activated K<sup>+</sup> Channel (mGIRK1) and Distinct Distributions of 3 GIRK (GIRK1, 2 and 3) mRNAs in Mouse Brain. *Biochem. Biophys. Res. Commun.* **1995**, *208*, 1166-1173.
5. Karschin, C.; Dissmann, E.; Stuhmer, W.; Karschin, A., IRK(1-3) and GIRK(1-4) inwardly rectifying K<sup>+</sup> channel mRNAs are differentially expressed in the adult rat brain. *J. Neurosci.* **1996**, *16*, 3559-3570.
6. Harkins, A. B.; Fox, A. P., Cell death in weaver mouse cerebellum. *Cerebellum* **2002**, *1*, 201-206.
7. Carter, K. P.; Young, A. M.; Palmer, A. E., Fluorescent Sensors for Measuring Metal Ions in Living Systems. *Chem. Rev.* **2014**, *114*, 4564-4601.
8. Terai, T.; Nagano, T., Small-molecule fluorophores and fluorescent probes for bioimaging. *Pflügers Archiv., EJP* **2013**, *465*, 347-359.
9. Kaufmann, K.; Romaine, I.; Days, E.; Pascual, C.; Malik, A.; Yang, L.; Zou, B.; Du, Y.; Sliwoski, G.; Morrison, R. D.; Denton, J.; Niswender, C. M.; Daniels, J. S.; Sulikowski, G. A.; Xie, X.; Lindsley, C. W.; Weaver, C. D., ML297 (VU0456810), the First Potent and Selective Activator of the GIRK Potassium Channel, Displays Antiepileptic Properties in Mice. *ACS Chem. Neurosci.* **2013**, *4*, 1278-1286.
10. Cruz, H. G.; Ivanova, T.; Lunn, M. L.; Stoffel, M.; Slesinger, P. A.; Luscher, C., Bi-directional effects of GABA(B) receptor agonists on the mesolimbic dopamine system. *Nat. Neurosci.* **2004**, *7*, 153-159.
11. Moulton, B. C.; Fryer, A. D., Muscarinic receptor antagonists, from folklore to pharmacology; finding drugs that actually work in asthma and COPD. *Br. J. Pharmacol.* **2011**, *163*, 44-52.
12. Bradley, S. J.; Tobin, A. B., Design of Next-Generation G Protein-Coupled Receptor Drugs: Linking Novel Pharmacology and In Vivo Animal Models. *Annu. Rev. Pharmacol. Toxicol.* **2016**, *56*, 535-559.

13. Weaver, C. D.; Harden, D.; Dworetzky, S. I.; Robertson, B.; Knox, R. J., A thallium-sensitive, fluorescence-based assay for detecting and characterizing potassium channel modulators in mammalian cells. *J. Biomol. Screen.* **2004**, *9*, 671-677.
14. Lavis, L. D.; Raines, R. T., Bright Building Blocks for Chemical Biology. *ACS Chem. Bio.* **2014**, *9*, 855-866.
15. Sabnis, R. W., *Handbook of Fluorescent Dyes and Probes*. Wiley: Hoboken, US, 2015.
16. Lavis, L. D.; Rutkoski, T. J.; Raines, R. T., Tuning the pKa of Fluorescein to Optimize Binding Assays. *Anal. Chem.* **2007**, *79*, 6775-6782.
17. (a) Nekongo, E. E.; Popik, V. V., Photoactivatable Fluorescein Derivatives Caged with a (3-Hydroxy-2-naphthalenyl)methyl Group. *J. Org. Chem.* **2014**, *79*, 7665-7671; (b) Wysocki, L. M.; Grimm, J. B.; Tkachuk, A. N.; Brown, T. A.; Betzig, E.; Lavis, L. D., Facile and General Synthesis of Photoactivatable Xanthene Dyes. *Angew. Chem. Int. Ed.* **2011**, *50*, 11206-11209.
18. Lavis, L. D.; Chao, T.-Y.; Raines, R. T., Synthesis and utility of fluorogenic acetoxymethyl ethers. *Chem. Sci.* **2011**, *2*, 521-530.
19. Yang, Y.; Zhao, Q.; Feng, W.; Li, F., Luminescent Chemodosimeters for Bioimaging. *Chem. Rev.* **2013**, *113*, 192-270.
20. Baracca, A.; Sgarbi, G.; Solaini, G.; Lenaz, G., Rhodamine 123 as a probe of mitochondrial membrane potential: evaluation of proton flux through F<sub>0</sub> during ATP synthesis. *Biochem. Biophys. Acta.* **2003**, *1606*, 137-146.
21. Sun, W.-C.; Gee, K. R.; Klaubert, D. H.; Haugland, R. P., Synthesis of Fluorinated Fluoresceins. *J. Org. Chem.* **1997**, *62*, 6469-6475.
22. Brunet, A.; Aslam, T.; Bradley, M., Separating the isomers--efficient synthesis of the N-hydroxysuccinimide esters of 5 and 6-carboxyfluorescein diacetate and 5 and 6-carboxyrhodamine B. *Bioorg. Med. Chem. Lett.* **2014**, *24*, 3186-3188.
23. Grimm, J. B.; Sung, A. J.; Legant, W. R.; Hulamm, P.; Matlosz, S. M.; Betzig, E.; Lavis, L. D., Carbofluoresceins and Carborhodamines as Scaffolds for High-Contrast Fluorogenic Probes. *ACS Chem. Bio.* **2013**, *8*, 1303-1310.
24. Tsien, R. Y., A non-disruptive technique for loading calcium buffers and indicators into cells. *Nature* **1981**, *290*, 527-528.
25. Minta, A.; Tsien, R. Y., Fluorescent indicators for cytosolic sodium. *J. Biol. Chem.* **1989**, *264*, 19449-19457.
26. Hille, B., Potassium channels in myelinated nerve. Selective permeability to small cations. *J. Gen. Physiol.* **1973**, *61*, 669-686.

27. Bhave, G.; Lonergan, D.; Chauder, B. A.; Denton, J. S., Small-molecule modulators of inward rectifier K<sup>+</sup> channels: recent advances and future possibilities. *Future Med. Chem.* **2010**, *2*, 757-774.
28. Aryal, P.; Dvir, H.; Choe, S.; Slesinger, P. A., A discrete alcohol pocket involved in GIRK channel activation. *Nat. Neurosci.* **2009**, *12*, 988-995.
29. Kubo, Y.; Reuveny, E.; Slesinger, P. A.; Jan, Y. N.; Jan, L. Y., Primary structure and functional expression of a rat G-protein-coupled muscarinic potassium channel. *Nature* **1993**, *364*, 802-806.
30. Kobayashi, T.; Ikeda, K.; Kojima, H.; Niki, H.; Yano, R.; Yoshioka, T.; Kumanishi, T., Ethanol opens G-protein-activated inwardly rectifying K<sup>+</sup> channels. *Nat. Neurosci.* **1999**, *2*, 1091-1097.
31. Ramos-Hunter, S. J.; Engers, D. W.; Kaufmann, K.; Du, Y.; Lindsley, C. W.; Weaver, C. D.; Sulikowski, G. A., Discovery and SAR of a novel series of GIRK1/2 and GIRK1/4 activators. *Bioorg. Med. Chem. Lett.* **2013**, *23*, 5195-5198.
32. Kennedy, J. P.; Williams, L.; Bridges, T. M.; Daniels, R. N.; Weaver, D.; Lindsley, C. W., Application of Combinatorial Chemistry Science on Modern Drug Discovery. *ACS Comb. Sci.* **2008**, *10*, 345-354.
33. Wickman, K. D.; Iniguez-Lluhl, J. A.; Davenport, P. A.; Taussig, R.; Krapivinsky, G. B.; Linder, M. E.; Gilman, A. G.; Clapham, D. E., Recombinant G-protein beta gamma-subunits activate the muscarinic-gated atrial potassium channel. *Nature* **1994**, *368*, 255-357.
34. Pravetoni, M.; Wickman, K., Behavioral characterization of mice lacking GIRK/Kir3 channel subunits. *Genes Brain Behav.* **2008**, *7*, 523-531.
35. Wen, W.; Wu, W.; Romaine, I. M.; Kaufmann, K.; Du, Y.; Sulikowski, G. A.; Weaver, C. D.; Lindsley, C. W., Discovery of 'molecular switches' within a GIRK activator scaffold that afford selective GIRK inhibitors. *Bioorg. Med. Chem. Lett.* **2013**, *23*, 4562-4566.
36. Mori, A.; Arai, I.; Yamamoto, H.; Nakai, H.; Arai, Y., Asymmetric simmons-smith reactions using homochiral protecting groups. *Tetrahedron* **1986**, *42*, 6447-6458.
37. Baldwin, J. E. B., Samuel, Jr., Stereochemistry of the thermal isomerizations of (1R,2R)-1-[(E)-styryl]-2-methylcyclopropane to 3-phenyl-4-methylcyclopentenes. *JACS.* **1993**, *115*, 10621-10627.
38. Forster, S.; Thumser, A. E.; Hood, S. R.; Plant, N., Characterization of Rhodamine-123 as a Tracer Dye for Use In *In vitro* Drug Transport Assays. *PLoS ONE* **2012**, *7*, 332-353.



39. Tsien, R. Y., New calcium indicators and buffers with high selectivity against magnesium and protons: design, synthesis, and properties of prototype structures. *Biochemistry* **1980**, *19*, 2396-2404.
40. Losonczy, A.; Makara, J. K.; Magee, J. C., Compartmentalized dendritic plasticity and input feature storage in neurons. *Nature* **2008**, *452*, 436-441.
41. Padmawar, P.; Yao, X.; Bloch, O.; Manley, G. T.; Verkman, A. S., K<sup>+</sup> waves in brain cortex visualized using a long-wavelength K<sup>+</sup>-sensing fluorescent indicator. *Nat. Med.* **2005**, *2*, 825-827.
42. Zimmerman, M.; Ashe, B.; Yurewicz, E. C.; Patel, G., Sensitive assays for trypsin, elastase, and chymotrypsin using new fluorogenic substrates. *Anal. Biochem.* **1977**, *78*, 47-51.
43. Lavis, L. D.; Chao, T.-Y.; Raines, R. T., Fluorogenic Label for Biomolecular Imaging. *ACS Chem. Bio.* **2006**, *1*, 252-260.
44. Musidlowska-Persson, A.; Bornscheuer, U. T., Recombinant porcine intestinal carboxylesterase: cloning from the pig liver esterase gene by site-directed mutagenesis, functional expression and characterization. *Protein Eng.* **2003**, *16*, 1139-1145.
45. Sueyoshi, K.; Nogawa, Y.; Sugawara, K.; Endo, T.; Hisamoto, H., Highly Sensitive and Multiple Enzyme Activity Assay Using Reagent-release Capillary-Isoelectric Focusing with Rhodamine 110-based Substrates. *Anal. Sci.* **2015**, *31*, 1155-1161.
46. Ellis, E. E.; Adkins, C. T.; Galovska, N. M.; Lavis, L. D.; Johnson, R. J., Decoupled Roles for the Atypical, Bifurcated Binding Pocket of the ybfF Hydrolase. *ChemBioChem* **2013**, *14*, 1134-1144.
47. Johnson, L. V.; Walsh, M. L.; Chen, L. B., Localization of mitochondria in living cells with rhodamine 123. *PNAS.* **1980**, *77*, 990-994.
48. Sweatman, T. W.; Seshadri, R.; Israel, M., Metabolism and elimination of rhodamine 123 in the rat. *Cancer Chemother. Pharmacol.* **1990**, *27*, 205-210.
49. Jager, W.; Winter, O.; Halper, B.; Salamon, A.; Sartori, M.; Gajdzik, L.; Hamilton, G.; Theyer, G.; Graf, J.; Thalhammer, T., Modulation of liver canalicular transport processes by the tyrosine-kinase inhibitor genistein: Implications of genistein metabolism in the rat. *Hepatology* **1997**, *26*, 1467-1476.
50. Barber, D. M.; Schonberger, M.; Burgstaller, J.; Levitz, J.; Weaver, C. D.; Isacoff, E. Y.; Baier, H.; Trauner, D., Optical control of neuronal activity using a light-operated GIRK channel opener (LOGO). *Chem. Sci.* **2016**, *7*, 2347-2352.
51. Wydeven, N.; Marron Fernandez de Velasco, E.; Du, Y.; Benneyworth, M. A.; Hearing, M. C.; Fischer, R. A.; Thomas, M. J.; Weaver, C. D.; Wickman, K., Mechanisms underlying the

activation of G-protein-gated inwardly rectifying K<sup>+</sup> (GIRK) channels by the novel anxiolytic drug, ML297. *PNAS*. **2014**, *111*, 10755-10760.

52. Williamson, K. S.; Michaelis, D. J.; Yoon, T. P., Advances in the Chemistry of Oxaziridines. *Chem. Rev.* **2014**, *114*, 8016-8036.

53. Andreae, S.; Schmitz, E., Electrophilic Aminations with Oxaziridines. *Synthesis* **1991**, *1991*, 327-341.

54. Vidal, J.; Guy, L.; Sterin, S.; Collet, A., Electrophilic amination: preparation and use of N-Boc-3-(4-cyanophenyl)oxaziridine, a new reagent that transfers a N-Boc group to N- and C-nucleophiles. *J. Org. Chem.* **1993**, *58*, 4791-4793.

55. Davis, T. A.; Vilgelm, A. E.; Richmond, A.; Johnston, J. N., A Preparation of (-)-Nutlin-3 Using Enantioselective Organocatalysis at Decagram Scale. *J. Org. Chem.* **2013**, *78*.

56. Harapanhalli, R. S.; Roy, A. M.; Adelstein, S. J.; Kassis, A. I., [125I/127I/131I]Iodorhodamine: Synthesis, Cellular Localization, and Biodistribution in Athymic Mice Bearing Human Tumor Xenografts and Comparison with [99mTc]Hexakis(2-methoxyisobutylisonitrile). *J. Med. Chem.* **1998**, *41*, 2111-2117.